# DECOMPOSITION AND METRICAL ANALYSIS OF SINGLE-JOINT MOVEMENT OF THE HEMIPARETIC UPPER-LIMB

By

MICHAEL T. WININGER

A Dissertation submitted to the

Graduate School − New Brunswick

Rutgers, The State University of New Jersey

and

The Graduate School of Biomedical Sciences

University of Medicine and Dentistry of New Jersey

in partial fulfillment of the requirements

for the degree of

Doctor of Philosophy

Graduate Program in Biomedical Engineering

written under the direction of

Dr. William Craelius

and approved by

_____

_____

_____

_____

New Brunswick, New Jersey

October, 2009

ABSTRACT OF THE DISSERTATION

Decomposition and metrical analysis of single-joint movement of the hemiparetic upper-limb

By MICHAEL T. WININGER

Dissertation Director:

William Craelius, Ph.D.

Observation of the voluntary movement of the upper-limb is the primary method by which recovery is determined in the motor-impaired. Here, an analytical infrastructure is presented for the decomposition of the kinematical record into two constitutive components: the essential motor activity, and spontaneous motor noise. These tools are subsequently used to perform novel hypothesis tests on the symmetry and variability of discrete single-joint articulation of the elbow in chronic stroke patients and healthy control subjects.

Firstly, elbow-joint goniometric data from 41 healthy volunteers was modeled with a high accuracy to a set of analytical curves, parameterized to account for movement delay and average velocity. From this it was determined that single-joint trajectories are not uniformly symmetric, nor are their trace morphologies highly stereotyped. Additional analysis of trajectory waveform variability following a pseudo-wavelet domain transformation revealed modest spontaneous behavior in the medial domains of joint articulation. Among 14 subjects with impaired motor control due to chronic stroke, though significantly greater transience was observed throughout the joint domain, cohort tendency to adopt symmetric trajectories within a narrow (but

non-singular) set of morphology themes did not depart significantly from that of unimpaired subjects.

It is concluded that motor dysfunction in the hemiparetic upper-limb, as observed via the motor activity of the elbow joint in stroke-afflicted persons, pertains to the proclivity to accelerative transience across the joint range, and not to an essential motor behavior associated with basic task execution.

ACKNOWLEDGEMENT & DEDICATION

To my family. A very inclusive designation, indeed.

# TABLE OF CONTENTS

**ABSTRACT OF THE DISSERTATION**……..ii

**ACKNOWLEDGEMENT & DEDICATION**……..……iv

**LIST OF FIGURES**..... x

**LIST OF TABLES**.....xiii

**LIST OF EQUATIONS**..... xv

**LIST OF ABBREVIATIONS**.....xviii

**1 INTRODUCTION**..... 1

*1.1.1 Statement of need*..... *1*

1.2 RESEARCH CONDUCTED UNDER THE THESIS PURVIEW..... 2

*1.2.1 Overview*..... *2*

*1.2.2 Devices*..... *2*

1.2.2.1 The Hand-Arm Rehabilitation Interface (HARI)..... 2

1.2.2.2 The Mechanical Arm Support & Tracker (MAST)..... 3

*1.2.3 Subject recruitment and demography*..... *4*

1.2.3.1 Healthy subjects with no known neurological impairments..... 4

1.2.3.2 Subjects with impaired motor control due to chronic stroke..... 6

*1.2.4 Subject protocol overview*..... *7*

*1.2.5 MAST movement protocols*..... *7*

1.3 HYPOTHESES..... 8

*1.3.1 Overview*..... *8*

*1.3.2 Raw SJTs can be approximated by analytical waveforms*..... *9*

*1.3.3 Essential movement patterns are symmetric and stable*..... *9*

*1.3.4 Stroke patients significantly less symmetric, stable*..... *10*

*1.3.5 Standard metrical resolution of motor proficiency*..... *11*

*1.3.6 Domain transformation yields robust motor assessments*..... *12*

1.4 THESIS OVERVIEW..... 13

*1.4.1 Analysis of standard, and novel SJT performance metrics*..... *13*

*1.4.2 Primary deliverables*..... *14*

1.4.2.1 Explanation for jerk failure..... 14

1.4.2.2 Proposal of a SJT transformation and operational scalars..... 14

1.4.2.3 Proposal of a noise-free SJT approximation..... 15

1.4.2.4 “Extension” of scope..... 15

**2 KINEMATICAL OBSERVATION**..... 17

2.1 THEORIES OF MOTOR CONTROL, AND KINEMATIC STUDY..... 17

*2.1.1 Minimum jerk*..... *17*

*2.1.2 Minimum change-of-torque*..... *17*

*2.1.3 Equilibrium point hypothesis*..... *18*

*2.1.4 Two-thirds power law*..... *19*

2.2 ARTIFACT IN THE KINEMATICAL RECORD..... 19

*2.2.1 Noise in the context of neuromotor research*..... *19*

*2.2.2 Error introduced in the data acquisition process*..... *19*

*2.2.3 Error introduced according to sampling frequency*..... *21*

*2.2.4 Error resulting from differentiation*..... *23*

*2.2.5 Artifact associated with inappropriate task constraints*..... *23*

*2.2.6 Artifact associated with legitimate movement phenomena*..... *24*

2.3 RATERS OF KINEMATICAL PROFICIENCY..... 25

*2.3.1 Basic kinematic parameters*..... *25*

2.3.1.1 Positional domain..... 25

2.3.1.2 Differentiated domains..... 26

*2.3.2 Waveform evaluation*..... *27*

2.3.2.1 Integrated jerk..... 27

2.3.2.2 Arrest periods..... 29

2.3.2.3 Velocimetric peaks..... 30

*2.3.3 Miscellany* ..... *31*
*2.3.4 Metric type and commutativity* ..... *31*
*2.3.5 Vectorial versus scalar metrics: local versus global analysis* ..... *32*
2.4 SUMMARY ..... 32

**3 EXTRACTING THE TRAJECTORY ESSENCE ..... 34**

3.1 INTRODUCTION ..... 34
3.2 SJT SHAPE: THEORY AND OBSERVATION ..... 34
*3.2.1 Physiology, task variables co-determine trajectory shape* ..... *34*
3.2.1.1 Agonist-antagonist activity ..... 34
3.2.1.2 Stretch reflex and velocity ..... 36
*3.2.2 Prediction of SJT shape from neuromotor control principles* ..... *37*
3.2.2.1 Minimum jerk velocity ..... 37
3.2.2.2 Two-thirds power law ..... 40
*3.2.3 Evidence of symmetric, approximately linear SJTs* ..... *41*
3.3 SJT APPROXIMATION BY ANALYTICAL FUNCTIONS ..... 43
*3.3.1 Need for suitable substrates in biomechanical analysis* ..... *43*
*3.3.2 Incorporation of analytical functions into biomechanics* ..... *45*
3.4 METHOD OVERVIEW: SIMULATION OF SJTS ..... 46
*3.4.1 Designing appropriate models for the angular trajectory* ..... *46*
*3.4.2 Global SJT model fitting by parameterization* ..... *47*
*3.4.3 Extraction of the Essential trajectory (ET)* ..... *50*
3.5 ANALYSIS AND DISCUSSION OF ET CURVES ..... 51
*3.5.1 Model assumptions* ..... *51*
*3.5.2 Trajectory-matching model in jerk analysis: limitations* ..... *52*
3.5.2.1 Choosing a model set ..... 52
3.5.2.2 Specific models chosen to represent angular trajectories ..... 52
*3.5.3 Trajectory-matching model in jerk analysis: utility* ..... *53*
3.5.3.1 Forward- and backward-testing of the two-thirds power law ..... 53
3.5.3.2 Assessing hand path for adherence to jerk cost minimization ..... 53
3.5.3.3 Generalizability of curve-matching model ..... 54
3.6 SUMMARY ..... 54

**4 VALIDATION OF THE ESSENTIAL TRAJECTORY ..... 56**

4.1 INTRODUCTION ..... 56
4.2 EXPERIMENTAL HYPOTHESES ..... 56
4.3 EXPERIMENTAL METHODS ..... 57
*4.3.1 Subjects and protocol* ..... *57*
*4.3.2 Signal processing and curve matching* ..... *58*
*4.3.3 Waveform comparison* ..... *59*
4.4 RESULTS ..... 60
*4.4.1 Basic performance measures* ..... *60*
*4.4.2 ET goodness-of-fit to the observed motion* ..... *61*
*4.4.3 Symmetry parameters: ET to SJT* ..... *62*
4.5 CLOSER LOOK: FILTER VALIDATION ..... 63
*4.5.1 Filter design* ..... *63*
*4.5.2 Filter assessment* ..... *65*
4.6 PEAK IDENTIFICATION: NEAREST-NEIGHBOR ANALYSIS ..... 66
*4.6.1 Spurious SJT peaks are randomly distributed* ..... *66*
*4.6.2 Veridical peak assessment* ..... *68*
4.7 SUMMARY ..... 71

**5 MOVEMENT PATTERNS FROM ET MODELS ..... 72**

5.1 INTRODUCTION ..... 72
5.2 EXPERIMENTAL HYPOTHESES ..... 72
5.3 EXPERIMENTAL METHODS ..... 73
*5.3.1 Subjects and protocol* ..... *73*
*5.3.2 Signal processing and curve matching* ..... *74*
*5.3.3 Curvature theme analysis and interpretation* ..... *74*
5.3.3.1 Essential Trajectory label histograms ..... 74
5.3.3.2 The Principal Trajectory (PT) ..... 75

5.3.3.3 Significant Trajectories (ST) ..... 75
5.4 HYPOTHESIS TESTING VIA SCREE ANALYSIS ..... 78
*5.4.1 Isogonic SJTs ..... 78*
5.4.1.1 Isogony principle and the two-thirds power law ..... 78
5.4.1.2 The isogony principle in single-joint motion ..... 79
*5.4.2 Trajectory pattern stability ..... 80*
5.4.2.1 Quantitative raters of trajectory variability ..... 80
5.4.2.2 Categorical metrics in trajectory variability analysis ..... 81
5.5 RESULTS ..... 81
*5.5.1 Isogony is common, but not universal ..... 81*
*5.5.2 Degeneracy of model themes typical ..... 83*
*5.5.3 Degeneracy persists at the single-session level ..... 85*
5.6 COMPARISON TO EXTENSION MOVEMENTS ..... 86
*5.6.1 Within-subjects analysis: Identical PT distributions ..... 86*
*5.6.2 Within-subjects analysis: Equivalently variable patterns ..... 87*
*5.6.3 Movement patterns across direction: no correspondence ..... 88*
5.6.3.1 "Hard" versus "soft" criteria for correspondence ..... 88
5.6.3.2 Chance PT prediction, weak ST overlap ..... 89
*5.6.4 Poor PT correlation to movement variables ..... 90*
5.7 DISCUSSION ..... 91
*5.7.1 Inference regarding trajectory selection ..... 91*
*5.7.2 Model space composition ..... 92*
5.7.2.1 Change in model space dimensionality ..... 92
5.7.2.2 Change in model space membership ..... 93
*5.7.3 Symmetry ..... 94*
*5.7.4 Single-joint protocols can be run in a single day ..... 94*
5.8 SUMMARY ..... 95

**6 TRAJECTORY ANALYSIS OF STROKE COHORT ..... 96**

6.1 INTRODUCTION ..... 96
6.2 EXPERIMENTAL HYPOTHESES ..... 96
6.3 EXPERIMENTAL METHODS ..... 97
*6.3.1 Subjects and protocol ..... 97*
*6.3.2 Signal processing and curve matching ..... 99*
*6.3.3 Degenerate behavior via scree analysis ..... 99*
6.4 RESULTS: PRINCIPAL TRAJECTORY ANALYSIS ..... 100
*6.4.1 Curve matching method equally accurate for stroke SJTs ..... 100*
*6.4.2 Stroke trajectory choices mirror those of normal subjects ..... 100*
6.5 RESULTS: DEGENERACY, DIRECTIONALITY ANALYSIS ..... 102
*6.5.1 Stroke subjects are equivalently degenerate to unimpaired ..... 102*
6.5.1.1 Within-subjects analysis ..... 102
6.5.1.2 Between-sessions analysis ..... 103
*6.5.2 Stroke subjects equivalently predictive in extension ..... 104*
*6.5.3 Prediction across movement direction ..... 105*
*6.5.4 Correlation to basic movement parameters ..... 105*
*6.5.5 Stroke subjects significantly more symmetric ..... 106*
6.6 MOVEMENT PATTERN VARIABILITY: STANDARD MEASURES ..... 107
*6.6.1 Variance Ratio ..... 107*
*6.6.2 Fluctuation in basic movement parameters ..... 108*
6.7 SUMMARY ..... 109

**7 RATERS OF MOTOR PERFORMANCE ..... 111**

7.1 INTRODUCTION ..... 111
7.2 FUNDAMENTAL THEOREM OF MOVEMENT SMOOTHNESS ..... 111
*7.2.1 General definition ..... 111*
*7.2.2 Basic principles of smoothness measurement ..... 113*
7.3 COUNTER-INTUITIVE RATER BEHAVIOR ..... 113
*7.3.1 Failure to discriminate obviously impaired cohorts ..... 113*
*7.3.2 Metrical contradiction ..... 114*
7.4 THE JERK PROFILE ..... 116
7.5 JERK AS A MEASURE OF MOVEMENT PROFICIENCY ..... 117

7.6 JERK NORMALIZATION ..... 118
*7.6.1 Need for normalization* ..... *118*
*7.6.2 Jerk normalization to total movement duration* ..... *119*
*7.6.3 Normalization by peak velocity* ..... *122*
*7.6.4 Normalization by average velocity* ..... *123*
7.7 ASSESSMENT OF JERK'S METRICAL VALIDITY ..... 125
*7.7.1 Study overview* ..... *125*
*7.7.2 Study protocol* ..... *126*
*7.7.3 Signal processing and analysis* ..... *126*
*7.7.4 Experimental hypotheses* ..... *127*
*7.7.5 Results: All jerk metrics spuriously correlated to speed* ..... *128*
*7.7.6 Results: Jerk metrics do not discriminate between cohorts* ..... *129*
7.8 SUMMARY ..... 130

**8 TRAJECTORY DOMAIN TRANSFORMATION ..... 131**

8.1 INTRODUCTION ..... 131
8.2 RATER ERROR INTRODUCED IN DISCRETE DIFFERENTIATION ..... 131
8.3 PERFORMANCE RATER DEPENDENCE ON TIME IS ILL-POSED ..... 132
*8.3.1 Motor performance: time independence* ..... *132*
*8.3.2 Motor performance: angular dependence* ..... *133*
*8.3.3 Increased positional dependence in hemiplegia* ..... *134*
8.4 SUPPORT FOR PERFORMANCE RATER BASED ON JOINT ANGLE ..... 134
*8.4.1 Isogony Principle & the Two-Thirds Power Law* ..... *134*
*8.4.2 Essential Trajectories suggest basic SJT themes* ..... *136*
*8.4.3 Fuzzy isogony: regionally straight trajectory curvature* ..... *136*
8.5 SPATIAL RESOLUTION OF MOVEMENT SMOOTHNESS ..... 138
*8.5.1 Approach overview* ..... *138*
*8.5.2 Even, n-wise segmentation along time* ..... *139*
*8.5.3 Hard lower-limit to segmentation* ..... *141*
*8.5.4 Linear approximants spanning observed angles* ..... *143*
*8.5.5 Distribution of error across segment domain* ..... *145*
*8.5.6 Correlation-based measurement of approximant error* ..... *147*
*8.5.7 Correlational error requires iterated normalization* ..... *149*
8.6 PUTTING IT ALL TOGETHER: CREATION OF THE SPATIAL MAP ..... 151
8.7 SUMMARY ..... 152

**9 MAPPING ACCELERATIVE TRANSIENCE ..... 154**

9.1 INTRODUCTION ..... 154
9.2 EXPERIMENTAL HYPOTHESES ..... 154
9.3 EXPERIMENTAL METHODS ..... 156
*9.3.1 Subjects and protocol* ..... *156*
*9.3.2 Transform method validation* ..... *156*
9.3.2.1 Determining the sensitivity to various curvatures ..... 156
9.3.2.2 Spatial acceleration versus raw acceleration ..... 157
*9.3.3 Data treatment and analysis* ..... *157*
9.3.3.1 Signal processing ..... 157
9.3.3.2 Standard smoothness raters: Average jerk and velocity peaks ..... 157
9.3.3.3 Scalar metrics of smoothness as a function of angle ..... 158
9.3.3.4 Trace feature analysis: Trace peak analysis ..... 159
9.4 RESULTS: METHOD VALIDATION ..... 159
*9.4.1 Robustness to global curvature, i.e. curved ETs* ..... *159*
*9.4.2 Comparison of spatial acceleration to raw acceleration trace* ..... *162*
9.5 RESULTS: HUMAN SUBJECTS TESTING ..... 165
*9.5.1 Basic performance measures* ..... *165*
*9.5.2 Integrated metrics: Area under S(θ) and J(t) curves* ..... *166*
*9.5.3 Ratiometric indices: Peak maximum to trace mean* ..... *167*
*9.5.4 Tallied metrics: Peak counting* ..... *167*
9.6 SPEED, TEMPORAL METRICS CORRELATED IN STROKE COHORT ..... 168
*9.6.1 Prolonged stall periods (high MAPR) skew jerk metrics* ..... *168*
*9.6.2 Spurious correlation: Jerk, speed in high-MAPR cohort* ..... *169*
9.7 SUMMARY ..... 170

**10 SUMMARY ..... 171**

10.1 KINEMATICAL MEASUREMENT OF THE UPPER-LIMB ..... 171
*10.1.1 Experimental methodology ..... 171*
10.1.1.1 Instrumentation ..... 171
10.1.1.2 Subjects and protocol ..... 171
*10.1.2 Analysis: Standard, novel metrics ..... 172*
10.1.2.1 Characterization ..... 172
10.1.2.2 Implementation ..... 173
10.2 RESULTS: BASIC MOVEMENT PARAMETERS ..... 173
*10.2.1 Cohorts not significantly different by standard measures ..... 173*
*10.2.2 Significant deficit apparent in SJT symmetry, variability ..... 176*
10.3 RESULTS: TRAJECTORY DOMAIN TRANSFORM ..... 176
*10.3.1 Method ..... 176*
*10.3.2 Jerk correlates to average velocity in high arrest conditions ..... 177*
*10.3.3 Transformed metrics: Velocity-independent, discriminative ..... 178*
10.4 RESULTS: ESSENTIAL MOVEMENT PATTERNS ..... 179
*10.4.1 Method ..... 179*
*10.4.2 Cohorts similar in essential motor behaviors, not symmetry ..... 180*
10.4.2.1 Degenerate movement patterns ..... 180
10.4.2.2 Identical model trace distributions ..... 180
10.4.2.3 Stroke subjects move with greater symmetry ..... 182
*10.4.3 Extension movement patterns reveal additional insight ..... 182*
10.4.3.1 PT distributions, degeneracy similar to that of flexion ..... 182
10.4.3.2 Poor prediction across movement direction ..... 183
10.5 CONCLUSIONS TO HYPOTHESES ..... 185
*10.5.1 Overview ..... 185*
*10.5.2 Chapter 4: Essential Trajectory as a valid SJT surrogate ..... 185*
*10.5.3 Chapter 5: SJTs symmetric, but unpredictably degenerate ..... 186*
*10.5.4 Chapter 6: Stroke patients equivalently isogonic, degenerate ..... 187*
*10.5.5 Chapter 8: Failure of jerk measures in cohort discrimination ..... 188*
*10.5.6 Chapter 9: Domain transformation yields valid substrates ..... 189*
10.6 CONCLUDING REMARKS ..... 190
*10.6.1 Thesis scope ..... 190*
*10.6.2 Thesis self-consistency ..... 191*
10.7 CONCLUDING PHILOSOPHY ..... 192

**APPENDIX ..... 193**

10.8 VARIABLES: CLASSICAL LATIN ALPHABET ..... 193
10.9 VARIABLES: GREEK ALPHABET ..... 195

**REFERENCES ..... 197**

**CURRICULUM VITA ..... 204**

# LIST OF FIGURES


| Figure | Caption | |
|---|---|---|
| Figure 1 | Mechanical Arm Support & Tracker (MAST). | 3 |
| Figure 2 | MAST Software Interface. | 4 |
| Figure 3 | Prediction of Linear Trajectory by *vmj:* The minimum jerk velocity plots a bell-shaped profile. | 40 |
| Figure 4 | Observations of symmetrical trajectories (Lacquaniti, Terzuolo et al. 1983; Hogan 1984; Flanagan and Ostry 1990; Feng and Mak 1997; Pfann, Hoffman et al. 1998; Amirabdollahian, Loureiro et al. 2002; Ju, Lin et al. 2002; Liang, Yamashita et al. 2008). | 42 |
| Figure 5 | Contamination of kinematic data by noise. | 44 |
| Figure 6 | Sample analytical models found in kinematic literature. | 45 |
| Figure 7 | Archetypal model curves. Basic trajectory model curves (angle of flexion vs. time) modeled against observed motions. + = acceleration, ++ = relatively swift acceleration; — = deceleration, —— = relatively swift deceleration; 0 = abrupt change in velocity. | 46 |
| Figure 8 | Snapshots of the iterative pseudo-convolution across the observed trajectory: Line (Top) and Sigmoid (Bottom). | 49 |
| Figure 9 | Sample best-fit curves. Three sample trajectories from a single subject, with the global best fit curve *B(l, p)* (generating label *L* for three repetitions). | 62 |
| Figure 10 | Frequency response profile of the 2nd-order low-pass Butterworth's filter used here: -3 dB reduction at approximately 12 Hz. | 64 |
| Figure 11 | Overlay of a sample trajectory $\theta$ and its Essential Trajectory approximant (c.f. Figure 9). | 70 |
| Figure 12 | Example of scree analysis: Determination of significant contributors to an simulated over-determined system according to a broken-stick scree line threshold. | 77 |
| Figure 13 | Adoption of ET model type across subjects. Proportion of subjects (N=41) yielding Principal Trajectories (PT) of each curve type ($\chi$ = A→F) for flexion SJTs. | 82 |
| Figure 14 | Frequency of model class as a significant dataset component. Proportion of subjects (N=41) yielding Significant Trajectories (ST) of each curve type ($\chi$ = A→F) for flexion SJTs. | 83 |
| Figure 15 | Results of curve-matching. Proportion of subjects (N=41) yielding Principal Trajectories (PT) of each curve type ($\chi$ = A→F) for both | 87 |

flexion (Left) and extension (Right) tasks.

Figure 16 Distribution of flexion Principal Trajectories for both cohorts. 100

Figure 17 Distribution of extension Principal Trajectories for both cohorts. 101

Figure 18 Distribution of stroke cohort Principal and Significant Trajectories. 102

Figure 19 Metrical Incongruence: Perturbation of ideal sigmoidal trajectory with parameterized noise, yields contradictory smoothness metric behavior. 115

Figure 20 Need for jerk normalization jerk: Trajectory θ1 (θ2: T1→T2=2T1 *Left)* yield disparate jerk profiles, skewing jerk according to average velocity (Right). 118

Figure 21 Artefact associated with jerk normalization to time: A sample flexion was assessed for jerk before (Top, *Left)* and after the insertion of simulated stalls (Middle, *Left)*. 121

Figure 22 Normalization of the jerk profile by maximum speed is more likely to skew the jerk metric by detection of velocity peaks related to spontaneous accelerations. 123

Figure 23 Partition Equivalence: Segmentation according to time guarantees approximately equal number of samples per partition. 140

Figure 24 Approximant construction: Three linear approximations to the data: scatter fit, linear fit from first data point, linear fit to segment ends. 143

Figure 25 Three error assignment methods: domain-wide attribution, and point-wise error assignment (direct, or nearest-neighbor, shown for sub-region inset). 145

Figure 26 Shortcomings of point-wise assignment: domain shift and non-surjective transformations. 146

Figure 27 Error vector generation: The first six iterations of partition and projection of E(θ), bar graph rotated to rise in the reverse-time dimension. 150

Figure 28 Spatial error vector generation: stacking, summing of A1→6 (θ); histogram representation of S(θ) (the sum is not subtracted or normalized). 150

Figure 29 Spatial error heat map generation: side-by-side comparison of flexion trace *θ(t),* spatial error generated from unsmooth trace features S(θ), and spatial error vector as a heat map. 152

Figure 30 Inverse weighting scale: S(θ) detects both gentle global curvatures and locally unsmooth activity, preferentially weighting small transients. 161

Figure 31 Accuracy and sensitivity of S(θ): two sample trajectories 164

demonstrate the accuracy of spatial error vectors to <5% error from peaks in the acceleration profile.

Figure 32 Sample spontaneous accelerations maps of healthy (Top) and stroke subjects (Bottom). 166

# LIST OF TABLES


| Table | Caption | Page |
|---|---|---|
| Table 1 | Demography of healthy subjects | 5 |
| Table 2 | Demography of stroke subjects | 6 |
| Table 3 | Basic kinematic variables of the positional domain | 25 |
| Table 4 | Standard kinematic variables of the differentiated domain | 26 |
| Table 5 | Analytical models for trajectory curve matching | 47 |
| Table 6 | Demography of healthy subjects: Trajectory modeling | 58 |
| Table 7 | Parameters of SJTs recorded from healthy subjects (N = 41) | 60 |
| Table 8 | Parameters of healthy subjects' ETs (N = 41) | 63 |
| Table 9 | Parameters of healthy subjects' unfiltered SJTs (N = 41) | 65 |
| Table 10 | Disparity of features extracted from SJT:ET trace pairs (N = 3334) | 67 |
| Table 11 | Comparison: ET peak against multiple SJT peaks (N = 3212) | 70 |
| Table 12 | Parameters of healthy subjects' ETs (N = 41) | 85 |
| Table 13 | Flexion trajectory degeneracy: Within-session analysis (N = 140) | 85 |
| Table 14 | Extension trajectory degeneracy: Within-subjects analysis (N = 41) | 87 |
| Table 15 | Flexion trajectory degeneracy: Within-session analysis (N = 140) | 89 |
| Table 16 | Correlation of ET model to motion parameters: Degenerate Sessions | 91 |
| Table 17 | Demography of stroke subjects: Essential Trajectory extraction | 98 |
| Table 18 | Flexion trajectory degeneracy: Stroke subjects (N = 11) | 103 |
| Table 19 | Flexion trajectory degeneracy: Within-session analysis (N = 120) | 103 |
| Table 20 | Comparative degeneracy of extension: Within-subjects (N = 11) | 104 |
| Table 21 | Directional prediction of PT and ST: Within-session (N = 140) | 105 |
| Table 22 | Correlation of ET model to movement parameters: Degenerate sessions | 106 |
| Table 23 | Symmetry comparison ETs recorded from stroke subjects (N = 11) | 107 |
| Table 24 | Comparison of movement parameter variability within-sessions | 109 |
| Table 25 | Smoothness raters | 112 |

| | | |
|---|---|---|
| Table 26 | Metrical contradiction among smoothness raters | 115 |
| Table 27 | Jerk metrics | 116 |
| Table 28 | Demography of cohort study: Accelerative transients | 126 |
| Table 29 | Correlation of jerk metrics to average velocity | 128 |
| Table 30 | Metrical results in cohort discrimination task | 129 |
| Table 31 | Smoothness map operations | 138 |
| Table 32 | Parameterization of domain transform | 148 |
| Table 33 | Parameters of SJTs from 15 Subjects | 165 |
| Table 34 | Peak counting of SJTs of 15 subjects | 166 |
| Table 35 | Ratiometric indices evaluated from SJTs of 15 subjects | 167 |
| Table 36 | Peak counting of SJTs of 15 subjects | 168 |
| Table 37 | Correlation of smoothness metrics to average speed $\rho(\bar{\theta}, X)$ | 169 |
| Table 38 | Results Summary: Basic parameters of upper-limb motion | 175 |
| Table 39 | Justification for, and analysis of, domain transform of kinematic data | 178 |
| Table 40 | Results summary: Flexion pattern via Essential Trajectory modeling | 181 |
| Table 41 | Results summary: Extension pattern via Essential Trajectory modeling | 184 |

# LIST OF EQUATIONS


| Equation | Expression | Page |
|---|---|---|
| (Equation 1) | $J = \kappa \cdot \int_0^T \left\| \frac{d^3}{dt^3}\theta(t) \right\|^2 \cdot dt$ | 27 |
| (Equation 2) | $MAPR = \sum_{i=1}^{N_s} \dot{\theta}_i < \delta_{\dot{\theta}}$ | 30 |
| (Equation 3) | $\pi_{\dot{\theta}} = 1 + \sum \frac{d}{dt}\left( \mathrm{sgn}\left( \frac{d}{dt}\left(\dot{\theta}(t)\right)\right)\right)$ | 30 |
| (Equation 4) | $\rho_{\dot{\theta}} = \frac{\dot{\theta}_{\max}}{\int_T \theta(t)dt}$ | 31 |
| (Equation 5) | $v_{mj} = \frac{\Delta}{T}\left( \frac{30t^4}{T^4} - \frac{60t^3}{T^3} + \frac{30t^2}{T^2} \right)$ | 39 |
| (Equation 6) | $v(s) = K(s) \cdot \left( \frac{R(s)}{1 + \alpha \cdot R(s)} \right)^{\beta}$ | 41 |
| (Equation 7) | $B_{iX}(l,p) = \left\{ \begin{matrix} \theta_{on} & 0 \le i < p \\ \theta_{on} + \theta_{ROM} \cdot b_{iX}(l,p) & p \le i \le p+l \\ \theta_{off} & p+l < i < T \end{matrix} \right\}_{\substack{p=0:T-l \\ l=5:T-1}}$ | 48 |
| (Equation 8) | $b_{i,X=A\cdots F}(l,p) = \left\{ \begin{matrix} \left(\frac{i-p}{l}\right) & A \\ \frac{1}{2}\cdot\left[1+\sin\left(\frac{i-p}{l}\pi - \frac{\pi}{2}\right)\right] & B \\ \left(\frac{i-p}{l}\right)^2 & C \\ \left[1-\left(\frac{i-p}{l}\right)^2\right] & D \\ \left(\frac{i-p}{l}\right)^{\frac{1}{2}} & E \\ \exp\left(-\left[\pi\left(\frac{i-p}{l}-1\right)\right]^2\right) & F \end{matrix} \right\}_{\substack{p=0:T-l \\ l=5:T-1}}$ | 48 |
| (Equation 9) | $\arg\min_{l,p} \sum_{i=1}^{T} \left( B_{i,\chi}(l,p) - \theta_i \right)^2$ | 50 |

(Equation 10) $$ET = B_{\chi}(l,p) \ \ni' \ \underset{\chi,l,p}{\arg\min} \sum_{i=1}^{T} \left(B_{i,\chi}(l,p) - \theta_i\right)^2$$ 50

(Equation 11) $$\rho = \frac{\sum_{i=1}^{T} \theta_i \cdot ET_i - T \cdot \bar{\theta} \cdot \overline{ET}}{\left(T-1\right) \cdot \sigma_{\theta} \cdot \sigma_{ET}}$$ 59

(Equation 12) $$h = \frac{\left\lfloor \ 0.04, \ 0.08, \ 0.04 \ \right\rfloor}{\left[ \ 1.0, \ -1.35, \ 0.51 \ \right]}$$ 63

(Equation 13) $$H_i = \left| \ L_j \ \right| \ \ni' \ L_j = \chi_i \ \ \forall \ \ 1 \le j \le N_{reps}, \ 1 \le i \le \left| \ \chi \ \right|$$ 74

(Equation 14) $$\Re^* = sort\left(\frac{\Re_k}{\sum_{i} \Re_k}\right)$$ 77

(Equation 15) $$V = K \cdot C(t)^{\frac{2}{3}}$$ 79

(Equation 16) $$V(s) = K(s) \cdot \left(\frac{R(s)}{1 + \alpha \cdot R(s)}\right)^{\frac{1}{3}}$$ 79

(Equation 17) $$VR = \frac{\sum_{i=1}^{T^*} \sum_{j=1}^{N_{reps}} \frac{\left(X_{ij} - \bar{X}_i\right)^2}{T^* \cdot \left(N_{reps} - 1\right)}}{\sum_{i=1}^{T^*} \sum_{j=1}^{N_{reps}} \frac{\left(X_{ij} - \bar{\bar{X}}\right)^2}{\left(T^* \cdot N_{reps} - 1\right)}}$$ 80

(Equation 18) $$O = \frac{ST^f \cap ST^e}{\left| \ ST^f \cup ST^e \ \right|}$$ 88

(Equation 19) $$J(t) \equiv \frac{d}{dt}\left(\ddot{\theta}(t)\right) = \frac{d^3}{dt^3}\theta(t)$$ 116

(Equation 20) $$MAPR = \frac{\sum \left|\dot{\theta}(t)\right| < \delta}{T}$$ 120

(Equation 21) $$\rho\left(J', \bar{\theta}\right) = \frac{1}{N-1} \sum_{i=1}^{N} \left(\frac{\overline{J'_i} - \bar{\bar{J'}}}{\sigma_{\bar{J'}}}\right)\left(\frac{\bar{\dot{\theta}}_i - \bar{\bar{\dot{\theta}}}}{\sigma_{\bar{\dot{\theta}}}}\right)$$ 127

(Equation 22) $$\theta(t) = \sum_{i}^{1 \le n \le N} \exp\left(-\left(n - \tfrac{N}{2}\right)^2\right)$$ 139

(Equation 23) $$n_p \propto \left.\frac{\nu}{\bar{\dot{\theta}}(t)}\right|_{\alpha \le t \le \beta}$$ 139

(Equation 24) $$n_p = \frac{\nu}{N_p}$$ 140

(Equation 25) $$1 \le j < J_{\lim},\ J_{\lim} \ni' \tau_{\zeta+1} - \tau_{\zeta} > 1 \quad \forall \quad \zeta \in \mathrm{N} < j$$ 142

(Equation 26) $$P_k = \left[ \frac{\Theta_{k+1} - \Theta_k}{T \diagup j} \cdot \left( i - \frac{k-1}{j} T \right) \right] + \Theta_k$$ 144

(Equation 27) $$k = \left| G \right| : G \subset \left\{ \frac{k-1}{j} \right\} < \frac{i}{T}$$ 144

(Equation 28) $$\left[ \frac{1}{\kappa} \sum_{i=1}^{N} (x_i - a)(b - c) \right]^{\gamma}$$ 147

(Equation 29) $$\rho(\theta_k, P_k) = \frac{1}{\frac{T}{j} - 1} \frac{1}{\sigma_\theta \sigma_P} \sum_{i \in \tau_k} (\theta_i - P_i)^2$$ 148

(Equation 30) $$E_k = 1 - \rho(\theta_k, P_k)$$ 148

(Equation 31) $$A_{j\cdot} = E^*(\theta) = \frac{E(\theta)}{\max(E(\theta))}$$ 149

(Equation 32) $$A_{j\xi} = E_k^* \quad \forall \quad \frac{k-1}{j} < \frac{\xi}{\eta} < \frac{k}{j}$$ 149

(Equation 33) $$S(\theta) = \sum_j A_{j\cdot}(\theta)$$ 151

(Equation 34) $$S^*(\theta) = \frac{S(\theta) - \min(S(\theta))}{\max(S(\theta) - \min(S(\theta)))}$$ 151

(Equation 35) $$J = \frac{1}{T} \int_0^T \left| \frac{d^3}{dt^3} \theta(t) \right|^2 dt$$ 158

(Equation 36) $$N_V = \sum_t \left[ \left\{ \frac{d}{dt} \operatorname{sgn}\left( \frac{d}{dt} \theta(t) \right) \right\} > 0 \right]$$ 158

(Equation 37) $$R = \frac{1}{\Delta\theta} \int_{\Delta\theta} S(\theta) d\theta$$ 158

(Equation 38) $$\pi_S = \sum_{\Delta\theta} \left[ \frac{d}{dt} (\operatorname{sgn}(S(\theta))) > 0 \right]$$ 159

(Equation 39) $$\varepsilon = \frac{\max(S(\theta))}{\bar{S}}$$ 159

(Equation 40) $$\Theta_e = \{\theta'\} \quad \ni' \quad \frac{d}{d\theta} S(\theta') < \delta$$ 162

(Equation 41) $$\tau_d = \{t'\} \quad \ni' \quad \frac{d}{d\theta} \ddot{\theta}(t') < \delta$$ 163

(Equation 42) $$\overline{\Delta p} = \frac{1}{\Delta\theta} \frac{1}{N_\cap} \sum_{i=1}^{N_\cap} \Theta_{ei} - \Theta_{di}$$ 163

# LIST OF ABBREVIATIONS

| | |
|---|---|
| ANOVA | Analysis of variance |
| AJ | Average jerk |
| CB | Cerebellopathy |
| DAQ | Data acquisition |
| DOF | Degree(s) of freedom |
| EMG | Electromyography |
| ET | Essential Trajectory |
| GUI | Graphical user interface |
| HARI | Hand-arm rehabilitation interface |
| IAJ | Integrated average jerk |
| IRB | Institutional review board |
| JM | Jerk metric |
| LDE | Linear differential equation |
| MAPR | Mean arrest period ratio |
| MAST | Mechanical arm support & tracker |
| MR | Measurement range |
| NARJ | Normalized average rectified |
| NHPT | Nine-hole peg test |
| PT | Prinicpal Trajectory |
| RMS | Root-mean square |
| RMSE | Root-mean square error |
| ROM | Range of motion |
| SJT | Single-joint trajectory |
| SNR | Signal-to-noise ratio |
| SR | Stretch reflex |
| SSE | Sum of squared error |
| ST | Significant trajectory |
| UL | Upper-limb |
| VR | Variance ratio |
| WR | Weaving ratio |

# 1 INTRODUCTION

### 1.1.1 Statement of need

Five million Americans have survived a cerebrovascular accident (stroke), with an annual affliction rate of approximately 700,000 clinical admissions annually (Gresham, Duncan et al. 1995). The resultant hemiparesis severely reduces the quality of life in stroke survivors according to the limitations of the activities of daily living (ADL), the widely accepted tasks constituting and independent lifestyle: grooming, eating, self-care and hobbies (King 1996). These activities are highly manual, requiring dexterous proficiency of all of the joints and musculo-tendinous complexes of the upper-limb.

At almost every juncture of the rehabilitation process, rigorous quantitative measurement of limb functionality is highly important: from preliminary diagnosis and design of therapeutic regimen, to monitoring of patient progress, and patient categorization for administrative and insurance purposes. Thus, reliable and robust measures of motor proficiency are an essential aspect of both clinical care provision, and laboratory-based development of rehabilitation tools and re-training paradigms. However, artifact sourced either in the empirical acquisition of biomechanical data, or in the ill-posed analysis of even putatively noise-free data can greatly bias the inferences generated in motion analysis. Here, an analytical infrastructure is developed for the accurate and informative analysis of kinematic data recorded from motor-impaired individuals.

## 1.2 Research conducted under the thesis purview

### 1.2.1 Overview

In the present work, a series of analytical investigations are performed on a single, large dataset of human subjects performing discrete flexion of the elbow, yielding single-joint trajectory (SJT) data. Here, a diverse set of theories of human movement and kinematic analysis are discussed either as long-standing and widely-tested conventions, or as novel hypotheses tested here for the first time. All human subjects testing described herein were approved by the Institutional Review Board of Rutgers University, in place of or in combination with that of the University of Medicine and Dentistry of New Jersey, and all protocol administrators were certified to work with human subjects via the Human Subjects Certification Program at Rutgers University.

### 1.2.2 Devices

#### *1.2.2.1 The Hand-Arm Rehabilitation Interface (HARI)*

The Hand-Arm Rehabilitation Interface (HARI) system is a family of instruments for the re-training of the upper-limb. The maxim of HARI is that of a set of simple rehabilitation tools of sturdy construction, comfortable design, and dependable performance, coupled with an intuitive graphical interface for real-time biofeedback display of a given measurement. HARI's softwares are written in consideration of client needs, with clear display, large fonts, audible commands, and a compliant, but rigid interface for the elbow, wrist, and digits. HARI's simplicity ensures reduced fabrication costs and setup, as well as interface interpretability and ease of operation, maximizing HARI's amenability to a broad cohort of individuals

with special needs, spanning a variety of ages, cognitive and attention deficits, visual and aural impairments, and motor limitations.

#### *1.2.2.2 The Mechanical Arm Support & Tracker (MAST)*

Third-generation MAST hardware was used in all experiments described herein. The MAST supports the arm against gravity, allowing movement in the transverse plane, while recording instantaneous joint angle as voltage returned from a variable resistor (potentiometer), stationed within the MAST, below the elbow pad (Figure 1). Movement is constrained to a single degree-of-freedom, articulation about the elbow, by strapping the forearm securely into a freely rotating walled platform, with the hand positioned in a neutral posture, palm down. The arm is secured at slightly below shoulder height, with a soft strap at the humerus to restrict shoulder movement, and also at the forearm, placing the elbow joint in-line with the goniometer axis. It is

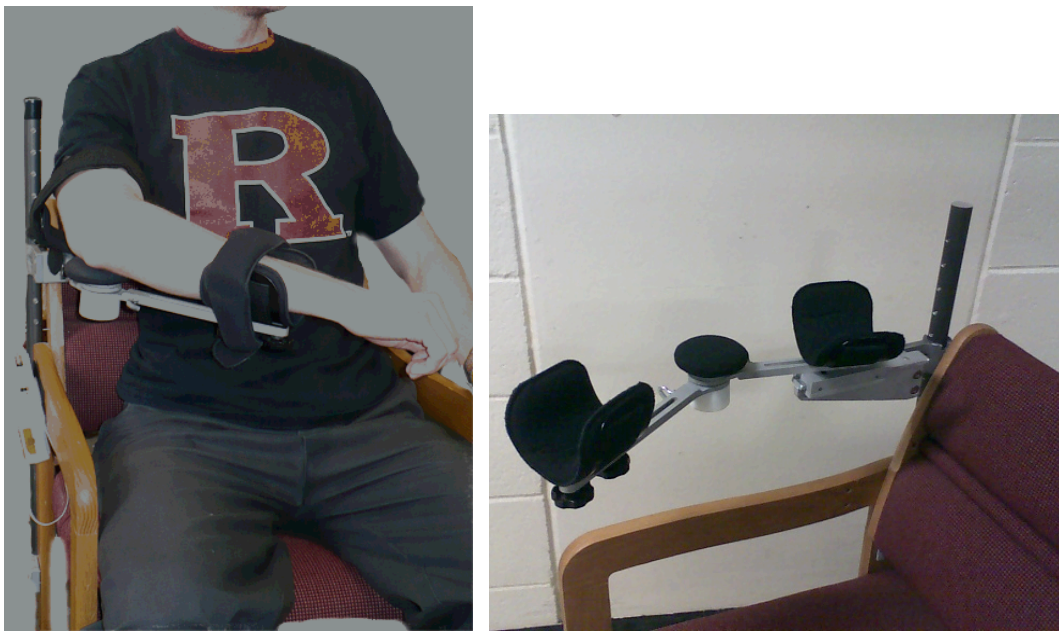


Figure 1 Mechanical Arm Support & Tracker (MAST).

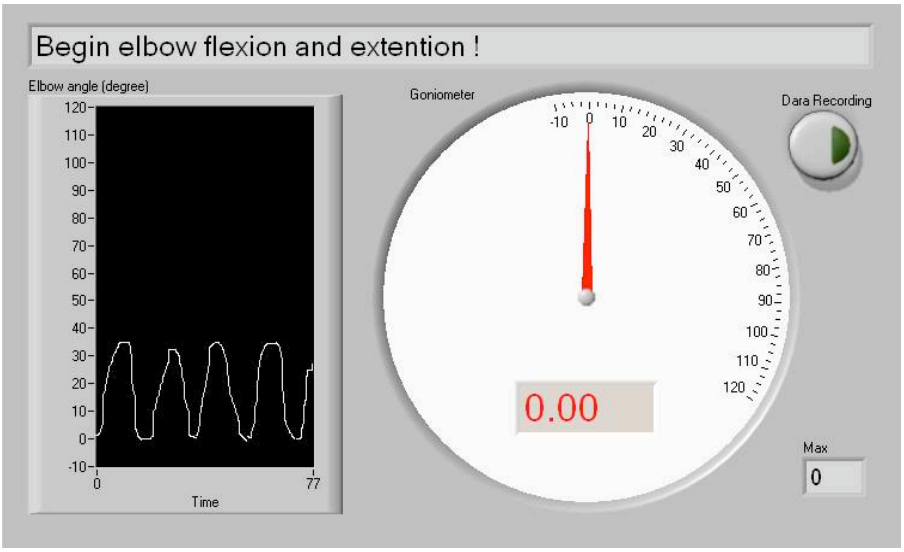


Figure 2 MAST Software Interface.

presumed, though has not been rigorously demonstrated, that the arm is securely strapped and does not translocate during a single or multiple movement cycles.

MAST interfaces with a National Instruments data acquisition board (DAQ, *National Instruments*, Austin TX, USA), which acquires data at 80 Hz, with 12 bits resolution. A real-time biofeedback display, programmed in LabView (National Instruments) provided real-time display of instantaneous joint angle, as well as an approximately 2-second buffer of recent movement history (Figure 2).

Minor processing was performed within LabView for display purposes, mostly pertaining to device calibration to the subject's total range of motion. However, only raw data were recorded to a tab-delimited text file and saved for downstream analysis.

### 1.2.3 Subject recruitment and demography

#### *1.2.3.1 Healthy subjects with no known neurological impairments*

Whereas HARI is a nascent technology whose development can be traced to the preliminary experiments of which some results are presented here, a wide variety

of subjects were recruited to perform repetitive movement tasks in the MAST. Healthy volunteers were taken in from the Rutgers University community, representing a variety of body types, ethnicities, age groups, and genders, as well as handedness, familiarity with computer-based and robotics-based rehabilitation, and from all education levels and backgrounds. For the results discussed here, a group of 65 healthy subjects provided data that could be used for at least one of the analyses (Table 1).

| Table 1: Demography of healthy subjects | | |
|---|---|---|
| | Group | Multiple visits |
| Number of Subjects | 41 | 19 |
| Age ($\mu \pm \sigma$)<br>Range (min/max) | 36.5 ± 16.2<br>21/68 | 26.0 ± 8.6<br>21/59 |
| Gender (M/F) | 21/20 | 15/4 |
| Side of affect (R/L) | 35/6 | 15/4 |
| Number of visits ($\mu \pm \sigma$)<br>Range (min/max) | 3.1 ± 3.0<br>1/17 | 5.5 ± 2.4<br>2/17 |
| $\mu$ = Mean, $\sigma$ = Standard deviation, min = Minimum, max = Maximum, M = Male, F = Female, R = Right, L = Left. | | |

In many cases, subjects were able to make repeated visits to the lab, in which case their data was incorporated into longitudinal studies comparing performance over several days. It is worth noting the somewhat narrowed profile of this cohort: because of the lab's situation in the Engineering Building at a large state university, persons capable of making multiple visits to the lab fit a stereotype of students enrolled in such a degree program.

*1.2.3.2 Subjects with impaired motor control due to chronic stroke*

Clinical collaborators of the Rutgers University Rehabilitation Lab at the JFK-Johnson Rehabilitation Institutes at Edison and at Hartwyck JFK Medical Center at Oak Tree (Edison, NJ) provided access to a consenting cohort of outpatient clients interested in an intramural rehabilitation experience. Over one dozen adults with spasticity have used the MAST either at the Rehab Lab on Rutgers University's Busch Campus, or at one of these regional facilities. Most individuals were interested in using the MAST system on repeated occasions, and some were compensated for their time.

Table 2: Demography of stroke subjects

| | Group | Multiple visits |
|---|---|---|
| Number of Subjects | 14 | 13 |
| Age ($\mu \pm \sigma$)<br>Range (min/max) | 56.8 ± 18.9<br>21/80 | 54.8 ± 19.6<br>21/80 |
| Gender (M/F) | 9/5 | 8/5 |
| Side of affect (R/L) | 8/6 | 7/6 |
| Number of visits ($\mu \pm \sigma$)<br>Range (min/max) | 10.4 ± 4.2<br>1/14 | 10.8 ± 3.6<br>3/14 |
| Months post-stroke ($\mu \pm \sigma$)<br>Range (min/max) | 22.4 ± 14.9<br>7/49 | 21.7 ± 15.2<br>7/49 |
| C-M arm score ($\mu \pm \sigma$)<br>Range (min/max) | 3.7 ± 1.2<br>3/7 | 3.6 ±1.2<br>3/7 |

$\mu$ = Mean, $\sigma$ = Standard deviation, min = Minimum, max = Maximum, M = Male, F = Female, R = Right, L = Left, C-M = Chedoke-McMaster stroke assessment.

Strict inclusion criteria of visual acuity, cognitive presence and attention span were evaluated by a licensed therapist, employed as facility Staff. Several functional evaluations were used, including the Nine-Hole Peg Test (NHPT) and the Chedoke-

McMaster arm score (Heller, Wade et al. 1987; Gowland, Stratford et al. 1993). Additional inclusion criterion of a Chedoke-McMaster score greater than 2+ or 5 completed tasks was employed; completion of the NHPT was not required, and is not presented in the present discussion. For subjects enrolled in the formal visitation program, these functional evaluations were administered before and after program completion, along with a pair of arm rating questionnaires, one of which was adapted from clinical literature (L'Insalata, Warren et al. 1997).

### 1.2.4 Subject protocol overview

All experiments described herein follow the same essential protocol except where otherwise indicated. Whereas the primary objective of this thesis document is to analyze behavioral motor control in its purest and simplest form, all analyses described herein are based on the *autonomous* single-joint flexion and extension of the elbow, meaning that the elbow was supported against gravity, pace self-selected, and no targets were imposed. “Warm-up” assistance was provided to the patients as requested, typically involving stretching of the involved joints, gentle massage, and periods of rest throughout the protocol.

### 1.2.5 MAST movement protocols

Single-joint elbow articulations were recorded from healthy and impaired individuals moving along a fixed pathway, where the only possible variable was angular velocity, as similarly adopted by previous studies (Nagasaki 1989; Wiegner and Wierzbicka 1992; Jaric, Gottlieb et al. 1998; Osu, Kamimura et al. 2004). Subjects were seated in the HARI with their dominant arm supported against gravity by the MAST. The elbow and hand were always positioned in the same horizontal plane as the shoulder, or just below, and the hand was never obscured from view.

Hemi-paretic individuals were seated with their affected arm in the MAST, irrespective of handedness.

| | |
|---|---|
| *Perform a series of maximally smooth flexions and extensions with your elbow. You can perform these at whatever pace you like, but you are asked to perform them as smoothly as possible, and to the bounds of your comfortable movement range.* | *Movement Instruction* |

Subjects were instructed to move as smoothly as possible, with large, but sub-maximal angular range. Movements were performed at a moderate and self-selected pace: no targets temporal or spatial were imposed on movements. Though not strictly controlled, the hand typically paused at movement reversal, i.e. all results reflect *discrete* and not cyclical movements. The arm was visible to the subjects, and biofeedback was provided as described above, however subjects were not specifically instructed to attend to this information: no hypotheses contained herein are considered to depend on the strict control of visual feedback, and this is considered a random variable.

## 1.3 Hypotheses

### 1.3.1 Overview

The present work represents a series of investigations into the characterization and analysis of human performance vis-à-vis both basic movement parameters and holistic assessments of movement proficiency via a family of smoothness metrics. A series of experimental hypotheses were put forth related to the assessment of human movement, and features of movement concerning both basic behavioral patterns, and their alteration under neurological deficit.

A review of these hypotheses and their conclusions follows:

### 1.3.2 Raw SJTs can be approximated by analytical waveforms

It is hypothesized that the single-joint trajectory record can be faithfully modeled by a surrogate trace, the Essential Trajectory (ET), an analytical curve parameterized to match the observed trajectory,

> *The single-joint trajectory can be accurately reconstructed by a parameterized analytic curve selected from among a small set of model traces, the so-called Essential Trajectory.* (Hypothesis 1)

and that the parameters extracted thereof would accurately reflect the veridical movement parameters contained within the SJT.

> *Features extracted from the Essential Trajectory will report information relevant to the observed movement with an accuracy that is competes with or exceeds those extracted from the observed single-joint trajectory.* (Hypothesis 2)

Several parameters, including the time to peak velocity, and the symmetry of the observed trajectory are used to leverage important hypotheses of human motor control, and thus it is incumbent to extract these features from noise-free traces, thus reducing error generated in the presence of empirical noise.

### 1.3.3 Essential movement patterns are symmetric and stable

Based on empirical laws, e.g. the isogony principle, and on copious abstraction within the literature, it was supposed that the basic motor behaviors of healthy subjects would yield highly linear, or at least symmetric SJT traces.

*Subjects single-joint movements will be largely isogonic and symmetric in both flexion and extension tasks.* (Hypothesis 3)

Furthermore, it is suggested that the basic motor behaviors of these subjects will be highly stable and stereotyped in the absence of external perturbations, and with the movement constrained, as in the MAST.

*Irrespective of the isogonic nature of the movement profile (Hypothesis 3), model adoption by subjects will be highly uniform, showing relatively high stability among the available model types.* (Hypothesis 4)

In the case that a degeneracy of movement themes should be observed, it is further hypothesized that "selection" of ET type could be related to basic parameters of the observed motion.

*In the cases where the primary model type is not observed in a given movement cycle, this deviation from the central behavioral theme can be explained as the result of some perturbation in basic movement patterns, i.e. angular velocity, angle of motion onset, or time.* (Hypothesis 5)

Thus, the basic tendency toward symmetric, stable movement is tested via a novel curve-matching paradigm: matching SJTs to ETs.

### 1.3.4 Stroke patients significantly less symmetric, stable

In order to characterize the essential movement behaviors of an impaired cohort, an investigation into the essential movement patterns of stroke subjects will be performed. First, it will be determined whether the ET is a satisfactory approximant of the SJT in stroke subjects.

*Essential Trajectory approximants of the SJT trace will yield equivalently strong trace reconstructions of trajectories recorded from hemiparetic individuals.* (Hypothesis 6)

Following this method validation, the ETs will be analyzed for their symmetry, as before with the healthy subjects. Whereas stroke subjects' neuromotor system is impaired, the hallmark symmetry of healthy human motion is hypothesized to deteriorate in the stroke condition

*Subjects with impaired motor control exhibit motor deficiency in the way of asymmetric movement patterns.* (Hypothesis 7)

Furthermore, it is suggested that the "choice" of movement pattern will depart from the healthy subjects, resulting in a higher degeneracy.

*Motor impairment will manifest as an increased variability in trajectory patterns, and this instability will have greater co-dependence on basic movement parameters.* (Hypothesis 8)

This analysis is a standard cohort comparison, testing the hypothesis of significant departure from the results observed in healthy subjects.

### 1.3.5 Standard metrical resolution of motor proficiency

Whereas it has been reported in the literature that standard jerk-based smoothness raters occasionally fail to report significant differences between cohorts, it is here supposed that this may relate to a spurious co-dependence of average angular velocity,

*Standard jerk metrics are independent of average velocity in "well-behaved" movements performed by healthy individuals.* (Hypothesis 9a)

and that this might pertain only to persons with impaired motor control.

*Jerk metrics exhibit spurious dependence on movement velocity in the special case of spastic movements characterized by significant periods of stall behavior.* (Hypothesis 9b)

The standard jerk metric is tested in several different formulations for its ability to discriminate an obviously impaired cohort,

*Jerk metrics can discriminate between healthy individuals and those with impaired motor control due to chronic stroke.* (Hypothesis 10)

Through this analysis, it will be determined whether, in the present dataset, standard proficiency metrics are sufficient for reliable assessment of motor skill in a diverse cohort with minimal constraints on the movement paradigm (and thus the maximally autonomous motion).

### 1.3.6 Domain transformation yields robust motor assessments

Temporal domain analysis of kinematic data results proficiency metrics that are not only highly prone to error, but are dependent on a relatively meaningless variable: time. In order to obviate the pitfalls of position-versus-time analysis, a pseudo-wavelet data transformation is proposed.

*Vectorial rendering of the single-joint trajectory, following transformation into the domain of linear approximant error as a function of angle, accurately reports movement proficiency in both healthy and impaired cohorts.* (Hypothesis 11)

Here, a subjective analysis of both special test cases, and empirical data yielded will assess the transformed representation of spontaneous accelerations in the angular domain. In order to support traditional analyses and hypothesis testing, a set of scalars will be defined from which the spatial acceleration map can be evaluated.

*Scalar smoothness metrics derived from the angular-domain trajectory transformation can discriminate healthy from impaired condition as well as standard metrics.* (Hypothesis 12)

As per the preceding investigation into spurious dependence of jerk-based metrics on average velocity (Hypothesis 9), scalars resulting from the domain transformation of positional data will be similarly tested.

*Measures derived from the angular domain are impervious to spurious co-dependence of angular velocity.* (Hypothesis 13)

Thus it will be determined whether either or both classes of proficiency metrics are sufficiently robust to yield dependable analysis of motor abilities in a broad cohort study.

## 1.4 Thesis overview

### 1.4.1 Analysis of standard, and novel SJT performance metrics

Here, standard measures of motor proficiency will be presented in the form of a review of the pertinent literature, and discussed for their respective applications.

Several metrics and data transformations will be discussed in considerable detail, from which it will be proposed that despite their wide incorporation into the analysis of SJTs, they are inherently prone to error due to either their formulation or their implementation, and therefore untenable for use in biomechanical analysis. To counteract the error associated with these data treatments, two novel SJT transformations are proposed, along with scalar metrics amenable to standard statistical analysis, and, where applicable, means by which to visualize the resultant information. These novel analyses espouse complementary approaches to trajectory waveform analysis: one a highly specific characterization of movement proficiency, at very high resolution; and the other, an extraction of the general trend of the trajectory pattern, in a setting devoid of higher-order trace activity. To conclude, several sequellae from this work are outlined for potential future work.

### 1.4.2 Primary deliverables

#### *1.4.2.1 Explanation for jerk failure*

Jerk is an oft-used measure of kinematic performance, but occasionally yields spurious and counter-intuitive results, particularly in the identification of impaired cohorts. Though this metric deficiency has been noted in some instances, the reason for jerk's failure is typically met with a superficial explanation, if any at all. Here, jerk is discussed for its dependence on an inherently noisy substrate, and its susceptibility to systematic deflation in the face of stalled movement, both a result of jerk's postulation as a time-domain metric.

#### *1.4.2.2 Proposal of a SJT transformation and operational scalars*

In order to ameliorate the extraction of salient performance parameters from the trajectory record, a transformation of angle-versus-time data to smoothness-

versus-angle is proposed. For most purposes, time is an arbitrary variable, with an undue influence on many smoothness metrics; a much more meaningful independent variable, one with relevance to skeletal muscle physiology, is joint angle. To operate on this new substrate, the transformed trajectory, several simple scalar metrics are presented, yielding comparable (and sometimes favorable) results in terms of cohort discrimination between healthy subjects and subjects with impaired motor control due to chronic stroke.

#### *1.4.2.3 Proposal of a noise-free SJT approximation*

Though motor *performance* is typically judged in terms of movement smoothness, many motor *control* hypotheses are predicated on the basic shape of the trajectory waveform. In this way, the important measurement is the SJT *essence*, and not the *incidence.* A model is presented for the abstraction of the global essence of the trajectory trace, based on noiseless, parameterized analytical curves fitted to each movement record. From these idealized trajectory representations, basic hypothesis tests of waveform parameters are performed, testing the notion of cycle-to-cycle invariance, trajectory straightness (equal angle in equal time: isogony), and these variables with respect to an impaired and a healthy cohort.

#### *1.4.2.4 "Extension" of scope*

The above analyses will be performed primarily on discrete (as opposed to cyclical) flexion of the elbow; however, select experiments will compare these results to data recorded from elbow extension, as well. Following a summary of these results, a brief outline of related methodologies is offered, and explained in sufficient detail to allow for adoption or adaptation, according to desire. Finally, the findings presented herein are discussed in the context of the central philosophy of this work, that it is

incumbent for researchers of the human neuromotor system to seek to identify not only those aspects in which the impaired differ from the unimpaired, but how they are alike.

# 2 KINEMATICAL OBSERVATION

## 2.1 Theories of motor control, and kinematic study

### 2.1.1 Minimum jerk

Most motor control researchers believe that minimum principles have some biological utility (Engelbrecht 2001). The notion of minimizing the rate of change of acceleration over some segment of a movement, i.e. maximizing smoothness, has postulated in terms of minimum endpoint jerk (Flanagan and Ostry 1990), and jerk over the entire course of movement (Hogan 1984). Trajectory formation under the principle of jerk minimization predicts bell-shaped tangential velocity profiles, and straight line pathways between the endpoints in higher-dimensional movements (Hogan 1984; Plamondon, Alimi et al. 1993).

The minimum-jerk has principle been prolifically applied to cohorts with impaired motor control, including upper motor neurone syndrome (Cozens and Bhakta 2003), spasticity (Feng and Mak 1997), chronic stroke (Rohrer, Fasoli et al. 2002), and cerebellar ataxia (Goldvasser, McGibbon et al. 2001). However, the apparent asymmetry observed by some in simple, single-joint movement tasks, has led to criticism of the minimum jerk hypothesis in voluntary motion of unimpaired individuals (Nagasaki 1989; Wiegner and Wierzbicka 1992; Mutha and Sainburg 2007).

### 2.1.2 Minimum change-of-torque

Whereas jerk can be considered a kinematic cost, kinetic costs, derived from muscle-generated forces or torques applied to the arm, constitute a separate class of optimization variables. By minimizing the summed squares of torques applied to the

joints during movement or while a posture is maintained, it is thought that the minimum change-of-torque principle, a rough correlate to metabolic energy consumed by the muscles, constitutes the most biologically relevant optimization principle (Hogan 1984; Uno, Kawato et al. 1989; Kawato, Maeda et al. 1990).

The relationship between torque and elbow joint angle has since been addressed in constant muscle activations in single- and multi-joint flexion movements (Gribble and Ostry 1999; Akazawa and Okuno 2006); and has been extended to special needs populations, including stroke and cerebellar ataxia (Dewald, Pope et al. 1995; Bastian, Zackowski et al. 2000). Invoking the movement invariance of single-joint movements in the context of a minimum torque-change principle, qualitative trajectory outcomes have been postulated according against which experimental data can be compared (Engelbrecht and Fernandez 1997).

### 2.1.3 Equilibrium point hypothesis

Suggested initially as a motor neuron activation threshold control, as opposed to force control (Asatryan and Feldman 1965), the notion of position sense comprising components other than an internal (e.g. muscle torque) model was originally suggested on the evidence of parallel control modalities associated the afferent and efferent mechanisms involved during movement under load (Feldman and Latash 1982). This equilibrium point hypothesis has been studied via kinematic and EMG studies of both autonomous and perturbed motion, in humans and sub-human primates (Bizzi, Accornero et al. 1984; Gomi and Kawato 1996; Adamovich, Levin et al. 1997; Sainburg, Ghez et al. 1999; Adamovich, Archambault et al. 2001).

### 2.1.4 Two-thirds power law

A non-linear relationship between tangential velocity and radius of curvature of hand trajectory in 2- and 3-dimensional motion is thought to be described by a power-law relationship, the two-thirds power law (Viviani and Terzuolo 1982; Viviani and Schneider 1991). This principal has been tested in a variety of boundary conditions, movement constraints, and task objectives, each according to the trajectory of the hand (Viviani and Schneider 1991; Viviani and Flash 1995; Todorov and Jordan 1998; Schaal and Sternad 2001). The adherence to or violation of this principle, according to movement task, is thought to imply the pre-dominance of rhythmic pattern generation, among other hierarchical control mechanisms.

## 2.2 Artifact in the kinematical record

### 2.2.1 Noise in the context of neuromotor research

Nearly all experimental data contains some element of noise, which often proves to be the limiting factor in the utility or performance capabilities of a medical instrument (Semmlow 2004). “Noise” can refer to machine error associated with the acquisition of biological data by a digital interface, or rounding error generated in the post-hoc analysis, or even legitimate signal content that detracts from the analyst’s ability to make a determination about some concurrent phenomenon. We thus define “noise” as any aspect of the kinematic trace which interferes with a given motor analysis.

### 2.2.2 Error introduced in the data acquisition process

In the experiments presented here, all data are obtained from the elbow joint via a variable resistor (potentiometer) goniometer, embedded in a sturdy aluminum manifold. Joint angle is recorded as a function of voltage out of the resistor, fed

through a data acquisition box (DAQ), which sends the digitized signal to an interpretation software in the computer, where it is stored. Error in the data acquisition process can occur at any juncture of this process, either due to mechanical failure of the goniometer, e.g. not fitted correctly to its housing, or sliding of the wiper within the potentiometer body; in the conversion of analog to digital signal at the DAQ box, or in the conversion of voltage data to numerical representation and subsequent storage as a file for downstream analysis (Flowchart 0).

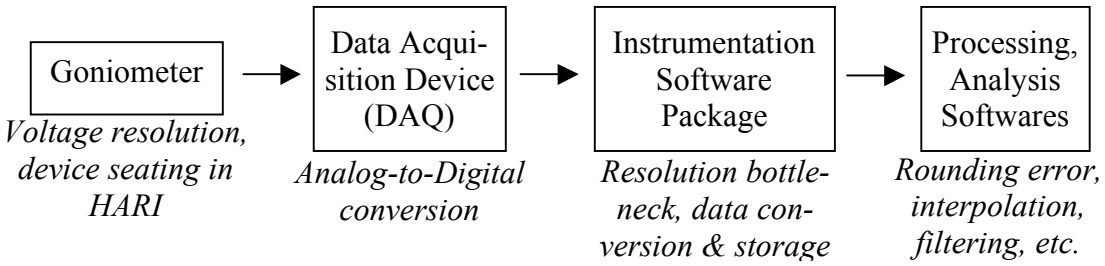


Flowchart 0 Data acquisition schematic. Error can be introduced into the recording of continuous human movement data as discrete, digital samples at any juncture.

Signal filtering, presents its own optimization process: filter design is an entirely separate field of study for which filter characteristics (ripple location in pass-band, stop-band, or both; filter roll-off), filter order, and filter coefficients, are determined not only by parameters of the data, primarily sampling frequency, but also by experimental objectives, e.g. the nature of the measurement, the specific hypothesis posed, and the movement task. Though “standard” filter characteristics are typical of niche research fields, it will be shown in subsequent Chapters that these are seldom ideal.

### 2.2.3 Error introduced according to sampling frequency

Above the Nyquist limit of minimum sampling frequency required to capture a given phenomenon, it is tempting to think that sampling frequency has little influence in the rendering of most processes (Shannon 1998). However, over-sampling any process creates as risk of generating instantaneous derivatives below the threshold of bit noise. Quantization of a continuous signal in the analog-to-digital conversion typically accounts for a trade-off between the signal-to-noise ratio and dynamic range by use of floating point sampling systems (c.f. fixed point systems with uniform sampling)[1]. In this way, if bit noise is large, and the ratio of dynamic range to sampling frequency sufficiently small, the resultant rate of change of signal may not supercede the error introduced in the system.

For example, any goniometric system, particularly those involving potentiometric measurements, the measurement range *MR* (voltage units V) of the variable resistor and the sampling frequency ν (time sample *c* per second *s*) act reciprocally to determine the voltage resolution $\rho$ (Volts per time sample):

$$\rho \propto \frac{MR}{\nu},$$

i.e. an expectation of Volts per sample *c*. In a scenario where the potentiometer is calibrated to a total range of motion $\Delta\theta_{\text{cal}}$, and a movement executed with a constant angular velocity $\bar{\dot{\theta}}$, voltage resolution will be

$$\rho = \frac{MR\,(V)}{\Delta\theta_{cal}\,(^{\circ})} \cdot \bar{\dot{\theta}}\,(^{\circ}/_{s}) \div \nu\,(^{c}/_{s}),$$

[1] Here the *dynamic range* denotes the usable voltage range of a given potentiometer, typically close to its total range, e.g. a 5V potentiometer with 4.8V of effective, non-saturated output.

yielding $\rho = \frac{MR}{\Delta\theta_{cal}} \cdot \frac{\bar{\dot{\theta}}}{\nu}$ $\left(V/c\right)$. Thus, voltage step size is *inversely proportional* to sampling frequency, creating potential for artifact in noisy systems.

To illustrate, consider a 5V potentiometer, calibrated to record a 60° angular displacement as voltages ranging from 0.5 to 4.5V, i.e. 4V representation of the dynamic range. For a 1.2s duration movement, sampled at 200 Hz, assuming constant angular velocity $\dot{\theta} = 60^\circ / 1.2s = 50^\circ / s$, voltage resolution is $\rho = \frac{4V}{60} \cdot \frac{50}{200c} = 0.0167 \frac{V}{c}$. This, of course, presumes a constant average velocity. Comparing this average resolution to the system noise tolerance, if signal error is on the order of 0.01V, the movement record could be compromised.

Indeed, constant movement speed is not physically realizable. For regimes of the motion where the instantaneous velocity is much larger than the average velocity $\dot{\theta}_i >> \bar{\dot{\theta}}$, i.e. towards the center of the bell-curve reported in the literature (), this resolution becomes larger: $\rho_i = \frac{4V}{60} \cdot \frac{\dot{\theta}_i}{\bar{\dot{\theta}}} \cdot \frac{50}{200c}$, reducing risk of error. However, it is easy to see that the lower bound for $\rho$ is $\rho_{\min} = \frac{4V}{60} \cdot \frac{\dot{\theta}_{\min}}{\bar{\dot{\theta}}} \cdot \frac{50}{200c}$, which in the limit as $\dot{\theta}_i << \bar{\dot{\theta}}$, greatly increases risk of error. This error is compounded in situations where differentiation is involved[2].

[2] It is incumbent at this juncture to assess whether this limit poses a problem for the data analyzed in the present discussions. It was determined that the version of MAST used to acquire all data presented here operated to within 0.05° tolerance. Presuming (conservatively) a 4V *MR*, and calibration to $\Delta\theta_{cal}$ = 120° for a range of motion $\Delta\theta_{cal}$ = 110° at a 2-second duration ($\bar{\dot{\theta}}$ = 55° $s^{-1}$). At a sampling rate of 80 Hz, presuming a slow movement with the 10th percentile of speed at $\bar{\dot{\theta}}$ = 3° $s^{-1}$, the change in voltage per sample for this system is given by $\rho_{10\%} = \frac{4V}{120} \cdot \frac{3}{55} \cdot \frac{110}{80c} = 2.5 \times 10^{-3}$ V$c^{-1}$. Whereas it has been determined that the potentiometer tolerance is $\frac{4V}{120^\circ} \cdot 0.05^\circ = 1.65 \times 10^{-4}$V, it is expected that the potentiometer, sampling rate, and calibration scales are entirely appropriate for our system, and its expected variable range.

### 2.2.4 Error resulting from differentiation

Various signal processing methods, such as low-pass filtering can reduce a considerable proportion of noise, but filter design espouses its own fuzzy and non-linear optimization process, and noise reduction presents a trade-off relationship with signal retention: it is possible to distort the meaningful signal in the process of removing meaningless content. Noise that remains is not only available to analysis and interpretation as a putative feature of ostensibly “clean” data, but is subject to all subsequent transformations on the original dataset, including differentiation with respect to time.

Differentiation of discrete time-series data by the central difference method is a notoriously noisy process, and will not only propagate, but amplify, errors with each iteration of the derivative (O'Haver and Begley 1981; Usui and Amidror 1982; Dabroom and Khalil 1999). Though filters are typically incorporated after each differentiation, amplified noise will require dynamic filter design; conventional filter protocol incorporates identical filters with each application. Thus, for any position-versus-time data to contain some noise content increases the probability that the velocity, acceleration, and jerk profiles are also contaminated, and possibly to a greater extent, constraining their utility as measurement substrates.

### 2.2.5 Artifact associated with inappropriate task constraints

Perhaps the least recognized limitation of biomechanical analysis is the lack of robust measures that can be implemented irrespective of a subject level of abilities. For instance, the simplest measure of motor proficiency, and the easiest to implement, is a target-tracking protocol. A simple mean-square deviation of the effector of interest (here the hand, directly reflecting joint angle) from the target allows for

impairment to be calculated instantaneously from within device software, or within readily available spreadsheet packages (e.g. Microsoft Excel).

The parsimony of such a paradigm notwithstanding, this protocol is utterly insufficient for determining the true limitations of an individual with impaired motor control. By definition, a special needs population will suffer from limited range of motion, joint articulation speed, and dexterity; their movements will be spastic and uneven, and may exhibit very dynamic behaviors across their angular range due to position-dependent spasticity, or across time, owing to fatigue or compromised attention. Subjects with impaired motor control often present with associated symptoms including visual or cognitive deficit, or other co-morbidities that render target-tracking tasks, no matter how parameterized, untenable.

### 2.2.6 Artifact associated with legitimate movement phenomena

Independent of signal error associated with the hardware or software interfaces, and even in the evaluation of healthy human subjects with no known neurological impairments, noise can be introduced into the movement record that detracts from the extraction of the essential movement pattern. These spurious trajectory trace features are detected by various proficiency metrics, and reported as unsmooth behaviors, even when this implication is contradictory to the underlying assumptions. Indeed, some proportion of the motor system can be attributed directly to noise generated by the motor system.

In the context of highly stereotyped movement patterns observed at many levels of the human nervous system, it has been postulated that the neural control signals underlying arm movements are corrupted by noise whose variance increases with the size of the control signal (Harris and Wolpert 1998). This noise influences the shape of the trajectory, and is selected in order to minimize end-point variance, at

the de-emphasis of trajectory smoothness. Irrespective of the veracity of this particular claim, and the magnitude of its impact in the trajectory signal, it is understandable that in the imperfect execution of some motor task, some noise will be overlaid on any putative essential trajectory pattern, associated with spurious, transient, and spontaneous accelerations produced throughout the movement execution, and unrelated to a hypothetical motor plan.

## 2.3 Raters of kinematical proficiency

### 2.3.1 Basic kinematic parameters

#### *2.3.1.1 Positional domain*

The primary characterization of motor execution is moored in the elemental features that can be extracted from the trajectory waveform. Amplitude $\Delta\theta$, which ostensibly represents angular range of motion, unless a movement is purposefully performed at a sub-maximal range[3], and temporal duration: total time $T$, synthesize or espouse several related metrics, including average velocity $\bar{\dot{\theta}} = \frac{\Delta\theta}{T}$, angular minima and maxima (maximum joint extension, and maximum joint flexion $\theta_{\min}$ and $\theta_{\max}$, as well as time to maximum position $\tau_{\theta_{\max}}$[4].

Table 3: Basic kinematic variables of the positional domain

| Metric | Symbol | Units |
|---|---|---|
| Movement amplitude | $\Delta\theta$ | degrees |
| Total movement time | $T$ | seconds |
| Total number of samples | $N_s$ | time sample |
| Average angular velocity | $\bar{\dot{\theta}}$ | deg/second |
| Maximum elbow extension angle | $\theta_{\min}$ | degrees |
| Maximum elbow flexion angle | $\theta_{\max}$ | deg/second |
| Time to maximum elbow flexion | $\tau_{\theta_{\max}}$ | seconds, time sample, or proportion of $T$[5] |

[3] It is strictly correct to reserve the nomenclature "Range of Motion" for the total range defined by the physiological limits of joint articulation for a given individual. In this discussion, we will adopt the convention that the ROM constitutes angular minimum to angular maximum for a given motion, which will be large, but sub-maximal and comfortable.

[4] Here, we will observe the convention that all temporal landmarks will be indicated with tau $\tau$, subscripted to denote the significance of the landmark, and super-scripted to identify the domain in which this landmark is assessed.

These metrics are typically available upon inspection of the trajectory waveform, and require little processing of the movement record. Note that $N_s = T \cdot \nu$ where $\nu$ is the sampling frequency in samples per second.

### *2.3.1.2 Differentiated domains*

By differentiating the position-versus-time trace, it is possible to calculate movement parameters with greater relevance to theories of motor control. For instance, the minimum-jerk theory postulates that the velocity profiles of healthy human movement are bell-shaped and symmetric about the time to maximum velocity $\dot{\theta}_{\max}$. This is typically quantified either by the time to peak velocity $\tau_{\dot{\theta}_{\max}}$, or by the ratio of time spent in acceleration to time spent in deceleration $\Gamma^{\ddot{\theta}} = \sum_{i=1}^{N_s} \ddot{\theta}_i > 0 \Big/ \sum_{i=1}^{N_s} \ddot{\theta}_i < 0$, the so-called symmetry ratio, (Jaric, Gottlieb et al. 1998).

Table 4: Standard kinematic variables of the differentiated domain

| Metric | Symbol | Units |
|---|---|---|
| Peak angular velocity | $\dot{\theta}_{\max}$ | degrees/second |
| Peak angular acceleration | $\ddot{\theta}_{\max}$ | degrees/second$^2$ |
| Time to peak angular velocity | $\tau_{\dot{\theta}_{\max}}$ | Proportion of $T$ |
| Time to peak angular acceleration | $\tau_{\ddot{\theta}_{\max}}$ | Proportion of $T$ |

[5] All temporal landmarks will hereafter be rendered as a proportion of $T$, i.e. on unity scale, unless otherwise stated.

Velocimetric parameters, defined within the $\dot{\theta}(t)$ domain can be extended to higher differentiations including acceleration, $\ddot{\theta}(t)$, and higher derivatives (jerk, snap, etc.).

### 2.3.2 Waveform evaluation

#### *2.3.2.1 Integrated jerk*

The jerk cost function[6] is a much studied tenet of human motor control, and has been called the "distillation of its essence" (Engelbrecht 2001). That each movement performed by a healthy individual seeks to maximize trajectory smoothness as defined by the integrated squared rate of change of acceleration

$$J = \kappa \cdot \int_0^T \left| \frac{d^3}{dt^3}\theta(t) \right|^2 \cdot dt, \qquad \text{(Equation 1)}$$

[6] Though *jerk* is, by definition a vectorial quantity reflecting the rate of change of acceleration in time, this trace will not be discussed frequently here; for this reason, the short-hand of "jerk" will be applied to the integral expressed in (Equation 1), or variant thereof, and will be referenced simply by the variable *J*. When necessary, the jerk trace $J(t) = \frac{d^3}{dt^3}\theta(t)$ will be identified appropriately.

where $\kappa$ is some constant, implies a kinematic motor plan of which hand path is the primary expression. This criterion is applied to angular position data $\theta(t)$, as a primary means by which rehabilitation is monitored in a clinical setting (Rohrer, Fasoli et al. 2002; Cozens and Bhakta 2003; Chang, Wu et al. 2005; Daly, Hogan et al. 2005; Fang, Yue et al. 2007) and motor control hypotheses are validated (Atkeson and Hollerbach 1985; Flash and Henis 1991; Wolpert, Ghahramani et al. 1995; Todorov 2004), as well as in the design of haptic interfaces (Piazzi and Visioli 2000; Amirabdollahian, Loureiro et al. 2002).

Despite its simple formulation, the parametrizability of jerk, via its upper-bound of integration and normalization coefficient, as well as data trace treatment, e.g. temporal normalization, makes jerk a cumbersome metric in terms of generalizability. For instance, $\kappa$ is typically chosen to account for some variable expected to bias the jerk integral. Normalization to total movement time (Kluger, Gianutsos et al. 1997; Engelbrecht 2001; Cozens and Bhakta 2003; Yan, Rountree et al. 2008) is most common, though division by total number of degrees of freedom (Viviani and Flash 1995; Feng and Mak 1997), maximum velocity (Rohrer, Fasoli et al. 2002), or not at all (Osu, Uno et al. 1997; Todorov and Jordan 1998; Goldvasser, McGibbon et al. 2001; Amirabdollahian, Loureiro et al. 2002; Richardson and Flash 2002). The correction for movement time not sufficient to counteract the implicit devaluation of the jerk integral by movement duration $T$. Indeed, it has been shown that the optimum movement under the jerk integral is that which endures for infinite time (Hoff 1994). Normalization by sampling frequency or total movement time, cannot resolve this scaling (Engelbrecht 2001).

The incorporation of the jerk integral into subject performance evaluation has been met with some controversy, for its propensity to yield counter-intuitive or

occasionally contradictory results. For example, chronic stroke patients, undergoing therapy of the upper-limb were determined to produce significantly jerkier movements after re-training (Rohrer, Fasoli et al. 2002). This observation contradicted four other smoothness measures, suggesting a fundamental limitation of the jerk metric. Other claims have been made of jerk's inability to discriminate between cohorts (Goldvasser, McGibbon et al. 2001; Cozens and Bhakta 2003), in various upper-limb movement paradigms. Here, it is noted that in the present discussion, "jerk" refers to the integral expressed in (Equation 1), as a measure of movement smoothness. This Section should not be interpreted as a discourse on the validity or veracity of the minimum jerk hypothesis, but an exposition on this particular evaluation of movement proficiency from a formulaic standpoint.

#### *2.3.2.2 Arrest periods*

Movements performed by individuals with compromised motor control, particularly resulting from severe spasticity, are often halting, interspersed with periods of low or zero velocity. Episodic movement is typical of patients in early stages of recovery, stopping multiple times before reaching their target (O'Dwyer, Ada et al. 1996; Blakeley and Jankovic 2002). That this stop-and-go movement behavior is endemic to a large subset of individuals, suggests the importance of a measure of the degree to which a given movement is punctuated with periods of angular velocity below some threshold.

The Mean Arrest Period Ratio (MAPR) quantifies the proportion of a movement task spent below an arbitrary threshold, for example, 10% of maximum velocity:

$$MAPR = \sum_{i=1}^{N_s} \dot{\theta}_i < \delta_{\dot{\theta}} \,, \qquad \text{(Equation 2)}$$

where $\delta_{\dot{\theta}} = 0.1 \cdot \dot{\theta}_{\max}$, and has units of time (here again, proportion of total time *T* (Beppu, Suda et al. 1984). Velocity threshold $\delta_{\dot{\theta}}$ can be set with respect to the expectations of the cohort: a low threshold is suitable for healthy subjects, for example.

#### *2.3.2.3 Velocimetric peaks*

In addition to integrated metrics such as jerk and MAPR, and assessment of the area under some curve, kinematic trace tonicity can be rendered via counting metrics. Tallying the number of peaks in the velocity profile, for example, yields the number of directional changes in acceleration

$$\pi_{\dot{\theta}} = 1 + \sum \frac{d}{dt}\left(\operatorname{sgn}\left(\frac{d}{dt}\left(\dot{\theta}(t)\right)\right)\right), \qquad \text{(Equation 3)}$$

for which it is hypothesized that in typical movements performed by healthy individuals, the velocity profile is a singly-peaked trace resembling a bell curve, i.e. $\pi_{\dot{\theta}}$ = 1. The number of peaks in the velocity profile[7] has been used to quantify smoothness in healthy (Brooks, Cooke et al. 1973; Fetters and Todd 1987) and stroke patients (Rohrer, Fasoli et al. 2002; Kahn, Zygman et al. 2006); fewer peaks represent a smoother movement.

An indirect measure of jerk can be posed by assessing the ratio of the velocity trace maximum to the mean trace value:

[7] Often referred to as the "peaks metric," but this jargon is avoided in the present discourse, as we will introduced several scalars depicting peaks in various traces. Here, "peaks" is indicated by pi $\pi$, subscripted for the domain over which the peaks are being counted.

$$\rho_{\dot{\theta}} = \frac{\dot{\theta}_{\max}}{\int_T \theta(t)dt}. \qquad \text{(Equation 4)}$$

This so-called "power ratio" yields an estimate of the relative disparity between the peak velocity and average velocity, i.e. the magnitude of incidental transience associated with spontaneous accelerations, as compared to the velocity of the remainder of the movement. This ratio may not be appropriate for application to movements punctuated with prolonged arrest periods.

### 2.3.3 Miscellany

The art of feature extraction from any dataset involves a major component of creative waveform analysis. Myriad performance metrics have been proposed which variously assess some subset of peak features, which are thought to directly or indirectly report some aspect of motor proficiency. In the present discussion, attention will be focused primarily on the metrics described above, both for their simplicity, as well as their popularity amongst motor control and rehabilitation researchers. There are ample opportunities for the sufficiently ambitious analysts to develop new descriptors, both as scalars and as vectors, and indeed a small set of such novel metrics is presented in subsequent Chapters.

### 2.3.4 Metric type and commutativity

Though smoothness measures in laboratory research are typically of a quantitative nature, e.g. integrated jerk, RMS deviation for a target curve, or MAPR, these metrics may not necessarily be optimal for reporting the features of their respective substrates. For instance, jerk and RMS deviation are both subject to systematic bias due to experimental parameters (sampling frequency ν) and basic

kinematical parameters (total movement time $T$ or angular range $\Delta\theta$). Thus, the validity of these metrics extends only within a given protocol, and their cross-comparison to other protocols is meaningless. In this way, an ordinal measure, i.e. of a given trace having the maximally smooth or having a sub-maximal smoothness, may be preferred. In other situations, a categorical variable, placing a given movement cycle in one of several different categories may be the most informative means of taxonomy. This paradigm, along with the subset of categorizations restricted to binary classification ("on" or "off," "diseased" versus "healthy," etc.) is generally a *pattern recognition* problem.

### 2.3.5 Vectorial versus scalar metrics: local versus global analysis

Lastly, it is proposed that for some research questions, a scalar smoothness rater is insufficient for a complete and meaningful assessment of motor proficiency. All of the measures described to this point have predicated on a mathematical operation applied to excursion trace or some equivalent transformation, yielding a single scalar metric. While scalars are convenient for interpretability, and amenable to traditional statistical analyses, there is often need to resolve motor proficiency as a function of time or angle, i.e. to retain the measure as a function of some independent variable. In this way, it is proposed that vectorial smoothness measures may provide crucial insight into the nature (location and magnitude) of the limitations of an individual's neuromotor system.

## 2.4 Summary

Kinematic data constitutes the primary variable incorporated into basic research of the human motor system, and serves as the substrate of evaluation in clinical applications. These data, however, typically contain noise not associated with

the motor plan, and whose source is rarely understood. The metrics used to evaluate these traces are not universally accepted, limited in scope, and may not generalize across protocols. Further, these metrics are scalar when a vectorial rendering may be more appropriate, quantitative when a categorical or ordinal variable would be more informative, and may themselves be prone to amplifying signal artifact.

Whereas abstractions of human movement are often formulated in terms of smoothness metrics, and subsequently used to assess the veracity of models of motor control, it is the burden of biomechanists to first demonstrate the validity of these parameters as fiduciary indices of motor output.

# 3 EXTRACTING THE TRAJECTORY ESSENCE

## 3.1 Introduction

The collection of kinematic data presents occasion for contamination of empirical data by noise unrelated to the true variable of interest. Research activities in which the trajectory curve is evaluated by some waveform operation, are subject to bias in the presence of trace artifact. For instance, even low amplitude transient accelerations in the flexion-versus-time record can greatly increase the peak content in the thrice-differentiated position-versus-time curve (jerk); this artifact skews all related metrics and invalidates hypothesis tests related to the adherence to a minimum-jerk trajectory. The incorporation of the kinematical data into basic research into human motor control, and characterization of motor deficiency in impaired subjects, evidences the importance of ensuring that the analysis of the trajectory waveform, and indeed the trace itself, is free from artifact. Here, the single-joint trajectory will be discussed in terms of its shape, i.e. the evolution of joint angle in time, and the extraction of the trajectory *essence* without undue alteration from empirical *incidence*.

## 3.2 SJT Shape: Theory and observation

### 3.2.1 Physiology, task variables co-determine trajectory shape

#### *3.2.1.1 Agonist-antagonist activity*

That the kinematic trace has utility as a proxy to neuromuscular activity within the motor hierarchy has been demonstrated in the high correlation between electromyographic signs of antagonist activation and kinetic parameters of movement (torque and velocimetric aspects of the movement) in a variety of conditions (Bouisset

and Goubel 1973; Gottlieb, Corcos et al. 1989; Gottlieb, Latash et al. 1992). Features of the agonist bursts, as detected by EMG, co-vary with the torque required to decelerate the limb (Gottlieb, Latash et al. 1992); increased agonist activity correlate with movement speed (Corcos, Gottlieb et al. 1989; Hoffman and Strick 1990), and possibly movement distance and peak acceleration c.f. (Marsden, Obeso et al. 1983; Mustard and Lee 1987; Gottlieb, Corcos et al. 1989; Hoffman and Strick 1990). Indeed, SJTs reflect a complex interaction of several interdependent variables related to the movement task and the underlying physiology.

Angular velocity of the hand about the elbow can be expressed as a second order linear differential equation reflecting the sum of torques generated by the flexor and extensor muscles

$$I\frac{d^2\theta}{dt^2} + B\frac{d\theta}{dt} = \sum T$$

where $I$ is the moment of inertia, $B$ is the coefficient of viscosity, and $T$ is the net muscle torque (Lemay and Crago 1996). Net torque about a joint is the resultant of torque by the flexor and extensor muscles. The torque exerted by a single muscle group $T_m$ can be expressed as

$$T_m = F_m d_m - \eta\frac{d\theta}{dt} - k\left(\theta - \theta_{eq}\right)$$

where $F_m$ is the active force produced by the muscle, $d_{\mathrm{m}}$ is the effective moment arm, $\eta$ is viscosity, $K$ is the elastic stiffness, and $\theta_{\mathrm{eq}}$ is the equilibrium joint angle.

Posture and movement control are facilitated by both viscoelastic properties of muscle and muscle activation (van Soest and Bobbert 1993; Milner 2002). Torque

production results from neuromuscular activation of the agonist-antagonist pair: biceps and triceps, or triceps and biceps in flexion, or extension. Electromyographic measurement of muscular activity is deterministic (Prasad, Wasson et al. 1984; Yang and Zhao 1998; Lei, Wang et al. 2001), however, the activations themselves in terms of the time of onset, duration, and magnitude, are formed by a non-linear combination of multiple sources, reflect stochastic processes (Tian and He 2003; Pohlmeyer, Solla et al. 2007).

#### *3.2.1.2 Stretch reflex and velocity*

Torque is a linear function of stiffness $K$, a 1st-order LDE (linear in activation $a$) with dependence on motor neuron pool input $u$:

$$K = f\left(a(t), u(t), \cdots\right).$$

which is scaled by stretch reflex, a function with dependence on muscle length $L$, velocity $\dot{L}_i$, and several physiologic constants

$$\text{stretch reflex} = f\left(L_i, \dot{L}_i, \cdots\right),$$

$L$ is reflexively determined by the angle spanned by the muscle across the joint, regulating the stretch reflex in a step-wise or zone-like fashion (Lemay and Crago 1996; Levin and Dimov 1997).

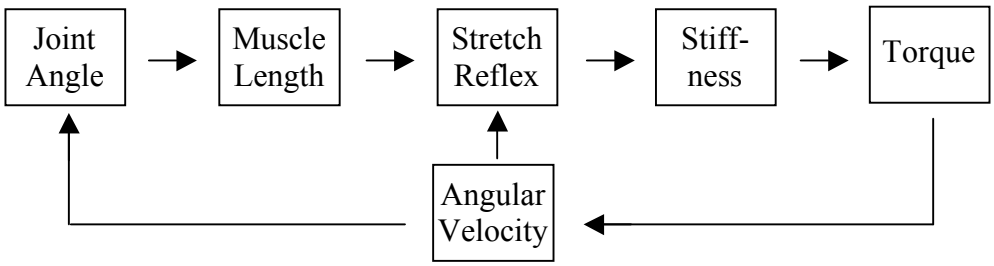


Flowchart 0 Factors influencing trajectory shape. Simplified, control-free model.

Task variables, and parameters of the skeletal muscles co-determine performance variables. For instance movement symmetry changes with peripheral factors such as different inertial loads, movement distances, or under certain instruction (Nagasaki 1989; Jaric, Gottlieb et al. 1998; Jaric, Milanovic et al. 1999), either due to the role of damping forces, central control patterns, or both (Jaric, Blesic et al. 1999).

### 3.2.2 Prediction of SJT shape from neuromotor control principles

#### *3.2.2.1 Minimum jerk velocity*

The jerk minimization theory poses that the motor system seeks to move with a maximally smooth motion according to the reduction of jerk as measured by some metric of the differentiation of acceleration in time. Suppose that for a given motion $\vec{r}(t)$, it is determined that its sixth derivative is equal to 0[8]. Thus

[8] This supposition is based on the original derivation submitted by Hogan (1984): The objective function $C = \int_0^d \gamma^2/2 \, dt$ is minimized as a function of state and input variables $\dot{\theta} = \omega$, $\dot{\omega} = \frac{K}{I}\theta_0 - \frac{K}{I}\theta - \frac{B}{I}\omega$ and $\gamma = \frac{K}{I}U - \frac{K}{I}\omega - \frac{K}{I}\dot{\omega}$. Taking the Hamiltonian of this system and minimizing with respect to control $U$, we generate a set of three co-state equations in $\lambda$, which form a six-equation set of linear differential equations solving $\dot{\theta}$, $\dot{\omega}$, $\dot{\theta}_0$, $\dot{\lambda}_1$, $\dot{\lambda}_2$, and $\dot{\lambda}_3$, where the characteristic polynomial is a sixth-order Laplacian (=0), yielding six eigenvalues, identically 0, and a

$$\vec{r}(t) = \frac{K}{5!}t^5 + \frac{L}{4!}t^4 + \frac{M}{3!}t^3 + \frac{N}{2!}t^2 + \frac{P}{1!}t + Q\,.$$

Substituting $A \to F$ for these coefficients, we impose the following boundary conditions

$$\begin{cases} \vec{r}(0) = 0 & \vec{r}(T) = \Delta \\ \dot{\vec{r}}(0) = 0 & \dot{\vec{r}}(T) = 0 \\ \ddot{\vec{r}}(0) = 0 & \ddot{\vec{r}}(T) = 0 \end{cases}.$$

where $\Delta$ is the total range of motion, yielding

$$\vec{r}(t) = At^5 + Bt^4 + Ct^3 + Dt^2 + Et + F\,.$$

where

$$\vec{r}(0) = A(0)^5 + B(0)^4 + C(0)^3 + D(0)^2 + E(0)^1 + F \to F = 0\,,$$

$$\dot{\vec{r}}(0) = A(0)^4 + B(0)^3 + C(0)^2 + D(0)^1 + E \to E = 0\,,$$

and

$$\ddot{\vec{r}}(0) = A(0)^3 + B(0)^2 + C(0)^1 + D \to D = 0\,.$$

Three boundary conditions remain to solve $\vec{r}(t) = At^5 + Bt^4 + Ct^3$. Setting up a system of equations differentiated as above, we get the following matrix problem:

---

fifth-order position trajectory given by $\theta(t) = b_0 + b_1 t + b_2 t^2 + b_3 t^3 + b_4 t^4 + b_5 t^5$. Euler-Poisson equation.

$$\begin{bmatrix} 5T^4 & 4T^3 & 3T^2 \\ 20T^3 & 12T^2 & 6T \\ T^5 & T^4 & T^3 \end{bmatrix} \cdot \begin{bmatrix} A \\ B \\ C \end{bmatrix} = \begin{bmatrix} 0 \\ 0 \\ \Delta \end{bmatrix}.$$

Performing some elementary row-reductions, we get the following in echelon form

$$\begin{bmatrix} T^2 & 0 & 0 \\ 2T^2 & 1 & 0 \\ T^2 & 1 & 1 \end{bmatrix} \cdot \begin{bmatrix} A \\ B \\ C \end{bmatrix} = \begin{bmatrix} \frac{6\Delta}{T^3} \\ \frac{-3\Delta}{T^3} \\ \frac{\Delta}{T^3} \end{bmatrix},$$

yielding the following:

$$A = 6\tfrac{\Delta}{T^5} \quad B = -15\tfrac{\Delta}{T^4} \quad C = 10\tfrac{\Delta}{T^3}.$$

Thus the positional vector which satisfies the jerk minimization criteria is as

$$\vec{r}(t) = 6\tfrac{\Delta}{T^5}t^5 - 15\tfrac{\Delta}{T^4}t^4 + 10\tfrac{\Delta}{T^3}t^3.$$

Differentiating once with respect to time, we generate the minimum jerk velocity $v_{\text{mj}}$

$$v_{mj} = \frac{\Delta}{T}\left(\frac{30t^4}{T^4} - \frac{60t^3}{T^3} + \frac{30t^2}{T^2}\right). \qquad \text{(Equation 5)}$$

From this bell-shaped velocity profile, a cumulative summation (effective integration), yielding degree of flexion in time, yields a sigmoidal plot analogous to the cumulative integration of the probability density function: the cumulative density

function. Invoking another analogue, that of the half-period sinusoid, it is proposed herein that by the small angle approximation $\lim_{\theta \to 0} \sin\theta = \theta$, the medial angles of flexion are transcribed at approximately constant velocity, i.e. plotting a linear trajectory (Figure 3).

Depending on the steepness and symmetry of the actual velocity plot, the linear regional trajectory may shift or occur over longer or shorter range of motion.

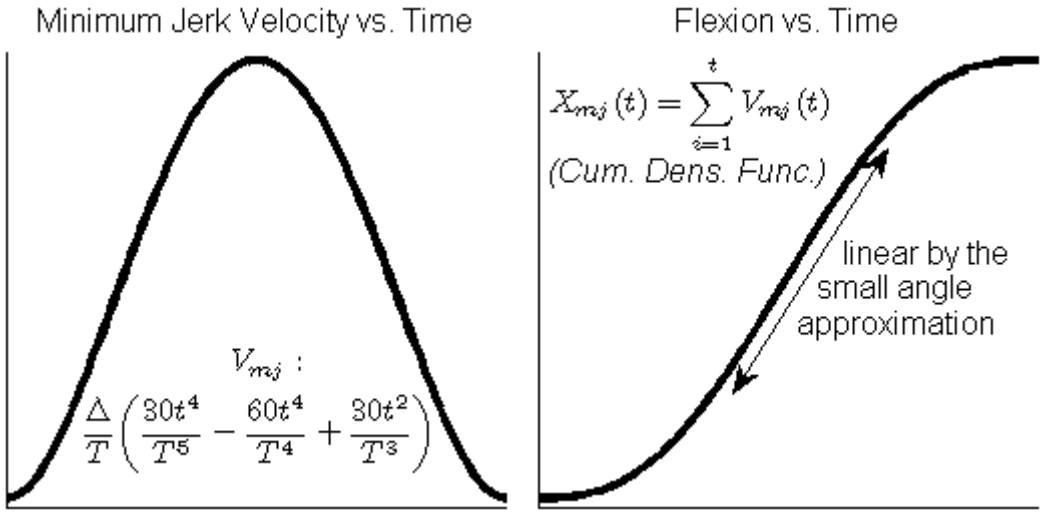


Figure 3 Prediction of Linear Trajectory by $v_{mj}$: The minimum jerk velocity plots a bell-shaped profile.

### *3.2.2.2 Two-thirds power law*

It was shown that within a singular motion segment, regions of constant curvature are transcribed with constant angular velocity: two-thirds power law (Viviani and Terzuolo 1982; Lacquaniti, Terzuolo et al. 1983). The two-thirds power

law relates the radius of curvature $R$ at any point $s$ along the trajectory with the corresponding tangential velocity

$$v(s) = K(s) \cdot \left( \frac{R(s)}{1 + \alpha \cdot R(s)} \right)^{\beta}, \qquad \text{(Equation 6)}$$

where $\beta \approx 0.33$ and $0 \leq \alpha \leq 1$. Though originally formulated for multi-DOF movement tasks, this relationship has been demonstrated in several paradigms that espouse some or all of the experimental protocol utilized here: planar movements where the trajectory has no points of inflection (i.e. a single movement segment) (Viviani and Schneider 1991) and movements under mechanical constraint (Viviani and Terzuolo 1982).

### 3.2.3 Evidence of symmetric, approximately linear SJTs

Single joint pointing movements are observed to transcribe bell-shaped velocity profiles with symmetric trajectory traces (Jaric, Blesic et al. 1999), having an approximately linear or gently curved (sigmoidal) morphology. This feature of motor behavior is abstracted as an invariant property of human motion, particularly under "low spatiotemporal accuracy requirements" (Atkeson and Hollerbach 1985). Figure 4 shows several examples of single-joint trajectories extracted from the relevant literature. Each trajectory (or ensemble) reflects an approximately symmetrical trajectory with a linear middle region, suggesting an either linear or sigmoidal trajectory curve.

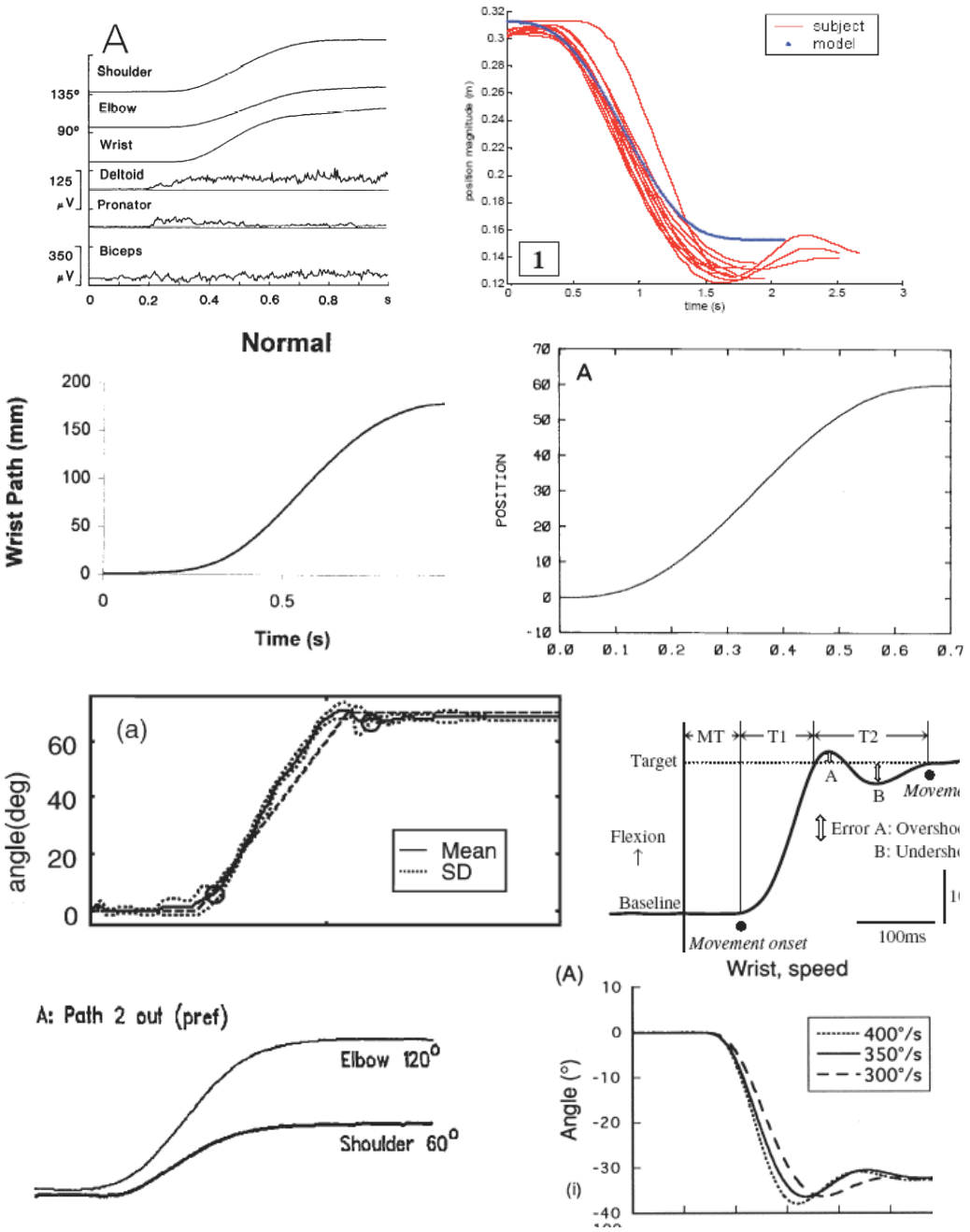


Figure 4 Observations of symmetrical trajectories (Lacquaniti, Terzuolo et al. 1983; Hogan 1984; Flanagan and Ostry 1990; Feng and Mak 1997; Pfann, Hoffman et al. 1998; Amirabdollahian, Loureiro et al. 2002; Ju, Lin et al. 2002; Liang, Yamashita et al. 2008).

Though kinematic plots reveal considerable information regarding the specific shape of single-joint trajectories, their actual shape, and the variability of this shape from motion-to-motion and from person-to-person has not been rigorously determined. What is the baseline kinematic behavior of a healthy individual, in autonomous reaching tasks, and how does this vary within and between persons? Moreover, is it possible to extract the basic pattern of a given record of single-joint motion, however noisy, and perform analyses of an individual's essential motor behavior free of signal artifact?

## 3.3 SJT approximation by analytical functions

### 3.3.1 Need for suitable substrates in biomechanical analysis

For situations where precise measurement of kinematical variables or keen representation of the global trends in movement is essential, trace noise may alter the SJT in such a way that it is no longer a tenable substrate for evaluation. Consider the following example. Let $y$ be an ideal sigmoid, created by a standard trigonometric function acting over the interval $-\frac{\pi}{2} \le t \le \frac{\pi}{2}$:

$$y = \sin(t) .$$

The "position versus time" graph of $y$ looks similar to that of the SJT traces found in the literature, and has a symmetric, bell-shaped velocity profile (Figure 5a). By doubly differentiating the velocity trace, the jerk curve is generated, and the jerk integral reads a value of approximately 0.01.

Now, very small amplitude noise is added by imposing

$$y' = y + t \cdot e^{-k \cdot \left(\left[-\frac{\pi}{2}+\frac{\pi}{4}\right]-t\right)^3} .$$

where $k = 1 \times 10^5$, manually set to minimally distort the simulated trajectory trace (Figure 5d).

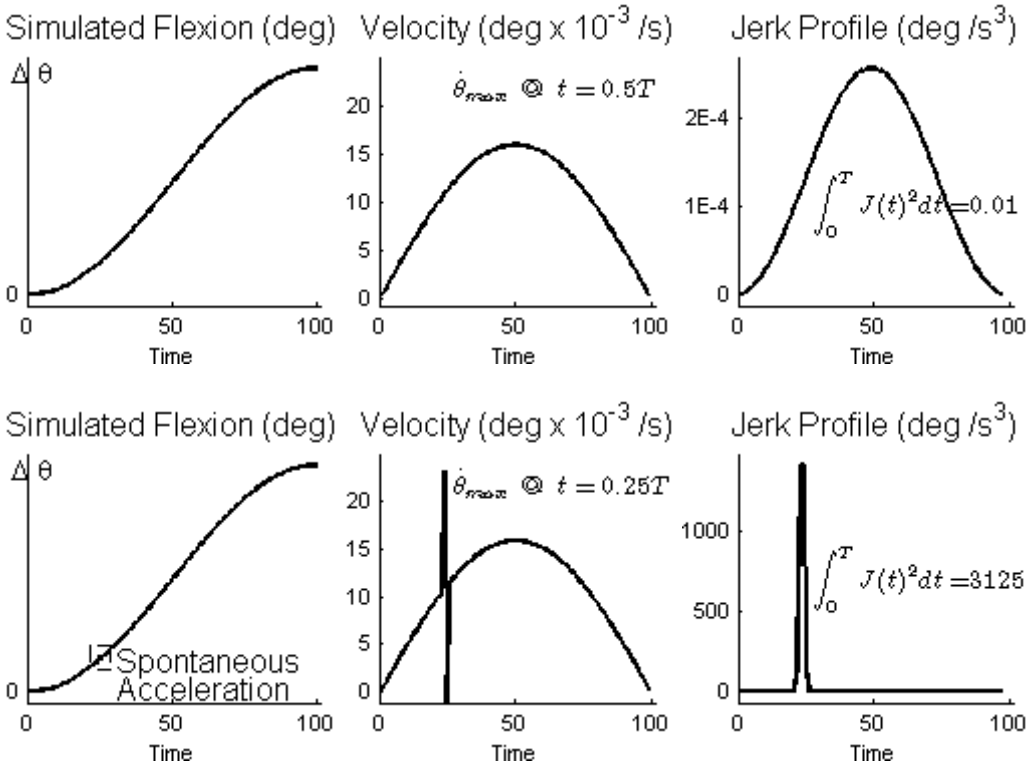


Figure 5 Contamination of kinematic data by noise.

The velocity trace $\frac{d}{dt}y'$ features a large peak at $t = 0.25 \cdot T = -\frac{\pi}{4}$, which is amplified in subsequent differentiations. The large area under the $J(t) = \frac{d^3}{dt^3}y'$ peak greatly increases the jerk integral (Figure 5f). Despite the relative insignificance of this transient disturbance in the position domain, the distortion of the jerk profile

invalidates its use in situations where even modest noise component may persist in the kinematical record.

In this way, it is possible for the *incidence* of movement to obscure the movement *essence*. It is suggested that a curve-matched trajectory surrogate, based on a simple analytical function, would provide a noise-free SJT approximation upon which hypotheses of motor control could be tested in the absence of contamination from incidental noise.

### 3.3.2 Incorporation of analytical functions into biomechanics

Mathematical models form the basis of forward dynamic simulations and performance criterion in a wide range of motor research and rehabilitation settings, and for many of these applications, analytical functions are ideal for their parametrizability. Velocimetric data is frequently modeled as a bell-shaped, i.e., Gaussian or Hanning function (Camilleri, Hull et al. 2007); periodic positional data is typically abstracted as a sigmoid or sinusoid (Hollerbach 1981; Soechting, Lacquaniti et al. 1986; Soechting and Terzuolo 1986); and geometric models such as square waves, triangular windows, and straight-lines are applied to rapid motion, impulse-data, and segmented motion (via the two-thirds power law) (Viviani and Terzuolo 1982; Viviani and Flash 1995; Camilleri, Hull et al. 2007) (Figure 6).

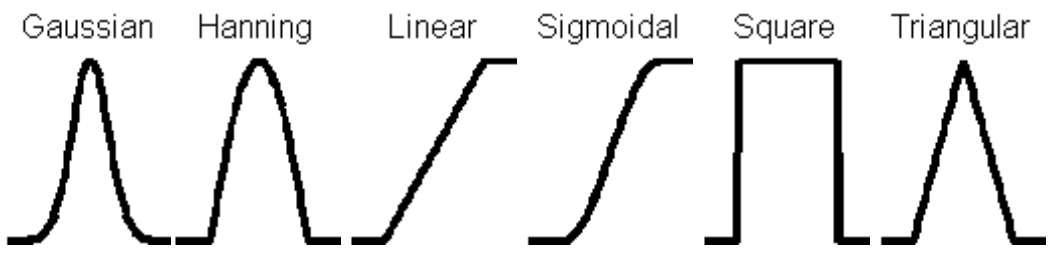


Figure 6 Sample analytical models found in kinematic literature.

Of course, whereas many of these models are devices of mathematical convenience, as opposed to physiological significance per se, their utility as an approximation cannot be underestimated in comparative studies as a basis for understanding the difference between health and disease (Wann, Nimmo-Smith et al. 1988).

## 3.4 Method overview: Simulation of SJTs

### 3.4.1 Designing appropriate models for the angular trajectory

In order to capture the essential pattern of angular trajectories recorded from healthy subjects in the MAST, six basic (archetypal) analytical curves are proposed, designed to simulate a range of features observed in a simple point-to-point reaching motion across the joint range of motion (Figure 7).


Figure 7 Archetypal model curves. Basic trajectory model curves (angle of flexion vs. time) modeled against observed motions. + = acceleration, ++ = relatively swift acceleration; — = deceleration, —— = relatively swift deceleration; 0 = abrupt change in velocity.

Whereas there are infinitely many ways by which to model the $\theta(t)$ curve of a simple flexion task (Harris and Wolpert 1998), it is argued here that six curves are sufficient to "span the space" of angular trajectory behaviors. Symmetric trajectories (Linear and Sigmoidal, A and B) depict nearly instantaneous and moderate accelerative and declarative behaviors, respectively, of approximately equal

magnitude. Quasi-Convex models (C) simulate moderate acceleration and swift deceleration; Quasi-Concave (D), the opposite. Sigmo-convex and concave models (E and F) depict alternately gentle and moderate accelerative/decelerative behaviors (Table 5).

Table 5: Analytical models for trajectory curve matching

| Model Type | | Description | Velocity Profile |
|---|---|---|---|
| A | Linear | Total isogony, negligible | Square wave |
| B | Sigmoidal | Medial isogony, symmetric and | Bell curve |
| C | Quasi-Concave | Distal isogony, reduced speed | Monotonically |
| D | Quasi-Convex | Proximal isogony, reduced speed | Monotonically |
| E | Sigmo-Concave | Comparatively slower distal | Positive skew bell |
| F | Sigmo-Convex | Comparatively slower proximal | Negative skew bell |

### 3.4.2 Global SJT model fitting by parameterization

In order to generate the optimal fit to the SJT within each model curve, two primary parameters must be considered: average movement speed and time of maximum velocity, $\boldsymbol{\tau}_{\max}^{\dot{\theta}}$. By presuming a symmetric velocity profile (see Chapter 2), the time to maximum velocity can be considered the equivalent to a benchmark of excursion beyond some minimum velocity.

Whereas the vast majority of the movement will be modeled by the idealized waveform (Table 5), any period of relative inactivity preceding this motion will be simulated as a rest interval by a pad *p* of zero-velocity content. The movement cycle,

defined from $t = 0$ to some time $T$, will thus contain two such rests, offsetting the majority of the simulated movement, lasting some time $l < T$, starting at $p > 0$ (Figure 6).

For some basic curve $b_{\chi=\mathrm{A..F}}$, we construct a baseline-padded curve $B_\chi$

$$B_{iX}(l,p) = \begin{Bmatrix} \theta_{on} & 0 \le i < p \\ \theta_{on} + \theta_{ROM} \cdot b_{iX}(l,p) & p \le i \le p+l \\ \theta_{off} & p+l < i < T \end{Bmatrix}_{\substack{p=0:T-l \\ l=5:T-1}}, \qquad \text{(Equation 7)}$$

is created, where $l \geq 5$ for the reason that a minimum of 5 points are necessary to construct a complete set of uniquely composed model vectors. $B_{i,\chi}$ is the basic curve $b_\chi$ of length $l$, pre-padded with $p$ time points of the angle of motion onset and appended with $T - (p + l)$ time points of the angle of motion cessation.

The analytical curves $b_{i,\chi}$ are given by

$$b_{i,X=A\cdots F}(l,p) = \begin{Bmatrix} \left(\frac{i-p}{l}\right) & A \\ \frac{1}{2}\cdot\left[1+\sin\left(\frac{i-p}{l}\pi - \frac{\pi}{2}\right)\right] & B \\ \left(\frac{i-p}{l}\right)^2 & C \\ \left[1-\left(\frac{i-p}{l}\right)^2\right] & D \\ \left(\frac{i-p}{l}\right)^{\frac{1}{2}} & E \\ \exp\left(-\left[\pi\left(\frac{i-p}{l}-1\right)\right]^2\right) & F \end{Bmatrix}_{\substack{p=0:T-l \\ l=5:T-1}} . \qquad \text{(Equation 8)}$$

Increasing the pre-pad value $p$ to accommodate all possible departure times, and decreasing the simulated motion length $l$ allows for an exhaustive modeling of all

possible average velocities of a movement starting at any time within the window of the repetition's definition (

Figure **8**).

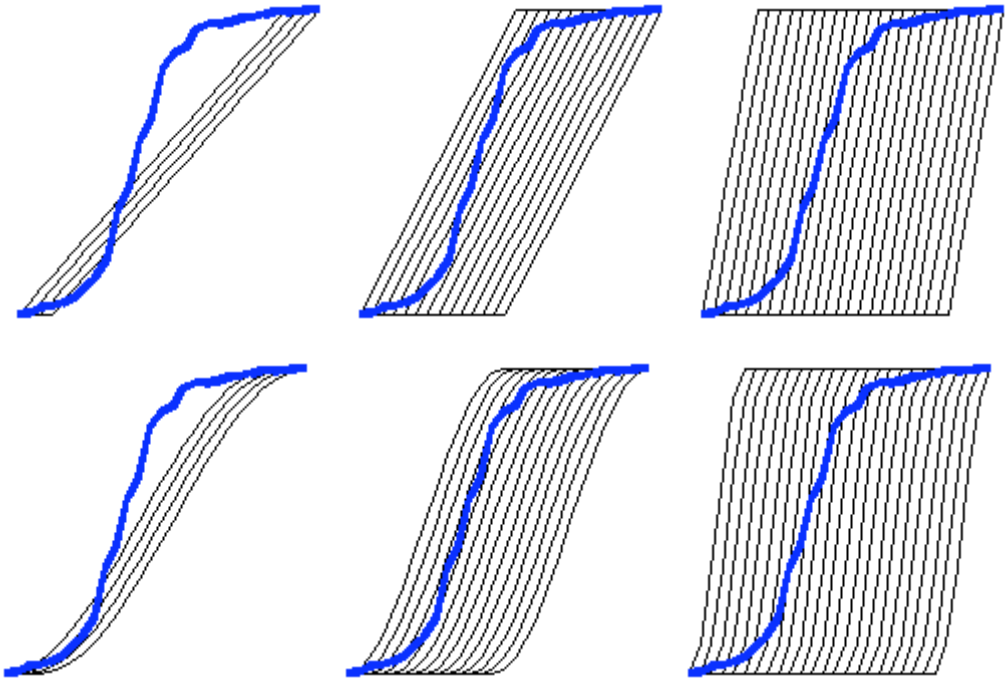

Figure 8 Snapshots of the iterative pseudo-convolution across the observed trajectory: Line (*Top*) and Sigmoid (*Bottom*).

Thus, the model universe comprises three parameters: average velocity, represented by time-in-motion, the length $l$ of the basic model curve; time of peak velocity, the equivalent of positive velocity start time, following a pad $p$ of rest, under the presumption of symmetric velocity; and model class $\chi$.

### 3.4.3 Extraction of the Essential trajectory (ET)

Among the paradigms by which the model curves $B$ could be evaluated for similitude to the observed trace $\theta$, the residual sum-of-squares was selected by convention. For each ordered pair of ($l$, $p$), model $\chi$ is compared against the recorded motion in a mean-squares way

$$\underset{l,\,p}{\arg\min} \sum_{i=1}^{T} \left(B_{i,\chi}(l,p) - \theta_i\right)^2 . \qquad \text{(Equation 9)}$$

By extension, from the global minimization over the entire model space, we define the *Essential Trajectory* (*ET*) as the single curve parameterized to best-match the observed trace over model type $\chi$, movement duration $l$, and movement start time $p$ :

$$ET = B_{\chi}(l,p) \quad \ni' \quad \underset{\chi,l,\,p}{\arg\min} \sum_{i=1}^{T} \left(B_{i,\chi}(l,p) - \theta_i\right)^2 . \qquad \text{(Equation 10)}$$

By virtue of approximation error minimization, the Essential Trajectory is the best idealized representation of the actual trajectory record, comprising a parameterized noise-free surrogate of the potentially noisy kinematical trace:

| | |
|---|---|
| *The Essential Trajectory (*ET*) is the single baseline padded model curve B which best approximated the observed kinematical trace θ. The* ET *is inherently noise-free and thus a preferable substrate for certain analyses.* | (Definition 1) *Essential Trajectory (ET)* |

It is proposed that from these well-conditioned waveforms, it will be possible to use highly sensitive functional operations, e.g. jerk, to ascertain the essential movement behaviors otherwise obscured by noise in the empirical data.

## 3.5 Analysis and discussion of ET curves

### 3.5.1 Model assumptions

Model construction is at its essence an optimization problem. Indeed, the primary criterion for model assessment presents an error minimization (Equation 10). Furthermore, it is imperative to minimize not only the number of model parameters required to synthesize the dataset to a given level of accuracy, but to place the model under the minimum number of assumptions. Here, two assumptions are made: 1) excursion is a monotonic process, and 2) the first time derivative of position is at most a unimodal process. These assumptions are fitting with the widely accepted generalizations of the SJT as a smooth trace, with a bell-shaped velocity profile. In fact, the incorporation of asymmetric velocity profiles (model classes $\chi$ = C, D, E, and F) account for the deviation of actual SJTs from this presumptive trajectory.

It is noted that three of the model curve types (Linear, Quasi-Concave, and Quasi-Convex; A, C, and D) simulate a step change in velocity either at the onset or cessation of excursion, or both. In terms of observable motion, this is physically meaningless and implies an infinite jerk cost; thus, these are seemingly untenable choices for forward-dynamic simulation. Two caveats contradict this conclusion: 1) in all cases, data is of a discrete nature, so at all time points, the velocity is literally step-wise posed, and 2) as with the processing of all kinematic data, filters can be applied either to the model itself, and following a large set of transformations applicable to the SJT downstream analysis, including all time derivatives.

In order to fully characterize the jerk profile of model curves as a function of model type $\chi$, a separate simulation was performed on a set of these curves.

### 3.5.2 Trajectory-matching model in jerk analysis: limitations

#### *3.5.2.1 Choosing a model set*

A fundamental consideration in the approximation of a trajectory curve by a series of analytical curves is the model set membership. Principally, any model must comprise a sufficiently replete set of basic curves to describe a large majority of the various species encountered within the dataset. If it should be determined that there exist some trajectory traces that are not adequately modeled by any of the archetypal curves, then it would be necessary to inject additional models. Model set expansion cannot continue *ad libitum*, however: haphazard model infusion creates a risk of fitting unimportant trajectory features, promoting their importance, and detracting from their "true essence." A direct analogy is that of over-fitting in cluster analysis, wherein boundaries are drawn around noise, skewing the bias-variance tradeoff, and destabilizing the discriminant (Hastie, Tibshirani et al. 2001). Care must be taken in choosing the appropriate type and number of models.

#### *3.5.2.2 Specific models chosen to represent angular trajectories*

As shown in Figure 4, angular trajectories assume a variety of shapes, including those with comparatively swift accelerations. In order to simulate the basic trends in acceleration thought to underlie most SJTs, six curves are chosen, simulating three levels of acceleration and deceleration in tandem: gradual (++/- -), moderate (+, -), and extreme (0) (Figure 7, Table 5). Of course, any analytical curve can be used, according to the nature of the task, and the tolerances in computation time and model complexity. However, the six curves used here were used for their ability to simulate simple global trends in trajectory formation, and their parameterization by only 2 variables. Polynomial curves, in particular, were avoided for their tendency to over-fit,

and for the linear increase in parameter set cardinality with increasing polynomial order[9].

### 3.5.3 Trajectory-matching model in jerk analysis: utility

#### *3.5.3.1 Forward- and backward-testing of the two-thirds power law*

In many fine motor tasks, the two-thirds power law predicts approximately linear trajectories within movement segments. Categorical assignment of a trajectory as having a predominantly linear morphology, from among a set of various canonical forms, permits a stringent examination of this relationship in broader circumstances. Conversely, by invoking the two-thirds power law in activities known to demonstrate this relationship, a backward test of the positional record may be made: portions of the movement matching best to a non-linear approximant would indicate multiple movement segments.

#### *3.5.3.2 Assessing hand path for adherence to jerk cost minimization*

The implications of this simulation are that for a given motion, the trajectory may be matched against a series of basic analytical curves, yielding a set of best-fit model curves (one for each curve class). From these, it can be determined immediately whether the path chosen was the minimally jerky path, as defined by the set of model curves. The hypothesis of tendency toward a minimally jerky movement can be tested directly, without contamination by error in the measurement, or the movement itself; model results yield categorical, as opposed to a quantitative variable. Whereas jerk calculation of a trajectory substrate yields a single scalar, the result can only be used for relative comparisons; no absolute information is gained with respect

[9] Most computational software packages, including Matlab, have a very efficient polynomial curve-matching routine, which would almost certainly out-perform the nested for-loop calculations required of the six models used here. However, the curve-padding paradigm would not be feasible with polynomial fits, and thus would make comparisons amongst curve classes laborious at minimum.

to the minimization of jerk. However, by defining a set of model curves with correspondence to meaningful trajectory parameters, a standard classification-by-error minimization forces a categorization of a motion as either the path with the minimum jerk, or some jerk score greater than the minimum jerk.

#### *3.5.3.3 Generalizability of curve-matching model*

The attractiveness of most modeling paradigms is contingent on the simplicity and fidelity of the model to its analogue in the kinematical record. The simplistic formulation of the present set of model curves (Equation 8), and the apparent morphological similarity to the expected trajectory record (forecasted in Figure 4) is suggestive of the power of a small set of simple analytical traces to reproduce a wide variety of SJT traces.

Though formulated in one dimension, for the purpose of illustrating application to historical problems in motor research, matching of the hand path can is readily generalized to higher dimensions. Many curves can be modeled as an analytical function, with some intuition of the underlying processes or of the nature of the curve itself. This has been done in the Rehab Lab and in the literature for a variety of phenomenon, not limited to biomechanics.

## 3.6 Summary

Empirical observation of the movement of the hand through space is a crucial activity in the research of human motor control and neuromotor dysfunction. However, the SJT is a mosaic of physiological processes, distorted by the compartments of the data acquisition process, thusly rendered as an inherently noisy trace. The subsequent subjectivity of this substrate to interpretation by metrics which many exhibit a large sensitivity to noise, suggests the need for a model-based method by which the

*essential* movement pattern is extracted without contamination from the movement *incidence*. Here, a method is proposed for extracting the *Essential Trajectory* based on a set of 6 basic trajectory behaviors, based on minimal assumptions, and parameterized to match average movement speed and time of maximum velocity. From this model, a single noise-free trajectory approximant results, upon which analyses of motor activity can be performed without contamination.

# 4 VALIDATION OF THE ESSENTIAL TRAJECTORY

## 4.1 Introduction

The evolution of elbow angle in time, the single-joint trajectory (SJT), is an essential measurement from which motor proficiency is assessed, and by which basic research into the human motor system is performed. The trajectory record, however, is highly prone to error both in the acquisition and processing of joint angular data, compromising the reliability of scalar metrics derived from these noisy substrates. In (Chapter 3), a method was proposed for the approximation of the SJT as a set of six idealized functions based on a pseudo-convolution search scheme with minimal assumptions.

Here the *essential trajectory* (ET) was extracted from raw trajectories recorded from healthy subjects performing discrete flexions of the elbow. ET traces were analyzed for the goodness-of-fit to the actual trajectory $\theta$, and features of each trace (ET versus $\theta$) will be analyzed for trace pairs. Also, the notion of a symmetric singly-peaked velocity profile will be directly tested.

## 4.2 Experimental hypotheses

Here, a method is proposed for the reconstruction of potentially noisy SJTs via noise-free Essential Trajectory surrogates. The present investigation sets out to demonstrate the validity of this trajectory approximation method.

*The single-joint trajectory can be accurately reconstructed by a parameterized analytic curve selected from among a small set of model traces, the so-called Essential Trajectory.* (Hypothesis 1)

Furthermore, it is hypothesized that important features of the SJT, related to the veridical, essential motor behavior, and not associated with noise in the movement record, can be extracted from the ET approximants.

> *Features extracted from the Essential Trajectory will report information relevant to the observed movement with an accuracy that is competes with or exceeds those extracted from the observed single-joint trajectory.* (Hypothesis 2)

Here the accuracy of reconstruction will be assessed via the coefficient of determination, comparing the SJT to its corresponding ET. Parameters related to peak velocity and other measures of symmetry will be assessed objectively on the level of cohort analysis, as well as on a trace-by-trace basis.

## 4.3 Experimental methods

### 4.3.1 Subjects and protocol

Forty-one healthy individuals with no known neurological impairments voluntarily participated in this study, and were observed in a single session typically lasting less than 30 minutes. A subgroup of 17 subjects was observed on multiple occasions, with visits separated by at least 24 hours (Table 6). All subjects gave informed consent based on the procedures approved by the IRB of Rutgers (Section 1.2.1).

Subjects were seated in the MAST, and instructed to flex and extend about the elbow across their "comfortable range of motion" in such a way that "maximized smoothness." Instantaneous visual feedback of joint angle, as well as a recent-history buffer of approximately 2 seconds, were provided by a real-time updating GUI appearing on a computer monitor, though subjects were not instructed to attend to this information. Pace was self-selected.

| Table 6: Demography of healthy subjects: Trajectory modeling | | |
|---|---|---|
| | Group | Multiple visits |
| Number of Subjects | 41 | 17 |
| Age (μ ± σ)<br>Range (min/max) | 36 ± 16<br>20/68 | 27 ± 9<br>20/59 |
| Gender (M/F) | 21/20 | 14/3 |
| Side of affect (R/L) | 35/6 | 15/2 |
| Number of visits (μ ± σ)<br>Range (min/max) | 3.4 ± 4.1<br>1/17 | 6.8 ± 4.7<br>2/17 |
| μ = Mean, σ = Standard deviation, min = Minimum, max = Maximum, M = Male, F = Female, R = Right, L = Left. | | |

### 4.3.2 Signal processing and curve matching

Single column vector data tracks were imported as raw elbow angular data, smoothed with a low-pass Butterworth's filter (2nd-order, 12 Hz cutoff), and divided into single cycles of flexion-and-extension, i.e. departure and return to maximal extension (elbow angle ~0°), automatically by a thresholded local minima.

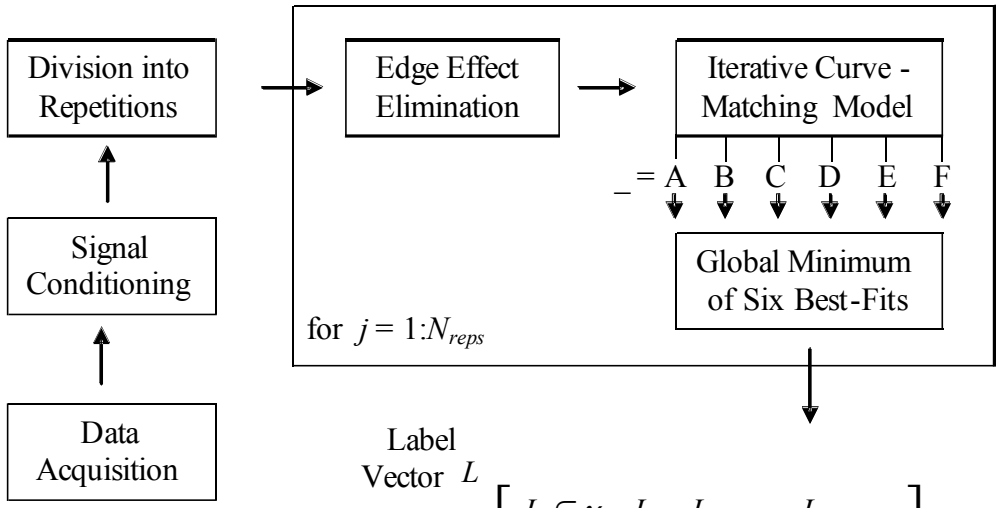


Flowchart 1 Iterative curve-matching protocol. A label vector $L$ of elements $L_j \in \chi$ is generated according to the single best-fit model approximation of the observed data.

Each repetition underwent an exhaustive curve matching process to determine the best-fit simulated trajectory waveform of synthesized from each of the six basic analytical curves $\chi$ = [Linear, Sigmoid, Quasi-Concave, …] defined previously (Section 3.4.1). For the $j^{th}$ motion, the best-fit model class was assigned to a label vector $L$ according to the curve type constituting the global minimum of modeling error. Thus label vector elements were coded variables $\chi$ = [A, B, C, … ]. This process is outlined in Flowchart 1.

### 4.3.3 Waveform comparison

The Pearson product moment correlation coefficient $\rho$ yields a scale-free rater of waveform agreement, independent of waveform length (number of points) and amplitude. Thus, the correlation coefficient was selected as the optimal measure of ET model fit to actual trajectory $\theta$:

$$\rho = \frac{\sum_{i=1}^{T} \theta_i \cdot ET_i - T \cdot \overline{\theta} \cdot \overline{ET}}{(T-1) \cdot \sigma_\theta \cdot \sigma_{ET}}. \qquad \text{(Equation 11)}$$

where $\overline{X}$ and $\sigma_X$ is average and the standard deviation of waveform $X$, and $T$ is the total number of samples in the waveforms. Recall that the waveforms are length-matched.

Other waveform similarity measures, e.g. the sum-of-squared errors (SSE), were discarded for metrical dependence on parameters of scale. Though temporal and amplitude normalization would have equated these variables, the SSE does not have a universal scale. The correlation coefficient, however scales $-1 \leq \rho \leq 1$, facilitating easy comparison across repetitions, between subjects, and against other protocols. It is noted that whereas all waveform comparisons here are, by construction, assessing

minute differences between a raw waveform and its ET approximant which will have identical trends (upwards for flexion, downwards for extension), $\rho$ is expected to be a positive quantity.

## 4.4 Results

### 4.4.1 Basic performance measures

Several basic parameters of movement listed in (Section 2.3) provide elementary indices of movement behavior. Here, the neurologically intact volunteers enacting smooth, discrete articulation of the elbow joint performed the task within an expected range of large amplitude but sub-maximal movements executed at a self-selected pace. Subject-wise averages are presented in (Table 7):

Table 7: Parameters of SJTs recorded from healthy subjects (N = 41)

| Metric | Value ($\mu \pm \sigma$) | Comparison to assumption |
|---|---|---|
| Movement amplitude $\Delta\theta$ | 91.3 ± 6.8º | |
| Average angular velocity $\bar{\dot{\theta}}$ | 90.6 ± 35.3º/s | |
| Time to maximum angular velocity $\tau_{\dot{\theta}_{\max}}$ | 0.36 ± 0.11·$T$ | <0.5, $P < 0.001$ |
| Symmetry ratio $\Gamma^{\ddot{\theta}}$ | 0.71 ± 0.15 | <1.0, $P < 0.001$ |
| Number of peaks in the velocity profile $\pi_{\dot{\theta}}$ | 5.1 ± 5.2 | >1.0, $P < 0.001$ |

All values $\mu \pm \sigma$.

Though speed of flexion was not strictly controlled, Table 7 reports that each movement cycle was completed in approximately 1 second ($\Delta\theta \approx \bar{\dot{\theta}}$), and that the movement amplitude was large, but did not approach the physiological limit of the

elbow joint (generally presumed to exceed 120º). Thus, the movements observed here are considered to represent natural, smooth movement at a comfortable pace, over a comfortable range.

In addition to basic kinematical parameters, two widely accepted notions of autonomous single-joint articulation were tested by inspection of the velocity and acceleration profiles. Specifically, the SJT velocity trace is thought to yield a singly-peaked, symmetric velocity profile. These assumptions were rejected at the $P < 0.001$ level of significance by a Student's *t*-test on subject means versus the expectation of a single velocity peak $\pi_{\dot{\theta}} = 1$ occurring at the temporal mid-point $\tau^{\dot{\theta}}_{\max} = 0.5 \cdot T$, with equal time spent in acceleration versus deceleration $\Gamma^{\ddot{\theta}} = 1$. Thus, SJTs were observed to yield neither symmetric, nor unimodal velocity profiles.

It is noted that the prevalence of multiple peaks persists in the velocity profile despite low-pass filtering. Whereas the velocity traces of corresponding to the ET models are by construction singly-peaked, their accuracy in reconstructing the $\theta$ curve must be asserted.

### 4.4.2 ET goodness-of-fit to the observed motion

Over 6000 angular position traces were recorded from forty-one subjects, some of whom made multiple (up to 17) visits. Each trace was compared against each of 6 archetypal curves, padded at either end to simulate all possible average velocities within the constraint of total motion time $T$ (in units of samples). This pseudo-convolution, started with analytical curve duration $l_{\min} = 5$, the minimum length at which the model curves were guaranteed to yield unique approximants. Thus, there were $\sum_{k=1}^{T-(l_{\min}-1)} k$ total simulations for each model curve. For six curve types, for a 1.5-second motion, sampled at 80 Hz, the global minimum represents the single best

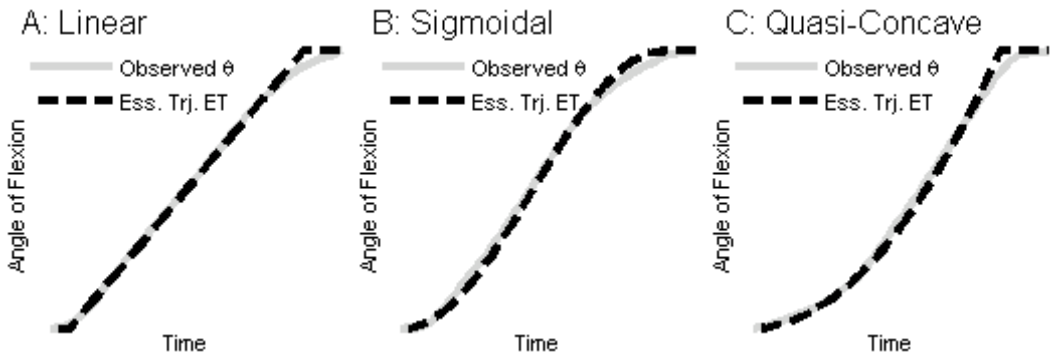


Figure 9 Sample best-fit curves. Three sample trajectories from a single subject, with the global best fit curve $B(l, p)$ (generating label $L$ for three repetitions).

approximation of the angular trajectory out of a total of $6 \cdot \sum_{k=1}^{(1.5\times 80)-3} k = 41418$ possible models. The Pearson product moment correlation coefficient for these best-fit curves against the observed motion was $\rho = 0.99 \pm 0.01$. Sample ET fits to raw trajectory data are shown in Figure 9.

Note that the movement records in Figure 9a-c have distinctly different morphologies that were fit well by the respective model curves.

### 4.4.3 Symmetry parameters: ET to SJT

Despite a very high correlation between the SJT traces and the idealized Essential Trajectory model curves, the multiply-peaked $\dot{\theta}$ profiles may pose a challenge to the extraction of features from the differentiated Essential Trajectory models, which, by construction, yield a single peak. The accuracy of differentiated ET traces in identifying the apparent asymmetry observed in the SJTs was subsequently tested by identical analysis:

| Table 8: Parameters of healthy subjects' ETs (N = 41) | | |
|---|---|---|
| Metric | Value ($\mu \pm \sigma$) | Comparison to filtered SJTs (Table 7) |
| Time to maximum angular velocity $\tau_{\max}^{\dot{\theta}}$ | $0.39 \pm 0.10 \cdot T$ | ≈0.36 |
| Symmetry ratio $\Gamma^{\ddot{\theta}}$ | $0.71 \pm 0.26$ | ≈0.71 |
| Number of peaks in the velocity profile $\pi_{\dot{\theta}}$ | $1 \pm 0$ | <5.1, $P < 0.001$ |
| All values $\mu \pm \sigma$. | | |

From Table 8, it is clear that the ET models correctly detected the asymmetry observed in the SJTs, while maintaining a uniformly unimodal velocity profile.

## 4.5 Closer look: Filter validation

### 4.5.1 Filter design

It has been determined that the SJT traces observed here depart considerably from the expectation of a singly-peaked velocity profile. Under the assumption that these peaks are unrelated to the essential movement pattern, and are therefore considered "noise," the simplest explanation for these peaks is that their persistence is a consequence of inadequate filtering. Thus, it bears disclosing the filter characteristics employed here. All data here were processed with a 2nd-order low-pass Butterworth's filter, with the following filter expression

$$h = \frac{\left[\ 0.04,\ 0.08,\ 0.04\ \right]}{\left[\ 1.0,\ -1.35,\ 0.51\ \right]}. \qquad \text{(Equation 12)}$$

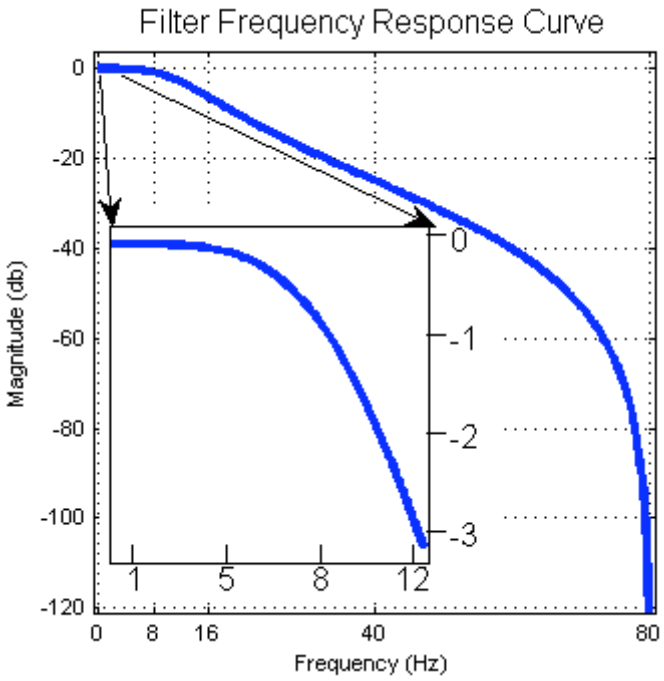


Figure 10 Frequency response profile of the 2nd-order low-pass Butterworth's filter used here: -3 dB reduction at approximately 12 Hz.

This filter exhibits a moderate roll-off following the pass-band, but does yield a cutoff of -3 dB attenuation after approximately 12 Hz. A frequency response curve is shown in Figure 10.

For kinematical analysis of SJT data, standard protocols typically specify a low-pass filter with a 6-15 Hz cutoff (Atkeson and Hollerbach 1985; Reina, Moran et al. 2001; Schaal and Sternad 2001; Cozens and Bhakta 2003; van Mourik and Beek 2004; Mutha and Sainburg 2007), and a low-order (3rd-order or less) Butterworth's filter is common (Feng and Mak 1997; Schaal and Sternad 2001; Ju, Lin et al. 2002; Mutha and Sainburg 2007). Thus, it is concluded that the filter design here is in keeping with the filtering conventions used in the literature for kinematical data, and that spurious peaks found here are not the result of a unique filter design, but could be found in a wide variety of protocols.

### 4.5.2 Filter assessment

Under the hypothesis that the filter does actually improve the quality of the signal, it is expected that the filtered trace contains fewer peaks, and the peaks that remain are attenuated. Here, peak amplitude will reflect the "power" of the maximum velocity: the peak normalized to the mean:

$$\dot{\theta}_{\max} = \frac{\dot{\theta}_{\max}}{\bar{\dot{\theta}}}.$$

It was found that there was a modest attenuation of peak power $\dot{\theta}_{\max}$ with filtering: 2.64 ± 0.57 versus 2.81 ± 0.63 in filtered versus unfiltered traces; however this difference was not significant at the $P < 0.05$ level (pair-wise *t*-test).

The number of peaks $\pi_{\dot{\theta}}$, time to peak velocity $\tau^{\dot{\theta}}_{\max}$, and symmetry ratio $\Gamma^{\ddot{\theta}}$ will also be calculated, for a standard of comparison.

| Table 9: Parameters of healthy subjects' unfiltered SJTs (N = 41) | | |
|---|---|---|
| Metric | Value (μ ± σ) | Comparison to filtered SJTs (Table 7) |
| Time to maximum angular velocity $\tau^{\dot{\theta}}_{\max}$ | 0.36 ± 0.11·*T* | ≈0.36 |
| Symmetry ratio $\Gamma^{\ddot{\theta}}$ | 0.80 ± 0.10 | >0.71, $P < 0.001$ |
| Number of peaks in the velocity profile $\pi_{\dot{\theta}}$ | 9.05 ± 9.16 | >5.1, $P < 0.05$ |
| All values μ ± σ. | | |

Here as before, a pair-wise *t*-test was performed comparing features extracted from filtered SJTs directly against those extracted from the raw trajectory waveforms. It is evident that application of a low-pass filter with the characteristics described here significantly reduces the higher-frequency trace activity related to low-amplitude peaks, while preserving the large major peak associated with the essential movement activity, from which the abstraction of a singly-peaked velocity profile is made. Thus, the filter design is not only appropriate, but selective and effective (Table 9).

Though it has been demonstrated that nearly half of the peaks found in the raw SJT are eliminated with low-pass filtering, it must now be determined whether the remaining peaks are sufficiently powerful to perturb SJT waveform parameter extraction. A cycle-by-cycle analysis of trace peaks follows.

## 4.6 Peak identification: Nearest-neighbor analysis

### 4.6.1 Spurious SJT peaks are randomly distributed

It is seemingly paradoxical that despite the significant reduction in peak count after processing, the features extracted from filtered versus unfiltered traces are approximately identical (Table 8). There are two possible explanations for this counter-intuitive result: 1) the peaks persisting in the SJT trace are small and inconsequential to trace analysis, or 2) the remaining peaks are large, but randomly distributed about the ET peak, and thus cancel out in the averaging over many movement cycles. In order to directly identify the true character of these peaks, a cycle-wise analysis was performed on trace pairs, comparing the filtered SJT against the ET. For context, an identical comparison was made between filtered and unfiltered SJT, to further characterize the potency of the filters used in kinematical analysis (viz. Section 4.5.2).

Features of each trace were extracted as described above, and trace-pair disparity was defined as their difference, normalized to the mean of the two values:

$$\Delta\Psi = \frac{\Psi_a - \Psi_b}{\frac{1}{2}\Psi_a + \Psi_b},$$

where $\Psi$ is a waveform feature: $\tau^{\dot{\theta}}_{\max}$, $\Gamma^{\ddot{\theta}}$, or $\dot{\theta}_{\max}$, and $(a, b)$ is an ordered pair indicating the trace pair of interest. This postulation poses the difference proportional metrical scale (Table 10).

| Table 10: Disparity of features extracted from SJT:ET trace pairs (N = 3334) | | |
|---|---|---|
| Metric | ET versus filtered SJT | Filtered versus unfiltered SJT |
| Time to maximum angular velocity $\Delta\tau^{\dot{\theta}}_{\max}$ | 0.14 ± 0.09 | 0.02 ± 0.01 |
| Symmetry ratio $\Delta\Gamma^{\ddot{\theta}}$ | 0.05 ± 0.34 | 0.12 ± 0.11 |
| Peak power $\Delta\dot{\theta}_{\max}$ | 0.23 ± 0.26 | 0.07 ± 0.03 |
| All values $\mu \pm \sigma$. | | |

Despite the apparent equivalence between ET and filtered SJT trace parameters seen in the subject-wise analysis (Table 7), it is revealed that there is considerable disparity between traces in terms of their feature extraction on a cycle-by-cycle basis. Though the symmetry ratio appears to deviate very little within this pairing, the large

variability indicates that this is an artifact of the approximately equivalent propensity for $\Gamma^{\ddot{\theta}}$ in either direction[10].

By contrast, the differences found between filtered and unfiltered SJTs did not significantly depart from those found at the within-subject level. The change in peak power over all traces, $\Delta\dot{\theta}_{\max} = 0.07 \pm 0.03$ (Table 10) agrees well with the subject-wise differences revealed in Section 4.5.2: $\frac{2.81 - 2.64}{0.5 \cdot (2.81 + 2.64)} = 0.06 \approx 0.07$. Likewise the change in symmetry ratio $\Delta\Gamma^{\ddot{\theta}} = 0.12 \pm 0.11 \approx \frac{0.80 - 0.71}{0.5 \cdot (0.80 + 0.71)} = 0.12$, and $\Delta\tau^{\dot{\theta}}_{\max} = 0.02 \pm 0.01 \approx \frac{0.36 - 0.6}{0.5 \cdot (0.36 + 0.361)} = 0$ (Table 9).

From this analysis, it is concluded that the peak content in the SJT trace consists of several large-amplitude transients, and that these peaks are randomly distributed about the single velocity peak simulated by the ET trace. This evidence, however, is not conclusive proof that the ET detects the *correct* peak, i.e. the single peak abstracted in common parlance. A more specific peak analysis is thus performed in order to determine whether the global maximum peak of the SJT is the best match to the true peak in velocity, approximated by the single ET peak.

### 4.6.2 Veridical peak assessment

That a large number of peaks persist in the differentiated SJT ($\pi_{\dot{\theta}} = 5.1 \pm 5.2$, Table 7) following a low-pass filter, and that largest peaks in the SJT traces appear to be randomly distributed about the putative true peak modeled by the ET ($\Delta\tau^{\dot{\theta}}_{\max}$ between ET and filtered SJT velocity $0.14 \pm 0.09$, Table 10) suggests two further possibilities: 1) the ET does not accurately detect the true velocity peak, and the veracity of the global maximum of the SJT is therefore undetermined, or 2) the

[10] Identicality would yield $\Delta\Gamma^{\ddot{\theta}} \to 0$, and $\sigma_{\Delta\Gamma^{\ddot{\theta}}} \to 0$

maximal peak in the filtered SJT profile reflects spurious noise in the trace, and that another sub-maximal peak in the filtered SJT velocity trace is the true peak, and is accurately reconstructed by the ET.

On the basis of the excellent waveform agreement of the ET trace to the SJT ($\rho$ = 0.99 ± 0.01, Section 4.4.2), and via its adherence to the assumption that the differentiated trajectory profile ought to have a single peak, the single ET peak is considered the *veridical peak*[11]. If the SJT maximum is the true maximum, it will be the closest peak to the ET peak, as determined by the difference in their respective peak times: $\boldsymbol{\tau}^{\dot{\theta}}_{\max}$. Thus, there should be peak such that there is a smaller temporal distance $\Delta\boldsymbol{\tau}^{\dot{\theta}}$ to that peak than $\Delta\boldsymbol{\tau}^{\dot{\theta}}_{\max}$ (calculated in Section 4.6.1). We define $\Delta\boldsymbol{\tau}^{\dot{\theta}}_{VP}$ as the distance between the ET peak and the nearest peak in the filtered SJT trace.

Under the hypothesis that the global maximum of the filtered and differentiated SJT trace is the veridical peak, $\Delta\boldsymbol{\tau}^{\dot{\theta}}_{VP} = \Delta\boldsymbol{\tau}^{\dot{\theta}}_{\max} \rightarrow \Delta\boldsymbol{\tau}^{\dot{\theta}}_{VP} = 0.14 \pm 0.09$ (Table 10). In this way, defining the rank $r_{VP}$ of this nearest-neighbor (and thus veridical) peak according to its amplitude in relation all other peaks in the differentiated SJT trace, $r_{\mathrm{VP}} = 1$ indicates the veracity of the SJT trace maxima; $r_{\mathrm{VP}} > 1$ suggests that the SJT velocity peak corresponds to trace noise, and that some other, sub-maximal peak should be considered the true peak. This analysis was performed on all multi-peaked filtered SJT velocity traces ($N$ = 3212 cycles, 96.3%).

[11] The robustness of this assertion is founded in the excellent waveform agreement. Based on this result, it is suggested that the counter-argument, i.e. that the ET peak does not correspond to any meaningful peak, is moot.

| Table 11: Comparison: ET peak against multiple SJT peaks (N = 3212) | | |
|---|---|---|
| Metric | Value ($\mu \pm \sigma$) | Comparison to |
| $r_{VP}$ | $2.08 \pm 1.36$ | $>1.0$, $P < 0.05$ |
| % of $r_{VP} = 1$ | $0.27 \pm 0.22$ | $<1.0$, $P < 0.001$ |
| $\Delta\tau_{VP}^{\dot{\theta}}$ | $0.07 \pm 0.03$ | $<0.14$, $P < 0.001$ |
| $r_{VP}$ = Rank of veridical peak in SJT velocity trace, $\Delta\tau_{VP}^{\dot{\theta}}$ = Temporal difference between single peak of ET curve, and veridical peak. | | |

The large rank of the nearest-neighbor SJT velocity peak to the single ET velocity peak $r_{\mathrm{VP}} > 1$, and the significantly smaller temporal distance to this peak $\Delta\tau_{VP}^{\dot{\theta}} < \Delta\tau_{\max}^{\dot{\theta}}$ is conclusive proof that the global SJT trace maxima does not correspond to the veridical peak simulated by the ET peak, but that there is frequently ($1 - 0.27 = 73\%$ of the time), a closer peak which is approximately the 2nd-largest ($2.08 \pm 1.36$) peak. Indeed, this sub-maximal veridical peak is located significantly closer to the ET velocity peak: $\Delta\tau_{VP}^{\dot{\theta}} = 0.07 \pm 0.03$, which is less than $\Delta\tau_{VP}^{\dot{\theta}}$ at the $P < 0.001$ (c.f. Table 10,Table 11).

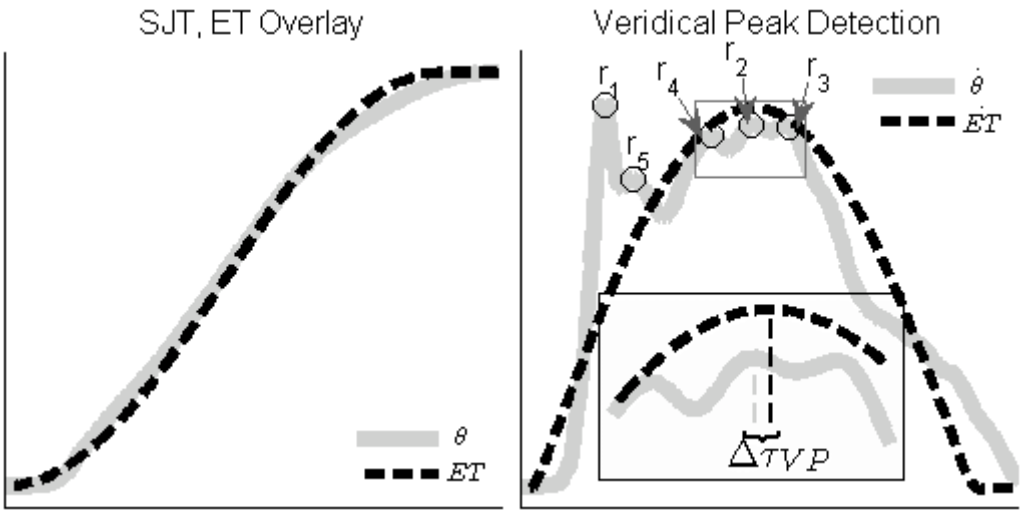


Figure 11 Overlay of a sample trajectory $\theta$ and its Essential Trajectory approximant (c.f. Figure 9).

A representative example of this result is shown in Figure 11: despite excellent agreement between the observed SJT and the ET model curve, their respective velocity traces reveal morphological dissimilarity and feature disparity. $\Delta\tau$ associated with the veridical peak $r_{VP} = 2$ is much smaller than that of the $\dot{\theta}$ trace maximum: $\Delta\tau << \Delta\tau_{max}$.

## 4.7 Summary

Here, three results have been presented: 1) despite adherence to a standard movement protocol on which fundamental tenets of single-joint motion are based, and implementation of standard filtering protocols, SJT traces were contaminated by randomly-distributed peak activity unrelated to the essential motor plan, 2) ET models provide a noiseless high-fidelity representation of the trajectory trace, and accurately extract the veridical peak activity associated with the basic movement pattern, and 3) joint angular trajectory profiles were observed to be moderately asymmetric (predominance of decelerative activity) by two independent measures (symmetry ratio and time to peak acceleration) operating on two different substrates: SJT and ET.

The widely accepted abstractions of SJTs as symmetric, is not universal in autonomous flexion of the elbow, and that the veracity of a singly-peaked velocity profile is a generalization that does not necessarily reflect the state of empirical data, even after conventional signal processing techniques. It is further concluded that the ET curve-matching paradigm yields noiseless trajectory surrogates which may provide useful insight into the human motor system in analyses where noisy substrates pose an untenably potent risk to metrical analysis and feature extraction.

# 5 MOVEMENT PATTERNS FROM ET MODELS

## 5.1 Introduction

As shown in Chapter 4, the basic shape of SJTs can be uniquely identified and classified into several variants. These shapes are determined by myriad interdependent factors and reflect the complex interplay between effectors at the many different stages of the motor hierarchy. Though trajectory formation has been studied extensively, the matching of raw trajectory patterns to idealized waveform models presents a novel opportunity to analyze both the nature and the variability of single-joint motion both within- and between individuals. Here, the essential movement pattern of single joint motion performed by both healthy and impaired subjects will be analyzed for thematic trends in trajectory curvature. The hypotheses of repeatable, isogonic SJTs will be tested directly by categorical analyses performed on ET approximations of the raw trajectory.

## 5.2 Experimental hypotheses

Having demonstrated the validity of the Essential Trajectory as a surrogate for the SJT, its utility as an index of basic movement behavior will manifest in a systematic analysis of the essential movement patterns in healthy subjects. Here, two central notions of human movement are tested: the adoption of highly symmetric trajectories of a consistent angular velocity in constrained tasks, and the highly stereotyped trajectories of repetitive movement

*Subjects single-joint movements will be largely isogonic and symmetric in both flexion and extension tasks.* (Hypothesis 3)

Isogony is measured simply by inspection of the results of the trajectory model: do linear or sigmoidal traces most frequently result the most common best-fit results. A separate test of the variability of this movement pattern is required.

> *Irrespective of the isogonic nature of the movement profile (*Hypothesis 3*), model adoption by subjects will be highly uniform, showing relatively high stability among the available model types.* (Hypothesis 4)

Movement theme stability will be showed directly by an analysis of the histogram of model results. Highly stable movement patterns will show a sharp spike at the singularly relevant model; unstable movement patters will exhibit a broad distribution over multiple model curves. Lastly, in cases where movement profiles are observed to exhibit high variability, an explanation will be sought vis-à-vis situational parameters.

> *In the cases where the primary model type is not observed in a given movement cycle, this deviation from the central behavioral theme can be explained as the result of some perturbation in basic movement patterns, i.e. angular velocity, angle of motion onset, or time.* (Hypothesis 5)

The relationship between "selection" of movement theme, and incidental variables will be assessed by standard statistical analyses.

## 5.3 Experimental methods

### 5.3.1 Subjects and protocol

Here as before, forty-one healthy individuals described in Section 4.3.1, performed a simple single-joint movement task, and the data were treated identically, as outlined in Section 4.3.2. Subjects were seated in the MAST, and instructed to flex

and extend about the elbow across their "comfortable range of motion" in such a way that "maximized smoothness." Visual feedback of joint angle was provided though subjects were not instructed to attend to this information. Pace was self-selected.

### 5.3.2 Signal processing and curve matching

As described in section 4.3.2, raw elbow angular data were smoothed with a low-pass Butterworth's filter ($2^{nd}$-order, 4 Hz cutoff), and divided into single cycles of flexion-and-extension by a thresholded local minima. Each repetition subsequently underwent an exhaustive curve matching process to determine the best-fit simulated trajectory waveform of synthesized from each of the six basic analytical curves (linear, sigmoidal, quasi- and sigmo-convex/concave, Chapter 3). A label vector $L$ listed the models which best fit each movement cycle, indexed by $j$, according to a RMSE-minimization criteria.

### 5.3.3 Curvature theme analysis and interpretation

#### *5.3.3.1 Essential Trajectory label histograms*

In order to determine the nature and variability of curvature themes in the SJTs, the distribution of model class labels for each repetition were analyzed ensemble. Matching each repetition to a set of archetypal waveforms yields a label vector $N_{\text{reps}}$ long, with elements $L_j \in \chi$ reporting the curve class for which repetition $j$ was best modeled according to a sum-of-squares error assessment. Computing a $1 \times |\chi| = 6$ histogram vector $H$ of the proportion of the dataset for which model $\chi_j$ was the global best-fit, we determine the relative frequency of each curve type:

$$H_i = \left| L_j \right| \ni' \ L_j = \chi_i \ \ \forall \ \ 1 \le j \le N_{reps}, \ 1 \le i \le \left| \chi \right|. \qquad \text{(Equation 13)}$$

Histogram elements are necessarily non-negative and sum to unity: $0 \leq H_i \leq 1$, $\sum_j H_j = 1$. Histograms typically comprised all waveforms of a single direction (flexion or extension) from a single visit, or across all visits performed by a single subject, as noted.

### *5.3.3.2 The Principal Trajectory (PT)*

Constructing $S$ as a sorted version of $H$ such that $S_1 \geq S_2 \geq S_3 \geq \ldots$, we define the *Principal Trajectory* PT as the label corresponding to the first element $S_1$, the model which produced the greatest proportion of Essential Trajectories for a given dataset.

> *The principal trajectory* PT *of an individual's dataset is the single analytical curve type which most frequently generated the global best-fit trajectory approximant.* $PT = \chi_i \ \ni' \ \left| L_j = \chi_i \right| > \left| L_j = \chi_k \right| \ \forall \ k \neq i, \ 1 \leq j \leq N_{reps}$, *and is the label associated with* $S_1$.
>
> (Definition 2) *Principal Trajectory*

Thus, the PT can be considered the predominant trend of trajectory curvature across a single dataset; this dataset will typically comprise all flexion or extension movements by a single subject in a single session, or across all sessions.

### *5.3.3.3 Significant Trajectories (ST)*

While it is important to ask "what is the single best model of an individual's trajectories?" the number of "good" trajectory models is equally valuable information. For instance, if a data session's histogram was nearly equally divided amongst two models H = [ 0, 0.45, 0, 0.55, 0, 0 ], then to report only the single best model (in this case PT = D, Quasi-Convex) would be to ignore the frequency with which another model (Sigmoidal, *B*) was the global best-fit.

For this case, it is clear that there are two and only two contributors to the dataset's model results space, each constituting a near 50% proportion. However, for an arbitrary case, for example H = [ 0.38, 0.30, 0.02, 0.06, 0.20, 0.04 ], a robust method is required in order to determine how many elements of *H* can be considered *Significant Trajectory* ST model classes, i.e. that a given model was sufficiently frequent to be a meaningful element of the trajectory modeling scheme.

*The significant trajectories* ST*s of an individual's dataset is the set of analytical curve types that generated the global best-fit trajectory approximant for a sufficiently large proportion of the dataset, according to some criterion* $\kappa_{(i)}$ *where* $\kappa$ *is either a vector or a scalar threshold:* $ST \subset \chi = \left\{ \chi_i \ni' \left| S_k = \chi_i \right| > \kappa_{(k)} \right\}$.

(Definition 3) *Significant Trajectory*

The matter of significance in a histogram is reduced to a *scree analysis*[12] problem, as typical of a principal components task where the minimum number of meaningful signals is sought. There are several major classes of scree analysis, each with their own set of considerations. Here, a broken-stick model was selected as the discriminant of choice as it has been found to yield the most consistent results (Jackson 1993; Cangelosi and Goriely 2007), and in fact, may be a conservative estimate of minimum dimensionality (Bartkowiak, Lukasik et al. 1991; Cangelosi and Goriely 2007). The broken-stick[13] method imposes a vector of threshold criterion, above which any element $S_i$ of the sorted histogram is considered a significant contributor to the system if $S_k > b_k = \Re_k^*$ where $\Re^*$ is the sorted vector of random values generated from uniform distribution on the interval [ 0, 1 ], $\Re = N\left(\frac{1}{2}, \infty\right)$:

[12] So-named because the monotonically non-increasing plot of sorted histogram values takes the shape of a mountain's scree slope.

[13] So-named because a straight-line vector of thresholds, descending over the sorted histogram separate the significant contributors (above the line) from those not contributing significantly (below the line).

$$\Re^* = sort\left(\frac{\Re_k}{\sum_i \Re_k}\right). \qquad \text{(Equation 14)}$$

Here, these $1 \times |\chi| = 6$ broken stick vectors $b$ actually reflect the averaging of 1000 sorted random-digit vectors $\Re^*$, to ensure uniformity across all iterations. Thus, viz. Definition 3, the number of STs is the count of curve types with a proportional representation in the dataset greater than some threshold $|S_k > \kappa_k = b_k|$. A rigid criterion is now defined for the assignation of significance to any member of the sorted histogram. This is demonstrated in Figure 12.

In summary, from the vector $L$ of repetition labels, determination of the predominant movement themes in a given dataset requires sorting a histogram of categorical variables.

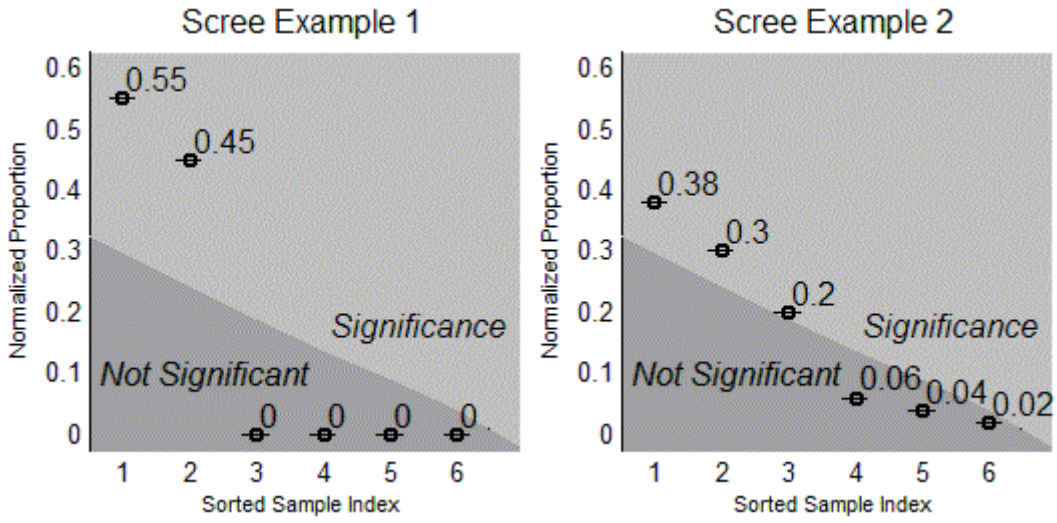


Figure 12 Example of scree analysis: Determination of significant contributors to an simulated over-determined system according to a broken-stick scree line threshold.

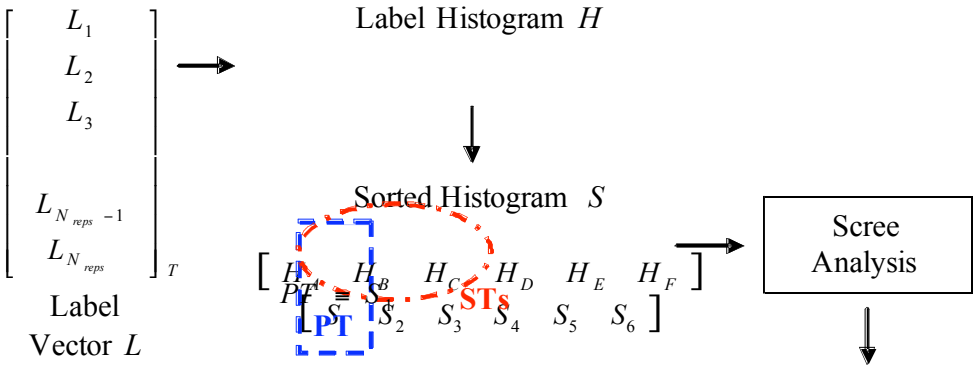


Principal Trajectory = most frequently best -fit # of Significant T rajectories

Flowchart 2 Curve-matching model analysis. A histogram $H$ reports the number of elements in $L$ labelled $\chi_j$. $S$ sorts $H$, with elements in descending order. From $S$, Principal and Significant Trajectories (PT, ST) can be ascertained.

The *Principal Trajectory* is identifiable by inspection; important contributors (*Significant Trajectories*) are determined via scree analysis (Flowchart 2).

## 5.4 Hypothesis testing via scree analysis

### 5.4.1 Isogonic SJTs

#### *5.4.1.1 Isogony principle and the two-thirds power law*

The dependence of trajectory curvature on movement velocity in multi-joint motion was noted in a number of early studies (Binet and Courtier 1893; Jack 1895), where the notion of isogony was first introduced as the co-variation of angular velocity with radius of curvature: equal angle in equal time. The specific relation between geometric properties of the spatial trajectory (curvature, $C$) and the kinematics (angular velocity, $V$) of the movement have been formulated via the two-thirds power law

$$V = K \cdot C(t)^{\frac{2}{3}}. \qquad \text{(Equation 15)}$$

More explicitly, the radius of curvature for a segment of movement *s* angular velocity has been shown to relate to the radius of curvature *R* according to

$$V(s) = K(s) \cdot \left( \frac{R(s)}{1 + \alpha \cdot R(s)} \right)^{\frac{1}{3}}, \qquad \text{(Equation 16)}$$

where $0 \leq \alpha \leq 1$ is a constant determined by the average velocity (Viviani and Schneider 1991). Thus, for movement over which the hand passes through a trajectory of constant radius of curvature, the angular velocity is thought to remain approximately constant, at a value relating to the trajectory curvature by a power-law.

#### *5.4.1.2 The isogony principle in single-joint motion*

The isogony principle has not been shown for movements of a single joint. However, there is sufficient evidence to suggest the possibility of isogony in single-joint motion at the elbow: the relationship between spatial and kinematic movement variables is invariant under mechanical constraint (Viviani and Terzuolo 1982). Whereas imposition of hand path does not appear to alter trajectory dynamics, it is possible that the restriction of UL motion to a track of a single-DOF, where the radius of curvature is uniform and highly controlled, would manifest approximately linear SJTs, corresponding to a constant velocity of excursion. Here, this claim is tested directly via the null hypothesis that all SJTs will be classified as predominantly linear, or at least sigmoidal, traces with uniform curvature throughout a large portion of the movement: PT = A.

### 5.4.2 Trajectory pattern stability

#### *5.4.2.1 Quantitative raters of trajectory variability*

The Pearson product moment correlation coefficient $\rho$ (Section 4.3.2) is the most commonly used measure of waveform similarity. However, the utility of the correlation coefficient extends to pair-wise comparisons of two curves, not to datasets comprising many repetitions. ANOVA-like raters exist for the purposes of comparing multiple traces, including the variance ratio (VR)

$$VR = \frac{\sum_{i=1}^{T^*} \sum_{j=1}^{N_{reps}} \frac{\left(X_{ij} - \overline{X}_i\right)^2}{T^* \cdot \left(N_{reps} - 1\right)}}{\sum_{i=1}^{T^*} \sum_{j=1}^{N_{reps}} \frac{\left(X_{ij} - \overline{\overline{X}}\right)^2}{\left(T^* \cdot N_{reps} - 1\right)}}, \qquad \text{(Equation 17)}$$

where $X$ is the set of temporally normalized (to $T^*$) data records, indexed by time $i$, and cycle iteration $j$; $\overline{X}_i$ represents the average across all repetitions at time point $i$, and $\overline{\overline{X}}$ is the "grand mean" or "global mean" of the entire dataset, i.e. column mean of the row-means.

The primary advantage of a metric such as the VR is that it reports the trace-to-trace variability as a single scalar value; this result is scaled between 0 (identical signals) to 1 (randomly generated signals). The minor variations in SJT morphology, however, may obsolesce quantitative metrics such as the VR, by obfuscating subtle alterations in the movement pattern. For instance, a dataset of 20 movement cycles comprising 10 identical SJTs modeled as class C and 10 identical trajectories modeled as class D, would generate some non-zero VR score. This score would be indistinguishable from another score of randomly matched repetitions with the right

set of parameters. Similarly, for a set of 20 repetitions to have identical curvature profiles, but performed at different speeds would obscure their mutual similarity by inflating the VR.

In this way, it is not possible to determine whether there were a large or small set of movement themes in the dataset. Thus, quantitative metrics present one facet of SJT waveform variability analysis; information as to the variability of essential trajectory curvature requires non-quantitative metrics.

#### *5.4.2.2 Categorical metrics in trajectory variability analysis*

Categorical modeling of each trajectory record as having a given morphology, i.e. linear or variously non-linear, provides a unique paradigm by which the repeatability of SJTs can be assessed. Assignment of a single best-fit model to each movement cycle creates a label set of model types found to best represent the SJTs in a given dataset. That a given trace is best matched to a given model class, at the exclusion of all other model types, suggests that trajectory pattern themes will emerge if the Principal Trajectory is sufficiently large. Here, the notion of trajectory pattern stability, the adherence to a restricted set of movement patterns, is tested directly via the null hypothesis that all SJTs in a given dataset will be classified uniformly, irrespective of the model type: $| ST | = 1$.

## 5.5 Results

### 5.5.1 Isogony is common, but not universal

For each dataset, a sorted histogram was constructed from the sorted label vector $L$, rendering the relative proportions of each model's representation as the best-fit approximant within the dataset. The Principal Trajectory PT was extracted as the

single model class which most frequently resulted in global error minimization (i.e. $S_1$, Definition 2).

No single model yielded PTs for a majority of the subjects; straight-slope models (class A) were the PT for a *plurality* of individuals in single-joint flexion and extension tasks. Sigmoids (B) were the next most frequent PT, also constituting the second-most PTs in both directions. These symmetric basic curves accounted for approximately 75% of all subjects' PTs. Two models with a non-monotonic and asymmetric velocity profile (Sigmo-Concave and Sigmo-Convex, Types E and F), did not yield any PTs, and were only considered a significant contributor to an individual's dataset in a few cases (Figure 13).

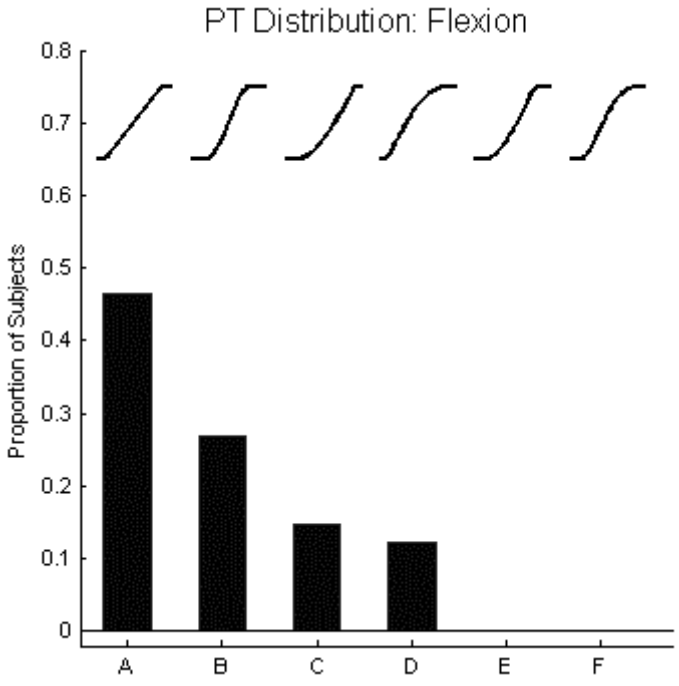


Figure 13 Adoption of ET model type across subjects. Proportion of subjects (N=41) yielding Principal Trajectories (PT) of each curve type ($\chi$ = A→F) for flexion SJTs.

That approximately 25% of individuals' PTs were neither linear nor sigmoidal suggests against isogony as a universal principle applicable to constrained motion of the elbow.

### 5.5.2 Degeneracy of model themes typical

Within each histogram, several model types were found to have non-zero components, i.e. some motion cycles were best-fit by a model other than the PT. In order to determine whether these non-PT models were "meaningful" contributors to the dataset's model space, a broken-stick scree analysis was employed (Section 5.3.3.3). These Significant Trajectories reveal the frequency with which a given

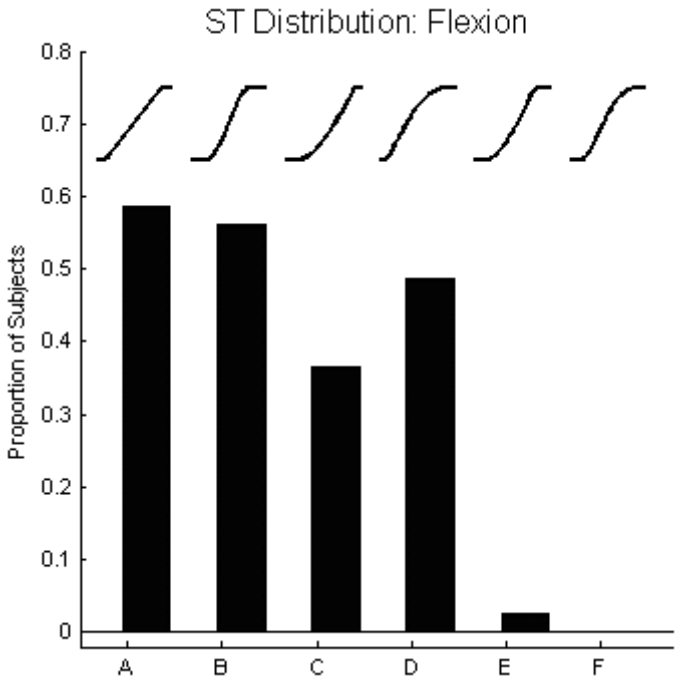


Figure 14 Frequency of model class as a significant dataset component. Proportion of subjects (N=41) yielding Significant Trajectories (ST) of each curve type ($\chi$ = A→F) for flexion SJTs.

model class was a significant contributor to a given dataset, irrespective of whether it was the single greatest component (the Principal Trajectory).

Here, it was typical for a given dataset to be best-modeled by a profile of ETs comprising a small set of curve types. Indeed, while the linear class ($\chi = A$) yielded PTs for 47% of subjects (Figure 13), an additional 59% − 47% = 12% of subjects' datasets a contained sufficient proportion of linear ETs to be considered "significant" by a scree analysis (Figure 14). Likewise, though sigmoidal, quasi-concave, and quasi-convex model curves were found to yield PTs in 27%, 15%, and 12% of subjects' datasets respectively, these models were Significant in 56%, 37%, and 49% of subjects.

It is apparent that for longitudinal analyses, i.e. inclusive of all movements performed over all sessions, subjects SJTs were not highly stereotyped, but were instead somewhat degenerate.

*A degenerate model set is one for which the Principal Trajectory was not the only Significant Trajectory, i.e.* $| ST | > 1$.

(Definition 4)
*Degeneracy*

Under the hypothesis that the movement patterns of SJTs are invariant and highly predictable, each dataset should yield a single Significant Trajectory, i.e. $| ST | = 1$, and thus the proportion of the dataset modeled by the Principal Trajectory should approach unity.

It was determined that the hypothesis of invariance in the movement patterns conveyed via the SJT can be rejected with a high level of certainty in comprehensive data profiles (Table 12). However, it is important to acknowledge that a subgroup of subjects contributed data to these profiles over several days, which may contribute to

the apparent degeneracy observed in this longitudinal analysis. In this way, the effects of observation on multiple days should be eliminated by an analysis of each session unto itself.

| Table 12: Parameters of healthy subjects' ETs (N = 41) | | |
|---|---|---|
| Model Set Parameter | Value ($\mu \pm \sigma$) | Comparison to assumption |
| \|ST\| ($\mu \pm \sigma$) | $2.02 \pm 0.72$ | >1, $P < 0.001$ |
| \|ST\| = 1 (proportion) | 0.24 | <1 |
| PT proportion | $0.49 \pm 0.14$ | <1, $P < 0.001$ |
| ST = Significant Trajectory, \|ST\| = ST set cardinality, PT = Principal Trajectory. | | |

### 5.5.3 Degeneracy persists at the single-session level

A separate analysis, identical to that performed on subject-wise datasets was performed for each session in order to test the hypothesis of highly invariant trajectory patterns in repetitive single-joint flexions, without artificial inflation of trajectory variability measures due to the consolidation of movements performed over several days' worth of sessions (Table 13).

| Table 13: Flexion trajectory degeneracy: Within-session analysis (N = 140) | | |
|---|---|---|
| Model Set Parameter | Value ($\mu \pm \sigma$) | Comparison to assumption |
| \|ST\| ($\mu \pm \sigma$) | $1.93 \pm 0.64$ | >1, $P < 0.001$ |
| \|ST\| = 1 (proportion) | 0 | <1 |
| PT proportion | $0.53 \pm 0.13$ | <1, $P < 0.001$ |
| ST = Significant Trajectory, \|ST\| = ST set cardinality, PT = Principal Trajectory. | | |

Here again it is clear that the null hypothesis of low cycle-to-cycle variation of the model classes comprising the Essential Trajectory profiles, i.e. low ST and PT comprising 100% of each session dataset, is rejected at the $P < 0.001$. Indeed neither the ST set cardinality | ST |, nor the proportion of PTs per session (Table 13) were significantly different than their corresponding values from within-subject analysis (Table 12) at the $P < 0.05$ level. This result suggests that in terms of trajectory analysis, parameters pertaining to trajectory variability do not change over time (average of 6.8 sessions), and a single session may be sufficient for investigations into related questions.

## 5.6 Comparison to extension movements

### 5.6.1 Within-subjects analysis: Identical PT distributions

In order to determine the effect of movement direction on trajectory shape, identical Principal Trajectory and Significant Trajectory analyses were performed on extension movements. Here, the hypothesis of general conservation of movement themes across movement direction was tested by the correspondence between PT distributions assessed in flexion and extension (Figure 15).

Interestingly, the distributions of PTs across curve types was identically ordered across both tasks, a 1-in-5! occurrence by chance. This suggests strongly that there is some prediction across movement direction of trajectory pattern as modeled by the Essential Trajectory. However, a within-session analysis is necessary to assess the veracity of this claim.

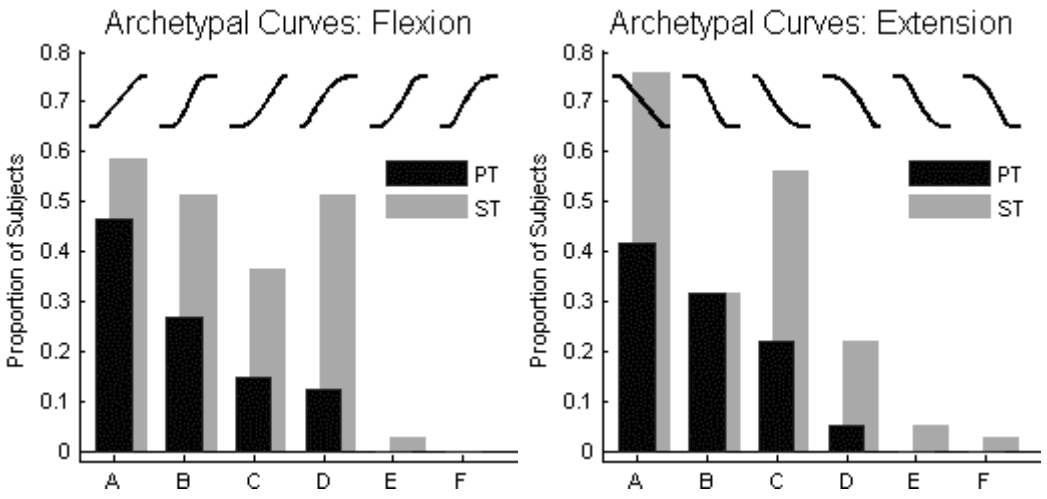


Figure 15 Results of curve-matching. Proportion of subjects (N=41) yielding Principal Trajectories (PT) of each curve type ($\chi$ = A→F) for both flexion (*Left*) and extension (*Right*) tasks.

### 5.6.2 Within-subjects analysis: Equivalently variable patterns

As before, with flexion SJTs, trajectory pattern variability was assessed by the number of Significant Trajectories and proportion of Principal Trajectories, both against the null hypothesis of 1. Here again, model sets were seen to be degenerate via a significant departure from the null hypothesis of invariance at the $P < 0.001$ level.

| Table 14: Extension trajectory degeneracy: Within-subjects analysis (N = 41) | | | |
|---|---|---|---|
| Model Set Parameter | Value ($\mu \pm \sigma$) | Comparison to Table 12 | Comparison to assumption |
| \|ST\| ($\mu \pm \sigma$) | 1.92 ± 0.81 | ≈2.02 | >1, $P < 0.001$ |
| \|ST\| = 1 (proportion) | 0.31 | >0.24 | <1 |
| PT proportion | 0.56 ± 0.16 | ≈0.50 | <1, $P < 0.001$ |
| ST = Significant Trajectory, \|ST\| = ST set cardinality, PT = Principal Trajectory. | | | |

From the statistical equivalence of PT proportion and ST counts in extension, it is concluded that the SJTs of extension movements are equally degenerate as flexion movement profiles. It is reported, though not shown in tabular form, that beyond for a low (0) proportion of subjects with unity ST profiles, within-session analysis again revealed compatible results with within-subject analysis: | ST | = 1.83 ± 0.38, and PT proportion 0.62 ± 0.18; neither differed from the within-subject analysis at the $P < 0.05$ level via a pair-wise *t*-test (Table 14).

### 5.6.3 Movement patterns across direction: no correspondence

#### *5.6.3.1 "Hard" versus "soft" criteria for correspondence*

Under the hypothesis that trajectory models were equivalent across directions, the PTs observed in flexion should match those of extension, i.e. $PT^f = PT^e$. However, for the same reasons that the PT is a somewhat limited measure of motor performance (that it ignores large sub-majority contributors, see Section 5.3.3.3), a "softer" criterion may be tested in order to provide a more detailed answer to the question of directional equivalence. We define ST overlap $O$ as the number of common elements between ST sets (the intersection $\cap$) divided by the number of total elements (the cardinality of the union $\cup$):

$$O = \frac{ST^f \cap ST^e}{\left| ST^f \cup ST^e \right|}. \qquad \text{(Equation 18)}$$

Thus, under the hypothesis of trajectory model equivalence across movement direction, $O$ on average should be close to the identity ($\overline{O} \to 1$), the proportion of identical subsets $O_1$: $ST^f = ST^e$ should be large, and there should be very few null

intersections ($ST^f \cap ST^e$ = null set, i.e., no common elements between the ST sets of flexion and extension, $O_0$[14] ).

### *5.6.3.2 Chance PT prediction, weak ST overlap*

Within each session, there was considerable diversity between model sets associated with flexion and those of extension. The proportion of sets with identical PTs was low (0.24), as was average overlap: $\overline{O}$ = 0.39. Though there were few sessions with non-intersecting model sets $O_0$ = 0.09, only 41% of datasets showed identical ST sets $O_1$ (Table 15).

| Table 15: Flexion trajectory degeneracy: Within-session analysis (N = 140) | | |
|---|---|---|
| Model Set Parameter | Value | Comparison to assumption |
| $PT^f = PT^e$ | 0.24 | <1 |
| Average ST overlap $\overline{O}$ | 0.39 ± 0.36 | <1, $P < 0.001$ |
| Unity ST overlap $O_1$ | 0.09 | <1 |
| Null ST overlap $O_0$ | 0.41 | >0 |
| ST = Significant Trajectory, \|ST\| = ST set cardinality, PT = Principal Trajectory. | | |

It is noted that whereas only 4 of the 6 ET model types were found to yield PTs at all (Figure 13), there is an approximately 1-in-4 chance of finding any one of these models as the PT. In this way, fixing one model type, e.g. $PT^f$, there is an approximately 0.25 chance in $PT^e = PT^f$ at random. In this context, it is concluded that there is very little correspondence between SJTs observed in flexion and extension.

[14] So-named $O_0$ because the cardinality of the null set is 0.

### 5.6.4 Poor PT correlation to movement variables

Single-joint motion is the realization of complex interplay between myriad effectors in the motor hierarchy. Changes in kinematics are expected under the condition of intentional adjustments in movement speed and range of motion, as has been shown for 1-D (Wiegner and Wierzbicka 1992; Jaric, Milanovic et al. 1999; Suzuki, Shiller et al. 2001; Mutha and Sainburg 2007) and less-constrained movements (Nagasaki 1989), and have been shown in 1-D motions. Another set of variables account for intrinsic muscle properties including the stretch reflex, activation, and stiffness. Within the scope of a purely kinematic experiment, it is not possible to ascertain these state variables. However, espousing these parameters in a collective variable, *fatigue*[15], it may be possible to ascertain suggestion of a change some combination of these parameters over time: specifically, changes in best-fit trajectory with time.

For three parameters: starting hand position $\theta_{on}$, average velocity $\bar{\dot{\theta}}$, and time (here indexed by the number of cycles performed $1 \leq j \leq N_{reps}$), correlative analyses were performed to determine the influence of these variables on trajectory model choice.

The proportion of sessions in each movement task for which multiple STs were found ($1 - 0.31 = 69\%$ and $1 - 0.41 = 57\%$ of sessions in flexion and extension) were analyzed; from each degenerate dataset, the two most prolific STs (the PT and the next ST), as well as the corresponding parameters associated with those motions. For quantitative parameters ($\theta_{on}$ and $\bar{\dot{\theta}}$) a Wilcoxon signed-rank test (a non-parametric alternative to the Student's *t*-test for when the assumption of normality is

[15] This does not necessarily mean to imply a measure of physical exhaustion, but rather to connote the time-dependency of performance, as measured here by the selection of trajectories from among the six model types.

not-valid); for ordinal variables (order of repetition, $j = 1 \ldots N$ were analyzed in a Wilcoxon rank-sum test.

| Table 16: Correlation of ET model to motion parameters: Degenerate Sessions | | |
|---|---|---|
| Movement parameter | Flexion | Extension |
| N (# of sets) | 97 | 82 |
| $\bar{\dot{\theta}}$ (proportion) | 0.14 | 0.12 |
| $\theta_{on}$ (proportion) | 0.09 | 0.12 |
| # of repetition (proportion) | 0.09 | 0.05 |
| $\bar{\dot{\theta}}$ = Average angular velocity, $\theta_{on}$ = Angle of motion onset. | | |

Of the 97/82 degenerate datasets evaluated in flexion/extension, fewer than 15% showed any significant relationship between trajectory model choice and the three basic parameters of motion outlined above. It is thus concluded that there is little dependence of model type on these movement parameters[16].

## 5.7 Discussion

### 5.7.1 Inference regarding trajectory selection

Of the 6 trajectory models, only 4 yielded PTs, and the remaining 2 resulted in STs for a limited number of individuals. For any one model should be assumed by random chance would occur with a frequency of 1-in-6. That any model should occur with frequency greater than 25 or 30% suggests its relevance as an approximant of the single joint trajectories generated in the present paradigm.

[16] It is noted that a mixed-effects model analysis was not performed, and thus it was not determined whether interaction between these parameters conspire to determine ET model type…

It was determined (Section 5.6.3) that trajectories of extension generated model sets with little correspondence to those of flexion. To reinforce this notion, consider that within the 6-dimensional model space, only 4 models yielded Principal Trajectories for the 41 subjects discussed here (Figure 15). Thus, the probability of an individual yielding a dataset for which a given archetypal curve class is the predominant best-fit (the PT), is 1-in-4. Supposing a subject's $PT^f = \chi_i$, the probability of $PT^e = \chi_j$ where $j = i$ is 1-in-4[17]. The equivalence analysis presented in Table 15 reports just that: that selection of trajectory models in either direction is essentially random.

### 5.7.2 Model space composition

#### *5.7.2.1 Change in model space dimensionality*

Whereas four models resulted in PTs in the present dataset, the question arises whether adding or subtracting models would change the distribution of PTs in Figure 15. It is prudent to note the role of these apparently non-contributory models to the PT distribution.

PTs are generated from an analysis of a histogram of the entire model space (the proportion of traces best-fit by each curve class). To remove a model is to displace the elements of its histogram to some other bin, i.e. those traces that will now be best-fit by some other curve. In this way, whereas an arbitrary curve type may not have yielded a PT, sufficiently many traces may have been best-fit by this function to alter the histogram in such a way that a new PT is reported. A low or zero-PT status for some model should not imply that it can be removed without impact on the model-space histogram.

[17] Strictly speaking, fixing *i* implies a 1-in-16 chance: $P = (¼)^2$ chance of a subject's $PT^f = PT^e = \chi_j$. However, our analysis allows for arbitrary *i*, constraining this variable, and limiting our degrees of freedom to 1: P = (¼ ).

*5.7.2.2 Change in model space membership*

In addition to judicious choice of the number of models, the models themselves must be carefully selected so as to represent a variety of possible trajectory curves, without "over-fitting." For instance, the six curves modeled here were selected for their collective representation of the diverse morphologies of the trajectory traces observed in the experiment (see Section 3.4.1 for explanation of their relevance and formulation). The present models were designed with simple underlying assumptions: 1) monotonic trajectory direction, 2) velocity profile with at most a single peak, and 3) departure from $\theta_{on}$ / arrival to $\theta_{off}$. More elaborate models can be chosen that either adhere to these constraints, or disregard them. For instance, higher-order polynomials may provide more accurate fitting, but would violate Assumption 2 (odd and even polynomials), or Assumption 1 and 3 (even polynomials). As with many modeling activities, it is possible to arrive at model that fits a large portion of the data with very fine accuracy, but its validity is constrained by the assumptions (or lack thereof).

It is clear that, some of the models used are posed in such away that implementation in a simulated human system, or as a performance criterion may be difficult to justify. For example, the straight-line trajectory is a physically unrealizable angular trajectory for the reason that it implies an infinite jerk cost in its discontinuous first derivative. This model's validity can be explained by the curve's *approximation* of a trajectory, implying a relatively brief acceleration/deceleration. Use of this model as a construct for simulated systems would require some filtering to obviate the errors associated with an impulse movement. However, the copious datasets for which this model was the Principal Trajectory, irrespective of its convoluted velocimetry, indicate its validity as a model of human motion.

### 5.7.3 Symmetry

The symmetry of single-joint trajectories has been discussed in the literature, with no clear resolution, partly owing to the variety of performance protocols c.f. (Nagasaki 1989; Jaric, Milanovic et al. 1999; Mutha and Sainburg 2007). It can be argued, however, that the question of movement symmetry may not necessarily be well-posed with respect to standard quantitative analyses. For instance, a small spontaneous ridge in the data trace, whatever the cause, may corrupt point-wise differentiations of the 1$^{st}$- or higher order (section 2.3.1.2). Here only two models could be considered symmetric: models A (linear SJT) and B (sigmoidal SJT). Subjects selected these models with sufficient frequency that together they comprise 47 + 27% = 74% and 42 + 32% = 74% of the within-subject PT distributions (Figure 15). Whereas the PT constitutes, on average, approximately 50-60% of any single dataset (Table 12, Table 13), and 26% of all subjects yielded datasets for which an asymmetric ET was the PT, it is concluded that symmetry is a common, but non-universal characteristic of SJT movements.

### 5.7.4 Single-joint protocols can be run in a single day

Analysis of human performance over extended time periods allows for the generalization of good-practices for experimental design. In the present set of experiments, a subgroup of 17 subjects made multiple visits, recording datasets with identical cyclic elbow articulation data, in a constrained system. Significant Trajectory analysis revealed a modest increase in trajectory waveform variability with additional sessions (up to 17) that did not reach significance at the $P < 0.05$ level, and ST overlap did not change substantially with multiple visits. There is little indication that a single session is insufficient to characterize the proficiency and variability of healthy individuals' single joint articulation.

## 5.8 Summary

Essential trajectory (ET) traces, matched so as to best approximate the observed single-joint trajectories (SJTs) for a single subject's profile were tabulated across all sessions, yielding histogram distributions of ETs per model type. The Principal Trajectory (PT, single most prolific ET type) and the Significant Trajectories (ST, all model types contributing importantly, as judge by a broken-stick scree analysis) were extracted to ascertain certain features of the observed SJTs. The notion of universal isogony (equal angle in equal time) in SJTs was rejected due to the wide prevalence of non-linear models (STs other than $\chi$ = A or $\chi$ = A, B); as was SJT symmetry, on the frequency with which non-linear STs were observed (STs other than $\chi$ = A, B).

Additionally, SJT movement patterns were found to be moderately variable: subjects tended to select from among 2 STs in both flexion and extension tasks, without relation to basic parameters of movement: time, movement speed, or angle of movement onset. There was no correspondence between movement patterns found in flexion and those in extension, and parameters found in sessional analysis did not differ significantly from those found within-subjects.

# 6 TRAJECTORY ANALYSIS OF STROKE COHORT

## 6.1 Introduction

Here, an ET analysis is performed on the SJTs recorded from a group of stroke patients. In addition to pattern analysis of the predominant movement profiles, analysis of the model distribution, both within-subjects and within-sessions will determine the stability of trajectory formation in persons with compromised motor control. In this way, single-joint movement in two cohorts will be exhaustively characterized for both its essential behavioral patterns, as well as transience in the movement profile.

## 6.2 Experimental hypotheses

The accurate extraction of trajectory features is made all the more important in the case of special populations, not only for the obvious implications in clinical and laboratory assessment, but for the reason that the present work has demonstrated the significantly greater noise component in stroke patients' movement profiles versus healthy subjects. Thus, it is incumbent to demonstrate that the surrogate Essential Trajectory traces are adequate representatives of trajectories observed from an impaired cohort.

> *Essential Trajectory approximants of the SJT trace will yield equivalently strong trace reconstructions of trajectories recorded from hemiparetic individuals.* (Hypothesis 6)

As before, a simple coefficient of determination will suffice in demonstration of model accuracy: detection of trace features, for example, time to maximum velocity, will follow as a presumption of satisfactory demonstration of SJT-ET

agreement. It is hypothesized that the results of the Essential Trajectory modeling, predicated on demonstration of Hypothesis 6, will reveal differences in the basic motor patterns of stroke patients.

*Subjects with impaired motor control exhibit motor deficiency in the way of asymmetric movement patterns.* (Hypothesis 7)

In addition to model "selection" within the stroke cohort, it is suggested that the proclivity for switching among movement patterns will manifest as a highly variable movement profile.

*Motor impairment will manifest as an increased variability in trajectory patterns, and this instability will have greater co-dependence on basic movement parameters.* (Hypothesis 8)

Here, a scree analysis, identical to that performed on healthy subjects' Significant Trajectory sets, will be expected to reveal not only degeneracy among the stroke subjects, but a significantly greater degeneracy than the corresponding findings in healthy subjects' motions.

## 6.3 Experimental methods

### 6.3.1 Subjects and protocol

Fourteen individuals enrolled in the JFK-Johnson outpatient stroke rehabilitation program, with a diagnosis of hemorrhagic or ischemic stroke greater than 6 months prior to study admission were recruited to participate, and were observed in a series of sessions typically lasting less than 30 minutes, enduring over 6 weeks. Of the 14, three were eliminated from analysis, for reasons relating to early

study withdrawal (1) or by the investigators on the basis of being judged to have insufficient residual motor function for inclusion in a study of moderately functional stroke patients. Of the 11 study subjects, only a single individual did not make multiple visits; for this reason, no subgroup of single-visitors was analyzed; the between-session analysis was performed on the 10 repeat-visitors. All subjects gave informed consent based on the procedures approved by the IRB of Rutgers (Section 1.2.1); subject demography is listed in Table 17.

As described earlier, subjects were seated in the MAST, and instructed to flex and extend about the elbow across their "comfortable range of motion" in such a way that "maximized smoothness." Subjects were uniformly tested on their affected side; no distinction was made between persons whose affected limb was collateral with their affected limb.

| Table 17: Demography of stroke subjects: Essential Trajectory extraction | |
|---|---|
| Number of Subjects | 11 |
| Age ($\mu \pm \sigma$)<br>Range (min/max) | 57.35 ± 17.35<br>21/80 |
| Gender (M/F) | 9/2 |
| Handedness (R/L) | 6/5 |
| Number of visits ($\mu \pm \sigma$)<br>Range (min/max) | 10.9 ± 4.78<br>1/16 |
| Months post-stroke ($\mu \pm \sigma$)<br>Range (min/max) | 22.4 ± 14.9<br>7/54 |
| C-M arm score ($\mu \pm \sigma$)<br>Range (min/max) | 3.13 ± 7.5<br>3/7 |
| $\mu$ = Mean, $\sigma$ = Standard deviation, min = Minimum, max = Maximum. M = Male, F = Female, R = Right, L = Left. | |

Subjects were admitted to the study based on satisfactory performance in testable performance criterion of in functional assays, and sufficient stamina to complete the MAST movement protocols was established prior to inclusion (Chapter 1).

### 6.3.2 Signal processing and curve matching

Goniometric data were smoothed with a low-pass Butterworth's filter ($2^{nd}$-order, 12 Hz cutoff), and divided into single cycles of flexion-and-extension, i.e. departure and return to maximal extension (elbow angle ~ 0°), automatically by a thresholded local minima, as described previously (Section 4.3.2). Six archetypal curve types, including linear and variously non-linear trajectory approximants were exhaustively matched to the observed trajectory signal in order to find the single best match for each trace over all six models. From each of these single Essential Trajectory (ET) results, and the single ET for which the greatest proportion of a dataset could be represented was extracted as the Principal Trajectory (PT).

### 6.3.3 Degenerate behavior via scree analysis

The models for which a large, but sub-maximal proportion of the dataset could be described yielded the set of significant trajectories (ST), as determined by a scree analysis. From these ST sets, analyses into the stability of movement themes could be quantified by the number of datasets for which | ST | = 1, as well as the average number of STs. Furthermore, trajectory trends in both movement directions were characterized by analysis of the ST sets in flexion and extension. Finally, correlational analyses were performed among degenerate datasets (those for which | ST | > 1), in order to determine the influence of basic movement parameters on SJT shape.

## 6.4 Results: Principal Trajectory analysis

### 6.4.1 Curve matching method equally accurate for stroke SJTs

Despite the apparent prevalence of higher-order noise in the stroke patient's trajectory traces, the goodness-of-fit of the Essential Trajectory waveforms found through the curve-matching process was high: $R^2 = 0.99 \pm 0.01$. Thus, one immediate conclusion can be drawn: that the curve matching paradigm proposed in this document is robust to moderate impairment, as found in the affected arms of hemiparetic individuals.

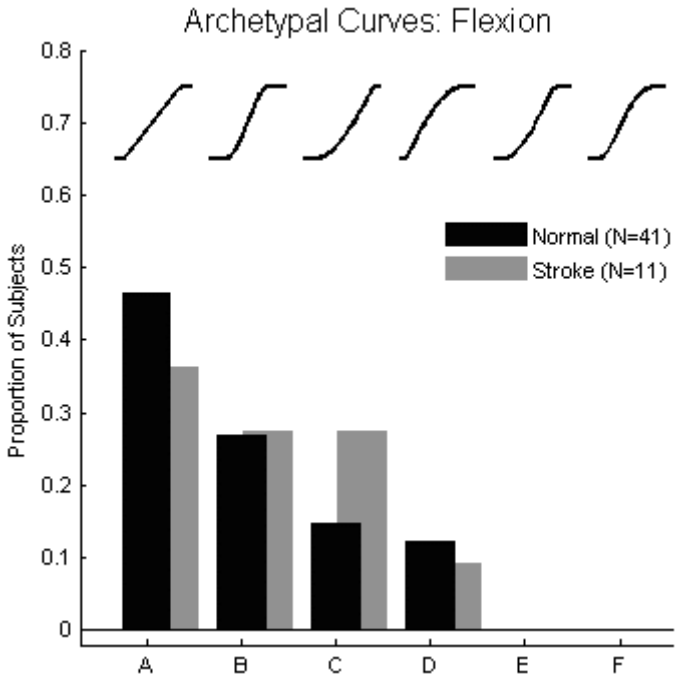


Figure 16 Distribution of flexion Principal Trajectories for both cohorts.

### 6.4.2 Stroke trajectory choices mirror those of normal subjects

In flexion tasks, the linear curve trace was the single-most prolific, i.e. the Principal Trajectory, in 36% of subjects, greater than sigmoidal (27%), quasi-concave

(27%) and quasi-convex (9%). Figure 16 shows the distribution of subjects for whom each trace was observed to result the PT. Here, the distribution of PTs (shown for stroke subjects in grey) is nearly identical to those of the healthy subjects (black).

For extension tasks, again the distribution was ordered identically, and nearly identical in composition to that of the healthy control subjects (Figure 17). To put this into context, consider that there are 6 possible traces from which a single PT could be "chosen." In this way, there are 6! orderings among the archetypal curve types. For the PT distribution in stroke subjects to match those of the healthy subjects, thus involves a 1-in-6! ≈ 0.0014 occurrence by chance, Here again, the order of trajectory models in extension matched those of flexion identically, itself an equally unlikely event to happen by random assignment[18].

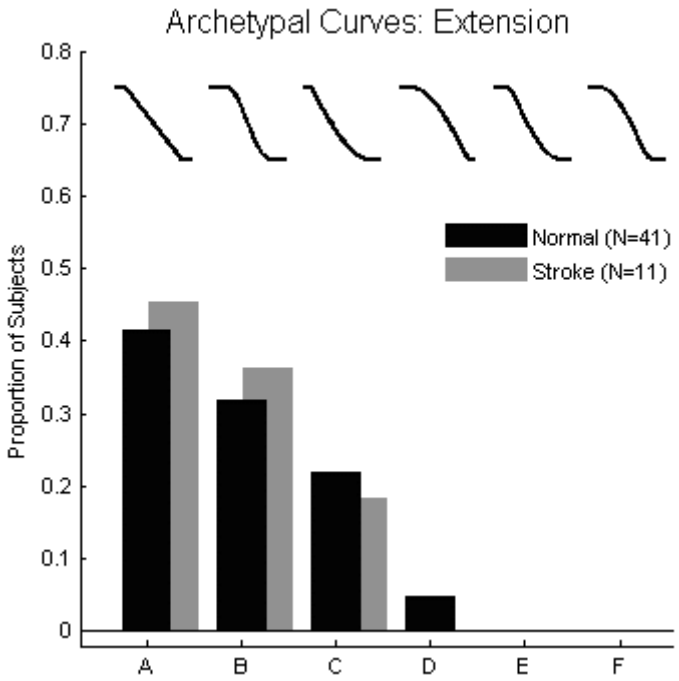


Figure 17 Distribution of extension Principal Trajectories for both cohorts.

[18] It is acknowledged that whereas only 4 of the six trajectory models were observed to yield PT, it is reasonable to ignore the sigmo-convex and sigmo-concave models from this interpretation of the low probability of identical random arrangements of PT distributions, increasing the probability to 1-in-4! ≈ 0.04.

## 6.5 Results: Degeneracy, directionality analysis

### 6.5.1 Stroke subjects are equivalently degenerate to unimpaired

#### *6.5.1.1 Within-subjects analysis*

A broken-stick scree analysis of stroke subjects Essential Trajectory distribution profiles revealed a degenerate movement profile in stroke subjects. ST distributions are shown in Figure 18.

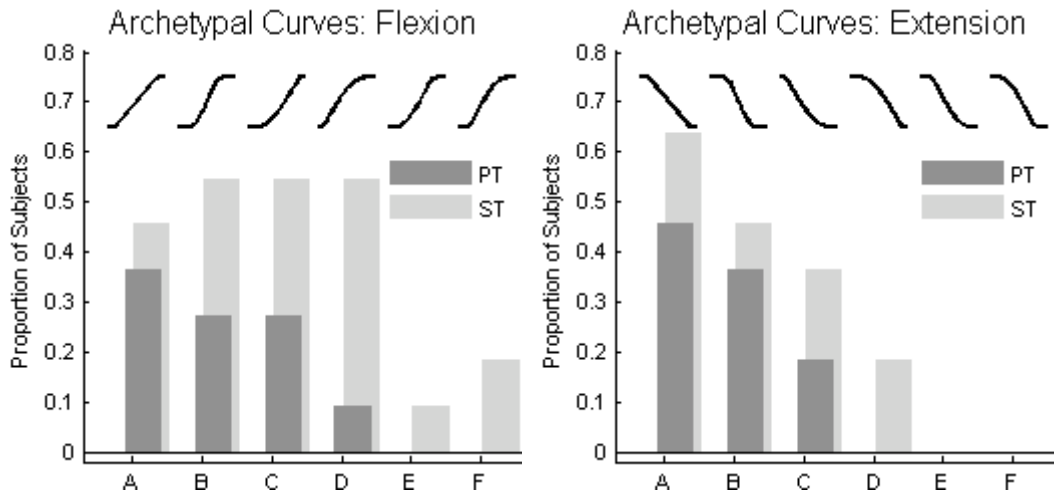


Figure 18 Distribution of stroke cohort Principal and Significant Trajectories.

On average, subjects' ST sets contained 2.36 ± 1.12, with only 3 subjects yielding datasets that were not degenerate in longitudinal analysis (Table 18).

| Table 18: Flexion trajectory degeneracy: Stroke subjects (N = 11) | | |
|---|---|---|
| Model Set Parameter | Value ($\mu \pm \sigma$) | Comparison normal (Table 12) |
| \|ST\| ($\mu \pm \sigma$) | $2.36 \pm 1.1$ | ≈2.02 |
| \|ST\| = 1 (proportion) | 0.27 | ≈0.24 |
| PT proportion | $0.48 \pm 0.18$ | ≈0.49 |
| ST = Significant Trajectory, \|ST\| = ST set cardinality, PT = Principal Trajectory. | | |

These findings were not significantly different from those of the healthy subjects c.f. (Table 12), however, these figures do represent a significant departure from the baseline hypothesis of | ST |=1 for all individuals.

#### *6.5.1.2 Between-sessions analysis*

Whereas ten of the 11 subjects performed single-joint articulations in multiple sessions, a session-by-session analysis was performed in order to determine the variability of trajectory themes day-to-day. Here, only modest decrease was observed in the degeneracy of single-day ET profiles, suggesting that there was not a significant increase in profile variability solely due to observation over multiple visits.

| Table 19: Flexion trajectory degeneracy: Within-session analysis (N = 120) | | |
|---|---|---|
| Model Set Parameter | Value ($\mu \pm \sigma$) | Comparison to normal (Table 13) |
| \|ST\| ($\mu \pm \sigma$) | $1.93 \pm 0.46$ | ≈1.93 |
| \|ST\| = 1 (proportion) | 0 | ≈0 |
| PT proportion | $0.52 \pm 0.17$ | ≈0.53 |
| ST = Significant Trajectory, \|ST\| = ST set cardinality, PT = Principal Trajectory. | | |

These results are not significantly different from those of healthy subjects c.f. (Table 13).

### 6.5.2 Stroke subjects equivalently predictive in extension

Here, as with flexion tasks, the Essential Trajectory profiles resulting from curve-matching of extension traces was found to be degenerate, with an ST set cardinality significantly greater than 1, and only 36% percent of subjects with a single ST (Table 20). Though there was a large difference across movement directions in terms of the trajectory degeneracy for stroke subjects ($1.63 \pm 0.50$ in extension, versus $2.36 \pm 1.12$ in flexion), the large variability among subjects prevented significance at the $P < 0.05$ level (Wilcoxon rank-sum). As with flexion tasks, the difference between cohorts failed to reach significance, with a degeneracy between 1.5 and 2 STs.

| Table 20: Comparative degeneracy of extension: Within-subjects (N = 11) | | | |
|---|---|---|---|
| Model Set Parameter | Value | comparison to Table 18 | comparison to normal (Table 14) |
| $\|ST\|$ ($\mu \pm \sigma$) | $1.63 \pm 0.50$ | ≈2.36 | ≈1.92 |
| $\|ST\| = 1$ (proportion) | 0.36 | ≈0.27 | ≈0.31 |
| PT proportion | $0.52 \pm 0.13$ | ≈0.48 | ≈0.56 |
| ST = Significant Trajectory, $\|ST\|$ = ST set cardinality, PT = Principal Trajectory. | | | |

Here again, the Principal Trajectory models typically accounted for half of all SJT traces.

### 6.5.3 Prediction across movement direction

An analysis of ST set composition in flexion and extension tasks revealed low prediction between directions of movement. Principal Trajectories in flexion matched those in extension in only 3 subjects (27%), which is approximately the same as the 1-in-4 chance found among healthy subjects (c.f. Table 15).

| Table 21: Directional prediction of PT and ST: Within-session (N = 140) | | |
|---|---|---|
| Model Set Parameter | Value | Comparison to normal (Table 15) |
| $PT^f = PT^e$ | 0.5 | ≈0.24 |
| Average ST overlap $\overline{O}$ | 0.44 ± 0.30 | ≈0.39 |
| Unity ST overlap $O_1$ | 0.08 | ≈0.41 |
| Null ST overlap $O_0$ | 0.25 | ≈0.09 |
| ST = Significant Trajectory, \|ST\| = ST set cardinality, PT = Principal Trajectory. | | |

ST sets in flexion and extension were found to have only modest intersection ($\overline{O}$ = 0.44 ± 0.31), and in only 3 subjects were the ST sets found to completely intersect ($O_1$ = 0.27). One subject yielded completely independent ST datasets (Table 21). As before, these results were comparable to the similar analyses performed on healthy subjects.

### 6.5.4 Correlation to basic movement parameters

In order to determine whether the class of ideal comparison trace best-fit to the observed SJT (the ET) was influenced by angle of motion onset, the average movement velocity, or the sequence of movement, a measure loosely analogous to

learning, fatigue, or adaptation, Wilcoxon signed-rank tests were performed on each degenerate dataset in both flexion (97 of 120 sets) and extension (82 sets).

| Table 22: Correlation of ET model to movement parameters: Degenerate sessions | | | | |
|---|---|---|---|---|
| | Flexion N = 97 sets | | Extension N = 82 sets | |
| Movement parameter | Value | comparison to normal (Table 16) | Value | comparison to normal (Table 16) |
| $\bar{\dot{\theta}}$ (proportion) | 0.13 | 0.14 | 0.07 | 0.12 |
| $\theta_{on}$ (proportion) | 0.05 | 0.09 | 0.07 | 0.12 |
| # of repetition (proportion) | 0.10 | 0.09 | 0.10 | 0.10 |
| $\bar{\dot{\theta}}$ = Average angular velocity, $\theta_{on}$ = Angle of motion onset. | | | | |

Similar to results observed in healthy subjects' degenerate datasets, there was little correlation to these variables, according to the low proportion of sessions yielding significance at the $P < 0.05$ level. Here, average velocity was most frequently correlated to curve type in flexion tasks (significance in 13% of sessions), with cycle sequence showing correlation in 10% of sessions in both flexion and extension movements (Table 22).

### 6.5.5 Stroke subjects significantly more symmetric

In addition to a marginal increase in the apparent preference of stroke patients for symmetric Essential Trajectories, a quantitative analysis revealed a significantly greater symmetry as measured by the time to maximum flexion. In terms of the ratio of time spent in acceleration versus deceleration, however, stroke subjects' flexion motions were equally asymmetric with respect to that of healthy individuals, however

the nature of this asymmetry was opposite: considerably greater time spent in acceleration in the case of impaired movement.

| Table 23: Symmetry comparison ETs recorded from stroke subjects (N = 11) | | |
|---|---|---|
| Metric | Value ($\mu \pm \sigma$) | Comparison to normal (Table 8) |
| Time to maximum angular velocity $\tau_{\dot{\theta}_{max}}$ | $0.51 \pm 0.16$ | >0.39, $P < 0.01$ |
| Symmetry ratio $\Gamma^{\ddot{\theta}}$ | $0.93 \pm 0.23$ | >0.71, $P < 0.001$ |

Though not explicitly reported here, similar results were found in extension tasks.

## 6.6 Movement pattern variability: Standard measures

### 6.6.1 Variance Ratio

The finding of degenerate model sets in healthy and stroke subjects contradicts the notion of highly stereotyped trajectory paths, which is a central assertion in several thrusts of motor research (Wolpert, Ghahramani et al. 1995). However, that the matching of Essential Trajectories is a categorical metric, while illuminating for its assignment of trajectory shape as having one specific morphology chosen from among a finite set, is somewhat limited in its ability to quantify the variability in SJT formation. For instance: all movement cycles in a single dataset could assume a precisely linear shape, but at a variety of different speeds, or from different starting points. These factors will strongly influence the trajectory patterns, irrespective of the essential movement pattern.

In order to quantify the cycle-to-cycle variability of an individual's single-joint trajectory record, the variance ratio was calculated for subjects' longitudinal datasets (Equation 17). The variance ratio reports the variability of a collection of temporally-normalized waveforms from 0 (identical signals) to 1 (noise). Here, healthy subjects were observed to move with relatively high stability across all repetitions in both flexion (VR = 0.09 ± 0.05) and extension (VR = 0.07 ± 0.03) tasks. Stroke patients, however, moved with considerably greater variability from cycle to cycle: VR = 0.32 ± 0.24 (flexion), and VR = 0.34 ± 0.21 (extension), which was significantly greater than the healthy cohort: $P < 0.01$ (Wilcoxon rank-sum).

### 6.6.2 Fluctuation in basic movement parameters

That stroke patients' SJTs are so highly variable, as reported by the Variance Ratio, and yet not significantly more degenerate than the healthy subjects' model-matched sets, suggests the need for an investigation into which specific parameters of the trajectory trace are more variable among the stroke patients. Thus, an analysis was performed on the variability of the two non-trivial movement parameters discussed elsewhere: average velocity $\bar{\dot{\theta}}$, and end-point position $\theta_{on} + \Delta\theta$. Under the hypothesis that stroke patients greater variability results from one of these parameters, it a Wilcoxon rank-sum test was performed comparing cohorts for parameter variation equivalence. Here, parameter variability φ is defined as the ratio of the variance to the mean. For parameter $\gamma$, this is expressed as

$$\varphi = \frac{\sigma_\gamma}{\mu_\gamma}.$$

As a cursory measure of performance difference between movement directions, the ratio of average speed in flexion was measured against the average speed of extension, presuming that their ratio would equate to the identity.

| Table 24: Comparison of movement parameter variability within-sessions | | | | |
|---|---|---|---|---|
| Parameter | | Healthy (N = 41) | Stroke (N = 11) | Comparison |
| Average velocity $\bar{\dot{\theta}}$ | Flexion | 0.00 ± 0.00 | 0.19 ± 0.14 | $P < 0.001$ |
| | Extension | 0.04 ± 0.01 | 0.19 ± 0.14 | $P < 0.001$ |
| End-point position $\theta_{on} + \Delta\theta$ | Flexion | 0.13 ± 0.04 | 0.03 ± 0.04 | →← |
| | Extension | 0.13 ± 0.05 | 0.09 ± 0.10 | ≈ |
| $\bar{\dot{\theta}}$ Flex:Ext | (ratio) | 1.08 ± 0.08 | 1.06 ± 0.08 | ≈ |
| All values (μ ± σ). →← = significance, in contradictory direction. Flex = Flexion, Ext = Extension. | | | | |

This variability analysis revealed a strongly suggestive result: that although the end-point error was approximately equivalent between cohorts, and indeed- was significantly reduced in stroke patients, at the $P < 0.05$ level, as indicated by the contradiction arrows in Table 24, the average velocity was significantly more variable within the stroke patients' datasets, whereas there was almost zero fluctuation in the velocity of healthy subjects' movements. Whereas flexion movements were performed with a significantly greater average velocity (6-8% faster than extension movements, $P < 0.001$), this was not significantly different between cohorts.

## 6.7 Summary

The present analysis served to validate the Essential Trajectory movement pattern extraction paradigm in cohort analysis, on the basis of a near-perfect goodness-of-fit. However, beyond method validation, the ET sets serve as new

substrates by which impairment can be described in the stroke cohort. Here it was shown that the distribution of Principal Trajectories was essentially identical in stroke patients, as healthy individuals, and that the ET sets were equivalently degenerate, meaning that the movement themes were pluralistic, but not significantly more so than healthy subjects, regardless of the domain of analysis: within-subjects, between-sessions, flexion or extension. However, variance ratio analysis showed a significantly more variable trajectory dataset in stroke patients. This variability was attributed to a large cycle-to-cycle variation in average movement velocity, which yielded significantly greater variability in stroke patients; end-point error was low in both groups. It is suggested that another possible source of SJT variability may be the dispersion of arrest periods, as will be presented in Chapter 7.

# 7 RATERS OF MOTOR PERFORMANCE

## 7.1 Introduction

In Chapter 3 a method was presented whereby the raw trajectory record was substituted for an idealized SJT surrogate, the Essential Trajectory (ET), which eliminates the noise associated with data acquisition, data processing, or spurious behaviors not associated with the essential motor plan. The ET thus eliminates errors associated with conditioning of the measurement substrate. The following chapters address the second major source of error in measuring motor performance: formulation of the metric by which the substrate is evaluated. A novel metrical analysis will be described, primarily for application to trajectory traces where spontaneous behaviors are not only prevalent, but the primary object of measurement.

Here, a critical analysis of widely-used smoothness metrics is conducted in the form of a review of the pertinent literature. A *fundamental theorem* of movement smoothness is proposed as a basic and universal tenet of what ought resemble a proficient motor activity, and several examples will be presented to illustrate fundamental shortcomings of smoothness raters commonly incorporated into clinical and laboratory research.

## 7.2 Fundamental theorem of movement smoothness

### 7.2.1 General definition

In addition to basic kinematical parameters of voluntary movement (e.g. range of motion, maximum velocity, average velocity, etc.), trajectory *smoothness* is often evaluated in biomechanical performance assessments. Though no standard formulation of movement proficiency exists, it is generally accepted that smooth

movements contain a minimum of transient accelerations. We define a fundamental theorem of movement smoothness as

| | |
|---|---|
| *A smooth movement is that which exhibits a minimum of accelerative transience.* | (Theorem 1) *Smoothness.* |

Various raters have been proposed as quantifiers of movement smoothness. Several such smoothness metrics are presented in Table 25.

Table 25: Smoothness raters

| Metric | Formulation | Source |
|---|---|---|
| Average Jerk | $\bar{J} = \frac{1}{T}\int_0^T \left( \left(\frac{d^3x(t)}{dt^3}\right)^2 + \left(\frac{d^3y(t)}{dt^3}\right)^2 \right) dt$ | (Flash and Hogan 1985) |
| Velocity Peaks | $\pi_{\dot{\theta}} = \sum \left[ \frac{d}{dt}\left(\mathrm{sgn}(v)\right) > 0 \right]$ | (Rohrer, Fasoli et al. 2002) |
| Mean Arrest Period Ratio | $MAPR = \frac{1}{T}\sum_t (v < \delta)$ | (Beppu, Suda et al. 1984; Hogan, Krebs et al. 2006) |
| Weaving Ratio | $WR = {}^{vel\ length}\!/_{SLP\ length}$ | (Beppu, Nagaoka et al. 1987) |
| Velocity Variance | $\sigma_{\dot{\theta}}^2 = \sum \frac{(v-\bar{v})^2}{T-1}$ | (Doeringer and Hogan 1998) |

Though these measures of motor proficiency are often used interchangeably, their respective formulations present a set of trace manipulation and feature extractions. Indeed, for each smoothness rater, there several parameters to consider in terms of data analysis and subsequent interpretation.

### 7.2.2 Basic principles of smoothness measurement

Each smoothness metric measures motor performance according to a unique cost function associated with the SJT trace. Many metrics require a data transformation such as differentiation with respect to time, or complex evaluative operations, e.g. integration under a curve. Thus, in the family of smoothness metrics, descriptors can be grouped according to their *substrate*, i.e. the trace domain: angular position in time, velocity, acceleration, or higher-order trace, etc., their *feature* of evaluation: the number of trace peaks, percentage of trace above a set threshold, area under the curve, etc., and their *operation:* discrete summation, ratiometry, integration, etc.[19]. The myriad possible substrate-feature-operation combinations available for evaluation of motor performance allows for a wide variety of smoothness measures, among which there is some risk for non-uniformity.

## 7.3 Counter-intuitive rater behavior

### 7.3.1 Failure to discriminate obviously impaired cohorts

Smoothness is used as an index of motor performance in both healthy subjects and persons with stroke (Trombly 1993; Platz, Denzler et al. 1994; Kahn, Lum et al. 2006), however, it is not uncommon for some metrics to fail to discriminate between healthy and afflicted individuals (Archambault, Pigeon et al. 1999; Goldvasser, McGibbon et al. 2001; Rohrer, Fasoli et al. 2002; Cozens and Bhakta 2003). The reasons for this counter-intuitive metrical behavior, especially considering the obvious motor impairments of the involved cohorts, are not well-known, and have been variously attributed to the merit of the rater itself, noise in the trace, and even to an over-estimation of the true level of disability of the recruited patients.

[19] Additionally, it is possible to discriminate according to *output*. Discrete sums yield non-negative integers, ratiometry and integration yield real numbers. Such a distinction may be necessary depending on the specific design requirements for metric resolution.

### 7.3.2 Metrical contradiction

Whereas each smoothness rater presents its own evaluation of the trajectory, subject to a unique set of constraints, it is not uncommon to incorporate multiple performance measures into a single kinesiological study. Here, there is risk of some metrics exhibiting contradictory behavior (Rohrer, Fasoli et al. 2002). A simple example will example the occasion for contradiction among smoothness raters.

Consider a simple ideal sigmoid over which a low jerk score is likely. Modifying this trace by the addition of two independent Gaussian features at various regions of the trace simulates a pair of spontaneous accelerations in the execution of a single-joint flexion motion, at proximal and distal reach. This trace is expressed generally by

$$y(t) = \sin(t) + A \cdot e^{-k(t-0.01\alpha)^2} + B \cdot e^{-k(t-0.01\beta)^2} \Big|_{-\frac{\pi}{2} \le t \le \frac{\pi}{2}},$$

where the "noisy" features are parameterized by [ A, B, α, β ]; let $k = 10^4$.

Inserting a single ridge into the otherwise smooth sigmoid, according to [ 0, 0.1, 0, 3π ] increases the number of peaks in the velocity profile $\pi_{\dot{\theta}}$ from 1 to 2, yielding a Mean Arrest Period Ratio of 0.202. Moving this ridge to a different position in the trace, simulating an acceleration at a position proximal to the torso via [ 0.1, 0, 3π, 0 ], the number of velocity peaks remains the same, but MAPR decreases to 0.172. Re-introducing the first perturbation, but reducing peak amplitudes ($\left\lfloor 0.1 \cdot \frac{\sqrt{2}}{2}, 0.1 \cdot \frac{\sqrt{2}}{2}, 0.3\pi, 0.3\pi \right\rfloor$), the MAPR returns to 0.202, despite the additional peak in the velocity profile. In all three cases, average jerk is approximately the same: $\bar{J} = 2.02 \times 10^{-6}$ (Table 26).

| Table 26: Metrical contradiction among smoothness raters | | | |
|---|---|---|---|
| Metric | $[0, 0.1, 0, 0.3\pi]$ | $[0.1, 0, 0.3\pi, 0]$ | $\lfloor 0.1 \cdot \frac{\sqrt{2}}{2}, 0.1 \cdot \frac{\sqrt{2}}{2}, 0.3\pi, 0.3\pi$ _ |
| $\bar{J}$ | $2.02 \times 10^{-6}$ | $2.02 \times 10^{-6}$ | $2.02 \times 10^{-6}$ |
| $\pi_{\dot{\theta}}$ | 2 | 2 | 3 |
| *MAPR* | 0.202 | 0.172 | 0.202 |
| $\bar{J}$ = Average jerk, $\pi_{\dot{\theta}}$ = Number of peaks in the velocity trace, MAPR = Mean arrest period ratio (10%). | | | |

The traces corresponding to these parameter sets are shown in Figure 19.

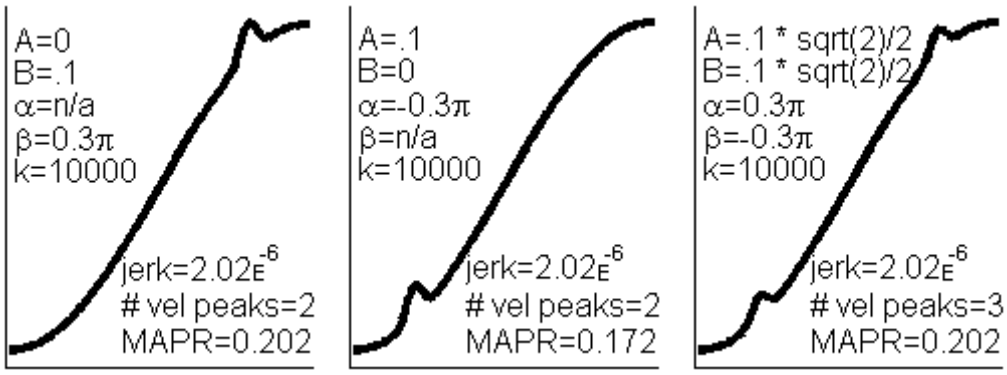


Figure 19 Metrical Incongruence: Perturbation of ideal sigmoidal trajectory with parameterized noise, yields contradictory smoothness metric behavior.

It is thus demonstrated that in some cases the relationship among smoothness metrics is neither predictable, nor congruent. In any assessment of empirical contradiction, determination of the erroneous elements is a difficult task: which rater is *modus errare*, and which is behaving *ad ferenda*, These simulated results suggest that an experimental analysis of this metric is warranted.

## 7.4 The jerk profile

Whereas acceleration is the essential variable of inertia-based control systems, its rate of change (i.e. jerk) is a standard measurement substrate in the assessment of movement smoothness. Jerk, however, is a function of time, and therefore not configured to report motor proficiency directly: scalar descriptors of this trace must be defined.

$$J(t) \equiv \frac{d}{dt}\left(\ddot{\theta}(t)\right) = \frac{d^3}{dt^3}\theta(t) \qquad \text{(Equation 19)}$$

Several indices of movement smoothness have been proposed, evaluating various features of the jerk signal, many of which are predicated on the area under the Jerk curve (Table 27).

Table 27: Jerk metrics

| Metric | Formulation | Source |
|---|---|---|
| Integrated Average Jerk (IAJ) | $IAJ = \int_0^T \left(\frac{d^3}{dt^3} x_i(t)\right)^2 dt$ | (Goldvasser, McGibbon et al. 2001) |
| Average Jerk (AJ)[20] | $AJ = \frac{1}{T}\int_0^T \left(\frac{d^3}{dt^3} x_i(t)\right)^2 dt$ | (Feng and Mak 1997) |
| Jerk Metric (JM)[21] | $JM = \mp\int_0^T \left(\frac{d^3}{dt^3} x_i(t) \cdot \frac{1}{\max \frac{d}{dt} x_i(t)}\right)^2 dt$ | (Rohrer, Fasoli et al. 2002) |
| Normalized Average Rectified Jerk (NARJ) | $NARJ = \frac{T^3}{T'^3}\left[\frac{1}{T}\int_0^T \left(\frac{d^3}{dt^3} x_i(t)\right)^2 dt\right]$ | (Cozens and Bhakta 2003) |

[20] The nomenclature employed herein is consistent with the literature. For the reason that different researchers name their metrics in the context of their development, descriptor names may not observe a

As can be seen, the above metrics differ primarily in their method of normalization: none, to time, and to velocity.

## 7.5 Jerk as a measure of movement proficiency

Previous attempts to track recovery from neurological impairment via jerk-based metrics have yielded inconclusive and sometimes counter-intuitive results. In training of thirty-one patients in a robotic therapy device, for example, and subsequent evaluation via five different smoothness metrics, four metrics reported a uniform improvement in movement coordination: the number of peaks in the speed profile, a ratiometric index of the peak speed to average speed, average movement speed, and the mean arrest period ratio (MAPR). The jerk metric (JM), however, curiously increased with training (Rohrer, Fasoli et al. 2002).

This contradictory result was attributed to the blending of submovements, discrete movement segments with a possibly invariant shape of which a small number (presumed to be two or three) comprise an single motion unit (Krebs, Aisen et al. 1999). A simulation was performed, convolving two fabricated Gaussian "submovements," assessing the JM as a function of curve overlap. It was reported that as these submovements blended, i.e. approached one another, the period of rest (the space between them) is shortened, increasing average jerk, decreasing smoothness. It is concluded that "at least during post-stroke recovery, jerk minimization may not be the primary criterion governing refinements in movement patterns," (Rohrer, Fasoli et al. 2002).

Sub-movements were also cited as an explanation for the failure of integrated average jerk (IAJ), to discriminate between seventeen cerebellopathy (CB) patients

---

logical or intuitive relationship. For instance, IAJ is so-called for its averaging across many repetitions; AJ reflects the averaging over time.

[21] The negative sign is convention employed to make JM a rater of *smoothness*, and not dysfunction.

and seventeen healthy control subjects at the $P < 0.05$ level .(Goldvasser, McGibbon et al. 2001). Here, the primitive neural activation commands, present in CB, and thought to underlie sub-movements, are considered to be more pronounced. These sub-movement activities are thought to reflect an internal jerk minimization process, applied not to the global movement, but to movement segments (sub-movements). Objective quantification of the form and process of sub-movements has not been demonstrated, despite a century from the original suggestion of their synthesis resulting in the observed continuous movements (Krebs, Aisen et al. 1999).

## 7.6 Jerk normalization

### 7.6.1 Need for normalization

In general, it is not the absolute average velocity with which an individual moves that is important to the evaluation of motor proficiency, but the inherent *smoothness* of the motion, irrespective of whether it was performed at a fast or slow pace. For example, a healthy human moving at a fairly rapid pace of 1 flexion-extension cycle per second should be scored equally by a jerk metric on equal smooth repetitions performed at half pace.

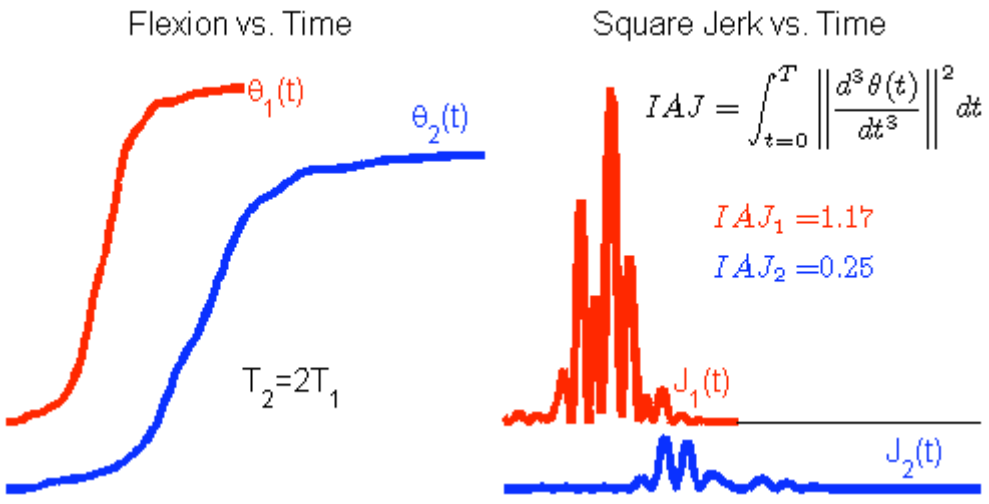


Figure 20 Need for jerk normalization jerk: Trajectory $\theta_1$ ($\theta_2$: $T_1 \rightarrow T_2=2T_1$ *Left*) yield disparate jerk profiles, skewing jerk according to average velocity (*Right*).

Figure 20 illustrates this scenario: ostensibly identical angular trajectories, to within a velocity scaling factor, yield jerk traces with similar morphologies, but scaled to different height and width. This transformation is not necessarily area conservative, and has been shown to artificially decrease non-normalized average jerk scores such as variants of IAJ, with increased duration (Cozens and Bhakta 2003).

### 7.6.2 Jerk normalization to total movement duration

Common to most scalar jerk metrics, either in combination with or in place of other normalization schema is an adjustment for total time of movement *T*. Division by total time serves two primary purposes: 1) to endow the metric with units: area under the curve is dimensionless, division by time gives a performance-score-per-unit-time of movement, and 2) to eliminate variability according to movement duration: it has been shown (here, and elsewhere (Rohrer, Fasoli et al. 2002; Cozens and Bhakta 2003), that identical movements performed at different paces yield drastically different integrated jerk values: $\theta_2 : T_1 \rightarrow T_2 = 2 \cdot T_1 \;\; \Rightarrow \;\; J_2 = \frac{1.7}{0.25} J_1$ (Figure 20).

In terms of scale adjustment, there are two essential shortcomings to a temporal normalization. Of primary concern is the uncertainty in the effect of movement speed on jerk: with decreased average velocity, i.e. greater *T*, it is not well-established whether jerk is prone to artefactual increase or decrease, and the dependence on the sign and magnitude of the effect vis-à-vis other movement parameters.

A further and more subtle counter-argument to the temporal normalization of jerk metrics becomes apparent in the evaluation of highly spastic movements. A spastic individual has a tendency to produce stop-and-go movements that are alternately still and swift, uncontrolled motion (Nielsen, Andersen et al. 1998). Thus, a spastic movement is likely to contain regions of *stall behavior*.

*A stall is any period within a movement sequence where the absolute velocity is below a given velocity threshold.* (Definition 5) *Stall.*

Stall behavior is traditionally quantified using the mean arrest period ratio (MAPR), the proportion of total movement time spent at a sufficiently low velocity, irrespective of movement direction (Beppu, Suda et al. 1984):

$$MAPR = \frac{\sum \left| \dot{\theta}(t) \right| < \delta}{T}, \qquad \text{(Equation 20)}$$

where $\delta$ is an arbitrarily small threshold velocity here set to 10% maximum velocity.

Take, for example, and arbitrary sample flexion executed by a neurologically intact subject (Figure 21). The jerk profile, resulting from two differentiations of the velocity profile, yields some IAJ score (here IAJ = 1.27).

Inserting two stall behaviors (instantaneous velocity << 10% maximum velocity), the jerk integral yields the same result: the area under the curve is not affected by the insertion of zero-jerk periods associated with the arrested motion. Scaling the independent variable $T$ to a normalized value, however, alters the jerk-profile in such a way that the integral is reduced in proportion to the increase in stall behavior: protraction of $\theta(t)$ to duration $1.5T$ (with the addition of 2 stalls of duration $0.25T$) decreases $J \rightarrow \frac{2}{3}J$.

Thus, where two identical movements, aside from the insertion of a period of stalled behavior, have equivalent absolute jerk scores, temporal normalization artificially *decreases* the apparent jerk associated with the spastic movement, where equal or greater jerk would be expectation. In this way, if jerk is to be adjusted by some factor, total movement time is not a tenable normalization parameter.

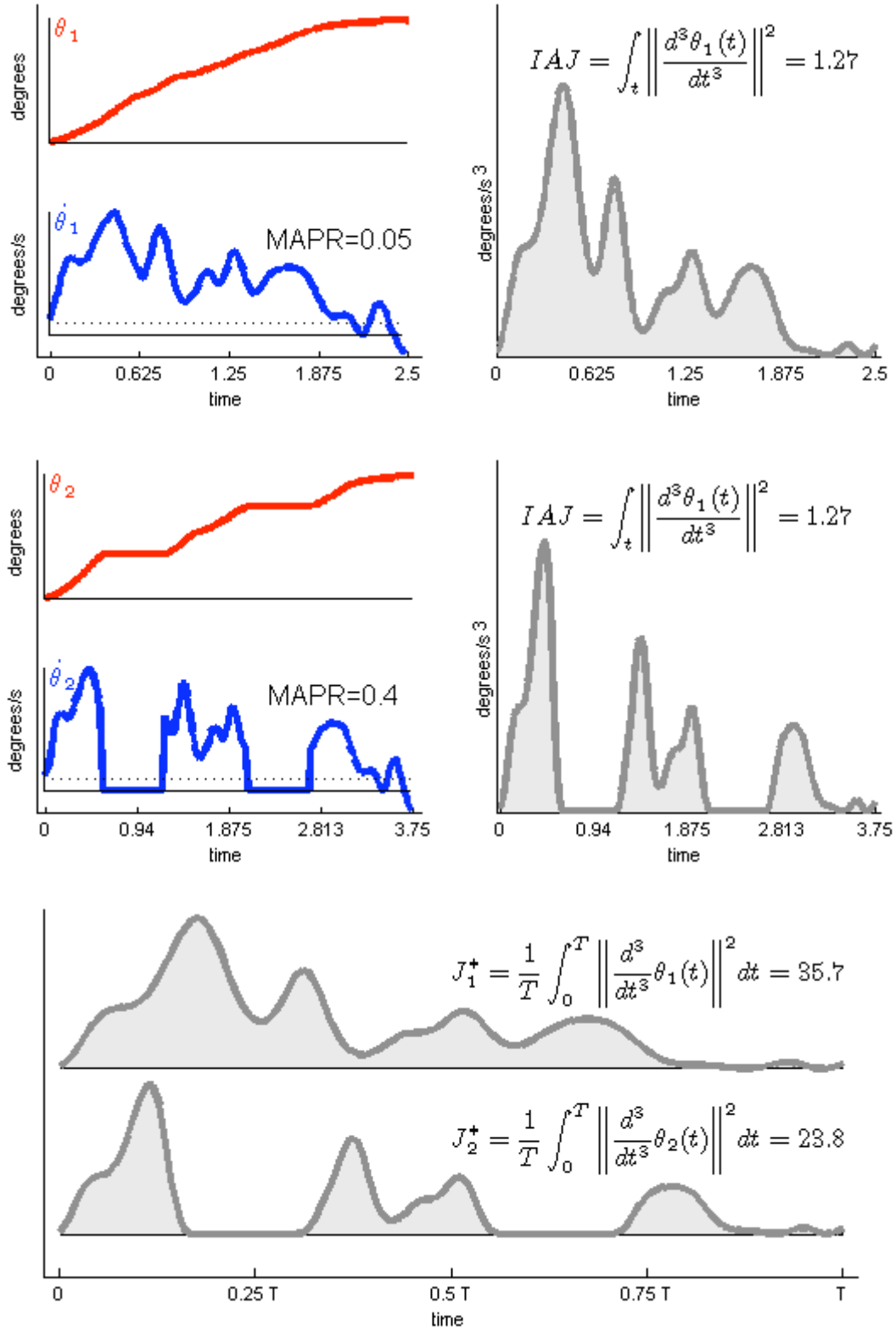


Figure 21 Artefact associated with jerk normalization to time: A sample flexion was assessed for jerk before (*Top, Left*) and after the insertion of simulated stalls (*Middle, Left*).

### 7.6.3 Normalization by peak velocity

By adjusting the jerk trace to peak velocity within each degree of movement freedom, it is proposed that the Jerk Metric accounts for differences in signal size/shape (Rohrer, Fasoli et al. 2002). Whereas this normalization may account for some affine transformations, it is apparent from a previous example (Figure 20), where $\dot{\theta}_2^{\max} = 2 \cdot \dot{\theta}_1^{\max}$, that a simple scale factor is not sufficient to make up the difference between jerk integrals. Despite the algebraic validity of this normalization[22], the peak-velocity normalized jerk does not withstand even simple perturbations of a given profile.

In general, peak velocity is not a particularly robust parameter by which to normalize a biomechanical dataset. Consider two flexion movements, one where a

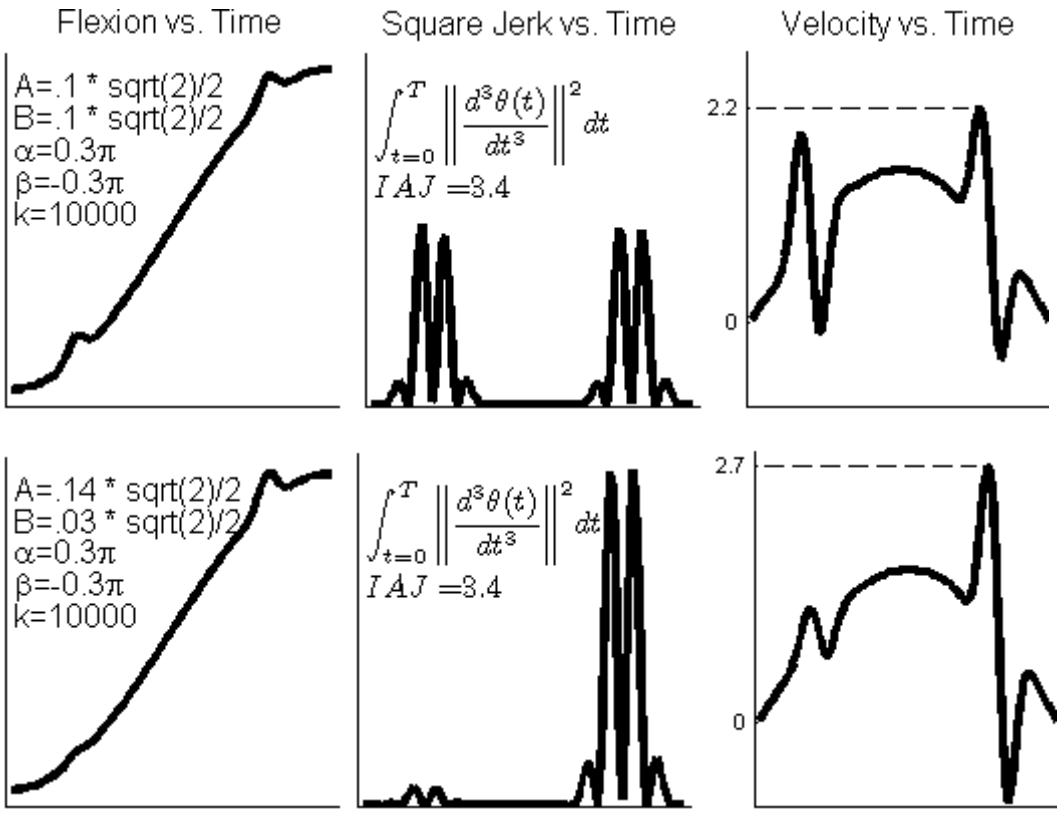


Figure 22 Normalization of the jerk profile by maximum speed is more likely to skew the jerk metric by detection of velocity peaks related to spontaneous accelerations.

moderate jerk is committed at both early and late flexion; one where a minor acceleration is committed early, and severe jerk late (Figure 22).

Ostensibly, the jerk profiles, though considerably different, yield the same integration, suggesting the equivalence of motor performance between the two movements. However, whereas the asymmetric jerk profile results from an asymmetric velocity profile, the single pre-dominant peak velocity will be extracted as the normalization factor for the second movement. Whereas peak velocities will typically be associated with spontaneous and unintentional features of the movement profile, it seems that *average velocity* would make for a much more meaningful scale factor.

### 7.6.4 Normalization by average velocity

A jerk scaling factor based on the average movement velocity has also been proposed (Cozens and Bhakta 2003). This method of normalization avoids spurious peaks in the velocity profile associated with transient accelerations, and is based on the proportional spectral scaling of identical repetitions of differing velocity.

An arbitrary trajectory x($t$) can be phrased as the infinite sum of a series of orthogonal functions of $t$, with coefficients X($\omega$):

$$x(t) = \frac{1}{2\pi}\int_{-\infty}^{\infty} X(\omega)\, e^{i\omega t}\, d\omega ,$$

where

$$X(\omega) = \int_{-\infty}^{\infty} x(t)\, e^{-i\omega t}\, dt ,$$

and $\omega$ is the angular frequency. An identical repetition performed at pace $p = \frac{T'}{T}$, where $T'$ is the duration of the new movement, is likewise expressed as $x' = x(p \cdot t)$ where the Fourier expansion now becomes

$$x'(t) = \frac{1}{2\pi}\int_{-\infty}^{\infty} X(\omega)\, e^{i\omega p t}\, d\omega .$$

Jerk, the third derivative of position, now obeys the chain rule of successive differentiation of exponentials $\frac{d^n}{dt^n} e^{f(t)} = \left(\frac{d}{dt} f(t)\right)^n \cdot e^{f(t)}$:

$$J(t) = \frac{1}{2\pi}\int_{-\infty}^{\infty} X(\omega)\, (i\omega)^3\, e^{i\omega t}\, d\omega$$

and

$$J'(t) = \frac{1}{2\pi}\int_{-\infty}^{\infty} X(\omega)\, (i\omega p)^3\, e^{i\omega p t}\, d\omega ,$$

where $J'(t) = p^3 \cdot J(t)$[23].

The normalized, average rectified jerk (NARJ) proposed by Cozens accounts for average velocity across the entire motion, as opposed to maximum instantaneous velocity, as the Jerk Metric described earlier (Rohrer, Fasoli et al. 2002). However, in

---

[23] Note that this presumes $\int_{-\infty}^{\infty} X(\omega) e^{i\omega t}\, d\omega = \int_{-\infty}^{\infty} X'(\omega) e^{i\omega p t}\, d\omega$, which is valid by the inclusion of the pace factor $p$ in the period arguments of both $x(t)$ (and thus $X(\omega)$) and $e^{iwt}$: $X'(\omega) = \int_{-\infty}^{\infty} x'(t) e^{-i\omega p t}\, dt = \int_{-\infty}^{\infty} x(pt) e^{-i\omega p t}\, dt$, i.e. a shift in frequency of each component by a factor of $p$, with preservation of amplitude Cozens, J. A. and B. B. Bhakta (2003). "Measuring movement irregularity in the upper motor neurone syndrome using normalised average rectified jerk." J Electromyogr Kinesiol **13**(1): 73-81..

the way that $\dot{\theta} \propto T^{-1}$, normalization to average velocity seems equivalently moot to normalization to total movement time.

In the context of jerk as a metric with no clearly defined paradigm for normalization, and a tendency to contradict other smoothness metrics, a metrical validation is warranted wherein each of the four jerk metrics are analyzed for their susceptibility to artifact rooted in basic variables of movement, i.e. movement speed.

## 7.7 Assessment of jerk's metrical validity

### 7.7.1 Study overview

Because movements of persons with compromised motor control are typically slower than healthy individuals, smoothness metrics should be independent of average velocity, and reflect only the intrinsic proficiency of the recorded movement (Cozens and Bhakta 2003).

In order to test the influence on jerk metrics of average movement speed, a correlation study was devised. It was proposed (Section 2.3.2) that jerk metrics may be adequate for "well-behaved," i.e. non-spastic, motions performed by healthy individuals, but become unreliable in the assessment of movement segments containing significant periods of stall activity. Accordingly, two cohorts of subjects were observed in the MAST, performing single-joint elbow flexion motions: a group of healthy volunteers, and a group of individuals with compromised motor control due to chronic stroke (Table 28).

| Table 28: Demography of cohort study: Accelerative transients | | |
|---|---|---|
| | Healthy | Stroke |
| Number of Subjects | 10 | 5 |
| Age ($\mu \pm \sigma$) | 54.9 ± 14.2 | 47.7 ± 20.8 |
| Gender (M/F) | 4/6 | 2/3 |
| Months Post-Stroke ($\mu \pm \sigma$) | 35/6 | 16 ± 8 |
| Chedoke-McMaster Arm Score | 3.1 ± 3.0 | 3.4 ± 0.5 |
| $\mu$ = Mean, $\sigma$ = Standard deviation, min = Minimum, max = Maximum, M = Male, F = Female, R = Right, L = Left. Stroke subjects all right-affected. | | |

### 7.7.2 Study protocol

Subjects were seated with their dominant (or affected) arm in the MAST, and asked to perform as series of autonomous flexions about the elbow at a comfortable, self-selected pace. Visual feedback was of their instantaneous hand position was provided, though not necessarily attended to, as described previously (Section 1.2.2.1). Subjects made a single visit, performing a minimum of 30 repetitions in the MAST.

### 7.7.3 Signal processing and analysis

Goniometric data was bi-directionally filtered with a Butterworth's low-pass filter (-3 db at 7.5 Hz). Repetitions were extracted from the continuous dataset by a thresholded local minimum, and edge effects were removed by truncating angular position data to those loci falling between the repetition onset and cessation, defined as the instant where angular velocity exceeds, and then recedes below, 2% maximum velocity. For simplicity, only flexion movements were considered; extension movements were discarded.

Each repetition was evaluated for two parameters: average movement velocity, and a series of jerk-metrics (Table 27). Traces were differentiated with a point-wise

difference, and filtered with identical characteristics as described above. Average velocity was defined simply as the mean of the filtered trace value, and the Mean Arrest Period Ratio (MAPR) was calculated at 10% maximum velocity. Integration of the square of the triply-differentiated (and iteratively filtered) flexion trace was performed by a trapezoidal integration.

### 7.7.4 Experimental hypotheses

In order to resolve the dependency of the various metrics on average velocity, the correlation between these sets of parameters was assessed on subject means of average velocity $\bar{\dot{\theta}}$ and each jerk metric.

*Standard jerk metrics are independent of average velocity in "well-behaved" movements performed by healthy individuals.* (Hypothesis 9a)

*Jerk metrics exhibit spurious dependence on movement velocity in the special case of spastic movements characterized by significant periods of stall behavior.* (Hypothesis 9b)

The test criterion of correlation between the jerk metrics and average velocity was a Pearson Product Moment Correlation Coefficient $\rho\left(J', \bar{\dot{\theta}}\right)$>0.7, where $J'$ represents one of the four jerk metrics presented in Table 27:

$$\rho\left(J', \bar{\dot{\theta}}\right) = \frac{1}{N-1}\sum_{i=1}^{N}\left(\frac{\bar{J}'_i - \bar{\bar{J}}'}{\sigma_{\bar{J}'}}\right)\left(\frac{\bar{\dot{\theta}}_i - \bar{\bar{\dot{\theta}}}}{\sigma_{\bar{\dot{\theta}}}}\right), \qquad \text{(Equation 21)}$$

where $N$ is the total number of subjects in a given cohort, $\bar{J}'_i$ and $\bar{\dot{\theta}}_i$ are the $i^{\text{th}}$ subject's sessional mean value for jerk metric $J'$ and average movement velocity,

respectively; $\overline{\overline{J'}}$, $\overline{\overline{\dot{\theta}}}$ and $\sigma_{\overline{J'}}, \sigma_{\overline{\dot{\theta}}}$ represent the cohort means and standard deviations of these parameters.

The ability of jerk to resolve cohort differences was tested here with all four jerk metrics.

| | |
|---|---|
| *Jerk metrics can discriminate between healthy individuals and those with impaired motor control due to chronic stroke.* | Hypothesis 10 |

This will be demonstrated with a simple hypothesis test on the difference of means between subject cohorts for each metric.

### 7.7.5 Results: All jerk metrics spuriously correlated to speed

All four jerk metrics were found to exhibit weak dependence $\rho < 0.7$ to average movement speed in the case of healthy subjects, mean velocity (expressed as a proportion of total range of motion per unit time) was faster than the stroke patients, although not significantly so at the $P < 0.05$ level (Table 29). Strong correlations, however, were found between stroke patient jerk scores and average velocity: $\rho > 0.8$.

Table 29: Correlation of jerk metrics to average velocity

| | Avg. Vel. (°/s) | MAPR @ 10% | IAJ | AJ | JM | NARJ |
|---|---|---|---|---|---|---|
| Healthy | 76.0 ± 19.8 | 0.09 ± 0.08 | 0.05 | 0.40 | 0.25 | 0.46 |
| Stroke | 66.6 ± 49.1 | 0.26 ± 0.19 | 0.84 | 0.85 | 0.91 | 0.90 |
| Significance | ≈ | ≈ | | | | |

Avg. Vel = Average velocity, MAPR = Mean arrest period ratio, IAJ = Integrated average jerk, AJ = Average jerk, JM = Jerk metric, NARJ = Normalized average rectified jerk. All values ($\mu \pm \sigma$).

By the reasoning outlined in Section 7.6.2, it is suggested that this strong dependence on movement speed is the result of a significant increase in the stall content of stroke patients' movements ($MAPR_{stroke} \approx 3 \times MAPR_{healthy}$, $P < 0.05$).

### 7.7.6 Results: Jerk metrics do not discriminate between cohorts

Though all jerk metrics reported greater dyscoordination in stroke patients versus healthy subjects, these impairments were not found to be significant at the $P < 0.05$ level using the Wilcoxon rank-sum test (Table 30). This test was used because of the non-normality of the datasets, owing to the small subject pool (5 and 15 subjects, respectively), and demonstrated in the Kolmogorov-Smirnov test (failure to generate KS score <0.05).

Table 30: Metrical results in cohort discrimination task

| | IAJ ($\times 10^{-3}$) | AJ ($\times 10^{-4}$) | JM ($deg/s^2 \times 10^{-3}$) | NARJ |
|---|---|---|---|---|
| Healthy | 12.5 ± 9.1 | 0.9 ± 0.7 | 9.5 ± 7.2 | 15.2 ± 16.7 |
| Stroke | 33.8 ± 32.4 | 4.1 ± 4.7 | 11.2 ± 4.1 | 40.2 ± 21.5 |
| Significance | ≈ | ≈ | ≈ | ≈ |

IAJ = Integrated average jerk, AJ = Average jerk, JM = Jerk metric, NARJ = Normalized average rectified jerk. All values ($\mu \pm \sigma$).

This lack of significance in jerk metric discrimination can be attributed to the high variability of these metrics within cohorts, where the variability ratio $\sigma/\mu$ is typically close to 1, and larger than the difference between group means $\mu_{stroke}$-$\mu_{normal}$. It remains unclear as to why there is such variability among subjects.

## 7.8 Summary

*Smoothness* is generally defined as the lack of accelerative transients in the trajectory record, and is quantified by any number of different proficiency metrics. However jerk-based metrics, despite their wide use in biomechanical applications, are prone to counter-intuitive, and occasionally contradictory behavior. It is shown here that this can be attributed to jerk's incompatibility with metrical normalization to movement time, average velocity, or peak speed. Further, it has been demonstrated both as an exercise, and using SJT data recorded from human subjects, that natural events related to spastic movement may artificially reduce jerk metrics, decreasing its discriminative power among obviously impaired cohorts. These inherent limitations on jerk-based metrics suggest the need for a smoothness measure less labile to basic movement variables.

# 8 TRAJECTORY DOMAIN TRANSFORMATION

## 8.1 Introduction

The previous chapter critically reviewed raters of motor performance, particularly those associated with movement smoothness. In this Chapter, the artifact associated with time-domain analysis of kinematic data is addressed via a transformation of temporal data into the angular domain. Two explicit outcomes of this work are expected: 1) a more accurate rendering of motor performance resulting from the obviation of a potentially noisy differentiation, and 2) a transformation of raw kinematic data into a domain where the independent variable is more relevant to kinesiological analysis.

## 8.2 Rater error introduced in discrete differentiation

In the analysis of trajectory data for information related to the essential motor behavior, noise-related artifact can occur at two junctures: systematic noise associated with the manifest end-effector activity, typically sourced in imperfect execution of the motor intention, and signal noise related to data processing post-hoc. Perhaps the most profound source of processing-induced noise is that of differentiation: many performance metrics predicate on this transformation of temporal data, despite the inherent risk of contamination.

The differentiation of discrete biomechanical data is typically performed via the finite difference method, based on the Taylor series truncated at various orders of the expansion

$$f'(x) = \frac{f(x+\delta) - f(x)}{\delta} + \Theta(\delta)$$

where $\Theta(\delta)$ indicates that the error is of the order $\delta$ (step size) (Hurley 1981). Digital acquisition of continuous data at a sampling rate $v = \delta^{-1}$ presents a trade-off between derivative approximation error (scaling with $\delta$), and representational error (introduced in the rounding of acquired data). The filtering of derivative-associated noise out of the differentiated data, presents a new optimization problem of filter design, for which the most parsimonious solution is simply successive (after each iteration of the derivative) application of a low-pass filter with characteristics identical to those used to smooth the raw positional data (Semmlow 2004). Alternative differentiation methods, such as spline-polynomial differentiation (Hsiang, Chang et al. 1999), and discrete-time observers (Dabroom and Khalil 1999), eliminate artefact associated with the finite difference, but pose separate and unique challenges of optimization. The introduction of noise into the differentiated data competes directly with the analysis of velocity and acceleration waveforms for the determination of movement smoothness.

## 8.3 Performance rater dependence on time is ill-posed

### 8.3.1 Motor performance: time independence

Parameter space both between and within subjects can be highly variable, confounding the analysis of biomechanical performance across the span of the task. In autonomous pointing movements, both average end-effector velocity and the shape of the velocity profile exhibit considerable variation (Levin 1996; Osu, Kamimura et al. 2004); self-pacing of non-targeting rhythmic reaching tasks varies naturally in a way that is partly determined by demography (age, gender, and relative fitness), physiologic state (rest, fatigued, stressed), and cognitive situation (neurological impairment, task attention, and presence and type of feedback), among other variables. In free reaching tasks, time is not necessarily a meaningful performance parameter.

### 8.3.2 Motor performance: angular dependence

Instantaneous joint angle $\theta$ is determined by the sum of torques generated at the flexor and extensor muscles:

$$I\frac{d^2\theta}{dt^2} + B\frac{d\theta}{dt} = T = T_f - T_e$$

where $I$ is the moment of inertia, $B$ is the coefficient of viscosity, and $T$ is the net muscle torque (Lemay and Crago 1996). Torque is primarily a function of stiffness $K$

$$T_i = m_i K_i + b_i,$$

Where $i$ = [ f, e ]. $K$ is a 1st-order LDE (linear in activation $a$) with dependence on motor neuron pool input $u$ :

$$K = f\left(a(t), u(t), \cdots\right).$$

which is scaled by stretch reflex $u_{\text{ifd}}$, a function with dependence on muscle length $L$, velocity $\dot{L}_i$, and several physiologic constants

$$u_{ifd} = f\left(L_i, \dot{L}_i, \cdots\right),$$

$L$ is reflexively determined by the angle spanned by the muscle across the joint, regulating the stretch reflex in a step-wise or zone-like fashion (Lemay and Crago 1996).

### 8.3.3 Increased positional dependence in hemiplegia

Smooth pointing movements are the result of precise execution of a series of activations of the antagonistic muscle pairs across the elbow joint. The stretch reflex (SR) is a mechanoreceptor-driven response to muscle lengthening, and serves to stabilize the joint by restoring antagonistic pairs to an equilibrium position (Voight and Cook 2001). In voluntary movement, this reflex activation is suppressed by reciprocal inhibition of the antagonist, accommodating an unopposed volitional contraction of the antagonist muscle by regulation of the SR. Deregulation of the central commands that coordinate these activations is a primary symptom of neurologic dysfunction: postural instability in hemiparetic individuals may result from either poor coordination of antagonist SR thresholds ─or a lack of detectable activational activity altogether─ within certain loci of the joint's range of motion (Levin and Dimov 1997; Levin, Selles et al. 2000).

## 8.4 Support for performance rater based on joint angle

### 8.4.1 Isogony Principle & the Two-Thirds Power Law

Appropriately constrained single degree-of-freedom may adhere to functional relationships describing force and kinematical observables in terms of task requirements. For instance, error in time to peak grasp force is affected by the time required to reach peak force, and peak force error scales with peak force magnitude (Schmidt's Law, (Schmidt, Zelaznik et al. 1979; Hancock and Newell 1985; van Galen and de Jong 1995)). Furthermore, average movement time for rhythmic reaching between fixed targets increases with the distance between targets, and decrease with the target error tolerance (Fitts' Law (Fitts 1954; Fitts and Peterson 1964)).

Velocimetric parameters also exhibit systematic response to geometrical considerations. In multi-dimensional upper-limb tasks, end-effector velocity has been shown to scale with trajectory curvature (Binet and Courtier 1893; Derwort 1938); for tasks such as handwriting and figure drawing, the comprehensive quantification of this relationship came in the form of the Two-Thirds Power Law (Viviani and Terzuolo 1982; Lacquaniti, Terzuolo et al. 1983):

*For a segment of motion $s$, trajectory radius of curvature $R$ and angular velocity $V$ conform to a power-law relationship*

$$V(s) = K(s) \cdot \left( \frac{R(s)}{1 + \alpha \cdot R(s)} \right)^{\frac{2}{3}}$$

*where K is an arbitrary constant (velocity gain factor), and $\alpha$ is an empirical constant on unity scale.*

(Theorem 2) $\frac{2}{3}$ *Power Law.*

This relationship is not necessarily conserved over the entire movement, but within sequential movement aspects. For instance, in the drawing of a cursive (and thus highly curved) letter, ligatures with similar curvatures will be traced with a similar angular velocity, regardless of character identity or size (Viviani and Terzuolo 1982; Lacquaniti, Terzuolo et al. 1983; Wann, Nimmo-Smith et al. 1988). Thus, for segmented motion, the isogony principle relates movement speed to angular velocity for a given curvature:

*Within a "unit of action," equal angles are transcribed in similar times, even though arc length may vary.*

(Definition 6) *Isogony.*

Though the isogony principle was originally demonstrated in higher-dimensional movements, its validity has been extended to a wider class of movements, including planar movements where the trajectory has no points of inflection (i.e. a single movement segment) (Viviani and Schneider 1991) and movements under mechanical constraint (Viviani and Terzuolo 1982). Thus, it is concluded that for motion constrained to a constant arc, in a device such the MAST, that typical SJTs should appear approximately linear, i.e. as having essentially constant angular velocity.

### 8.4.2 Essential Trajectories suggest basic SJT themes

The isogony principle, and its demonstration in a wide variety of movement protocols, including paradigms similar to those used here, suggests an approximately linear SJT. However, a trajectory curve-matching analysis revealed non-linear Essential Trajectories in many instances (Section 5.5.1). Whereas it is presumed that the protocol was strictly observed, or only sparsely broken, in a random and randomly distributed way, this regional linearity serves as a sturdy axiom by which to base a robust criterion for the assessment of motor smoothness.

### 8.4.3 Fuzzy isogony: regionally straight trajectory curvature

Symmetric and approximately linear angular trajectories of single degree-of-freedom motions are observed in a variety of protocols, and are predicted by empirical law. That mechanical constraint of the forearm into a wide, evenly arced hand path is robust to the 2/3 Power Law validates the assertion of constant angular velocity in the present experiment of self-paced elbow articulation with forearm and upper-arm secured. Indeed, single-joint movements committed by neurologically intact humans

tend to conform to the smoothest possible trajectory (Nelson 1983), which is typically abstracted as a linear or sigmoidal ramp curve (Section 2.1.1).

Within the generalization of global isogony in human single-joint motion (Hypothesis 3), is the implicit linear relation of adjacent time-points in a digitized signal. Discrete functions have the property that in the limit as two samples are chosen an arbitrary number of cycles *h* from one another, the data spanning these two points assumes a linear shape:

$$\lim_{h \to 1} \sum_{i=1}^{h} \left( f(x_i) - \left[ \frac{f(x_1 + h) - f(x_1)}{h} \cdot (i - 1) + f(x_1) \right] \right)^2 = 0 .$$

Thus, it is an explicit consequence of data acquisition that in the low-limit of data analysis (choosing an arbitrarily small segment of data), the curve trends linearly. In consideration of this basic tenet of differential calculus, and of the empirical evidence of gently curved global trajectory shapes in single-joint motion, the regional adherence to an approximately linear trajectory is assumed:

*Within arbitrarily defined segments of a single-joint trajectory, the trace should demonstrate an approximately linear shape.*

(Assumption 1) *Regional trajectory linearity.*

1. Behavior of sampled data in low-limit
2. Tendency towards smoothness
3. 2/3 Power Law
   —Valid in present protocol
   —Predicts constant angular velocity

## 8.5 Spatial resolution of movement smoothness

### 8.5.1 Approach overview

Rendering a scalar parameter as a dynamic variable across the domain space requires sensitive and specific feature detection, as well as easily interpretable and accurate representation. In the graduation from a scalar to a vector entity, several operations must be performed, each one representing a set of sequential arithmetic steps of which slight alterations may drastically alter the resultant spatial smoothness map. These operations are as follows

Table 31: Smoothness map operations

| Operation | Description | Decision |
|---|---|---|
| Segmentation | Division of trajectory profile into adjacent regional partitions | Data variable: time $t$, vs. angle $\theta$ |
| | | Segmentation rate |
| | | Segmentation limit |
| Evaluation | Imposition of an ideal straight-line trajectory against observed motion | 0-, 1-, or 2 best-fit "anchor points" |
| Assignment | Accurate, high-resolution attribution of performance deficit to loci of the spatial map | Domain averaging vs. point-wise attribution |
| | | Nearest-neighbor vs. correspondence |
| Measurement | Comparison to ideal straight-line trajectory | RMS error vs. correlation vs. other |
| Scaling | Normalization of segment errors | Normalization within segments, within iterations, or none at all |

Broadly, the generation of a spatial rendering of motor performance from the 1-D movement record will involve the assessment of movement smoothness according to the minimization of transient accelerations (Theorem 1) by the segmentation of the trajectory record into progressively smaller workspace sub-regions, and tabulating regional error to a straight-line trajectory.

### 8.5.2 Even, *n*-wise segmentation along time

Locating spontaneous departures from a constant angular velocity within the spatiotemporal trajectory record requires division of a single action unit (Definition 6) into segments of motion spanning smaller regions of the workspace. In a 1-D record, partitions within two domains are possible: the independent (time) and dependent (angle) data, each with its own relative merit as a segmentation variable.

Whereas single-joint trajectories are typically found to have approximately symmetric bell-shaped velocity profiles (Hogan 1984), partitions along $\theta$-space would allow the possibility of large variations in partition sample density. For example, a sigmoidal trajectory approximated by the cumulative density function

$$\theta(t) = \sum_{1 \le n \le N}^{t} \exp\left(-(n - \tfrac{N}{2})^2\right), \qquad \text{(Equation 22)}$$

exhibits gentle acceleration and deceleration at the motion onset and cessation, respectively. The number of points in a given partition $N_p$ are inversely proportional to average velocity over some interval $\alpha \le t \le \beta$, and directly proportional to constant sampling rate $v$

$$n_p \propto \left. \frac{v}{\bar{\dot{\theta}}(t)} \right|_{\alpha \le t \le \beta}, \qquad \text{(Equation 23)}$$

manifesting a concave histogram of distribution points per segment across the range of motion (Figure 23). Untoward consequences of this non-uniform regional distribution of points include the skewing of RMS-based error calculations, and the possibility of partitioning regions for which there are an insufficient number of

samples on which to base a comparison to a straight-line trajectory (see discussion of Segmentation Limit, below). By contrast, constructing a partition function within the time domain, by definition of a constant sampling rate, yields an identical number of samples (to within rounding error) in each partition

$$n_p = \frac{\nu}{N_p}, \qquad \text{(Equation 24)}$$

yielding an approximately flat histogram (Figure 23). Whereas it is often desirable to maintain equivalent partition sample sizes (for the reason that non-correlation-based raters might be used, c.f. Section 4.3.3), division in time is preferable to segmentation within angular space.

The segmentation rate, the method by which the movement record is partitioned along the chosen variable, poses an additional consideration, roughly equating to a parameter of sensitivity. A tradeoff exists between segmentation rate and the relative scaling of map features, according to the compounding of error found during each segmentation iteration. For instance, segmentation at a slow rate may insufficiently

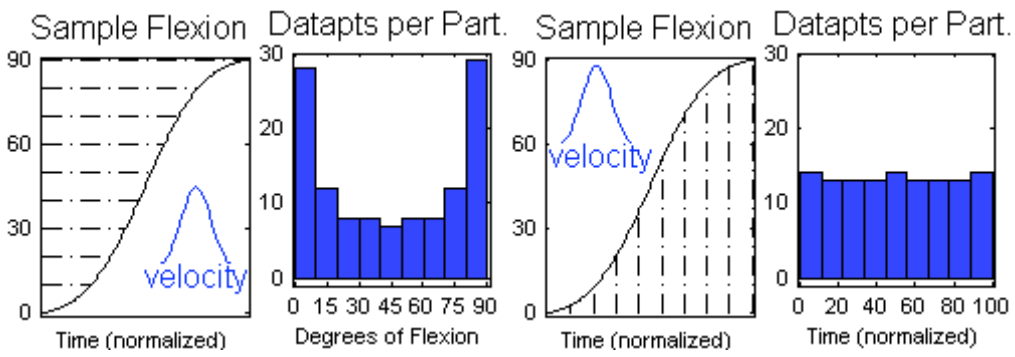


Figure 23 Partition Equivalence: Segmentation according to time guarantees approximately equal number of samples per partition.

resolve small and local features in the trajectory profile, by over-weighting the global non-linearities in curvature (Section 5.5); segmentation at a fast rate may exaggerate trajectory minutiae, essentially decreasing the signal-to-noise ratio (SNR).

Locations of unsmooth features in the movement profile are determined by comparing the trajectory curve against a series of temporally adjacent straight lines. This approach is similar to cell tracking assays in which the squared displacement vector over progressively larger time intervals is averaged over all interval sizes, yielding parameters that ultimately result in the random cell migration coefficient $\mu$[24] (Shreiber, Barocas et al. 2003). In this way, the present method will observe the convention of one-at-a-time interval adjustment, comparing the trajectory trace to one, two, three intervals, and so on.

### 8.5.3 Hard lower-limit to segmentation

A segmentation limit must also be defined. This limit recapitulates the resolution-noise tradeoff (Section 2.2.3): how many iterations can be performed so that the system is sufficiently rendered (with respect to locality and severity) without introducing artefact (distorting the performance map with amplified bit noise)? A terminal case exists wherein the number of elements in any partition interval $| P |$ is less than 2, the minimum number of points necessary to define a line[25]. However, by this logic, $| P | = 2$ is trivially "smooth" (as the two points defining the line will naturally coincide with the line: the departure is nil), and the number of data points in a non-trivial partition is $| P | \geq 3$.

---

[24] Though the present method was *inspired by* cell migration analysis, the resemblance beyond the initial construct of serial straight-line approximants is minimal: $\mu$ is a scalar determined by overlapping time intervals; spatial mapping of accelerative transients requires a non-intersecting comparison substrates (the straight lines) for determination of the precise locality in space of spontaneous accelerations.

[25] Unless otherwise stated, vertical brackets $| \times |$ will denote cardinality, i.e. the number of elements in a set.

In the segmentation of a discrete time vector, however, rounding of the partitioned indices is necessary in order to avoid non-integer partition bounds (e.g. a 9-point time vector cut into two segments would yield "half" vectors of 4- and 5-points, or 5- and 4-points, but not 4-and-a-half and 4-and-a-half points). In this way, it is expected that many segmentations in the "low-limit" will generate some combination of 2- and 3-point vectors (e.g. an 8-point vector segmented into three partitions of $| P_1 | = 2$, $| P_2 | = 2$, $| P_1 | = 3$. This presents an ill-posed segmentation, as zero error will be attributed to trivial partitions, which will give the appearance of comparatively smooth (indeed, perfectly smooth) movement, when the result is merely a rounding error artefact. Thus, a stopping rule is imposed where in no segmentation iteration $j$ can contain a single trivial partition:

$$1 \leq j < J_{\lim},\ J_{\lim} \ni' \tau_{\xi+1} - \tau_{\xi} > 1 \quad \forall \quad \xi \in \mathrm{N} < j. \qquad \text{(Equation 25)}$$

where $\tau = T \cdot \left\{ \frac{k-1}{j} \right\}$ is the set of partition boundaries (time units, up to total time $T$), $k \in \mathrm{N} \leq j+1$[26]. Note that adjacent time points need differ by greater than one (and not two) because elements of $\tau$ are vector indices, so index difference denotes degrees of freedom (i.e. number of elements -1); we require a minimum of three elements, so any difference of 2 or greater (i.e. >1) is permitted.

[26] For clarity, we define the following set theory notations: $\subset$: subset; $\in$: element of; $\{\times\}$ set containing $\times$. Number theory notation: N denotes the set of natural numbers (integers). Two logical notations: $\ni'$: such that; $\forall$ universal quantification "for all."

### 8.5.4 Linear approximants spanning observed angles

In designing a linear fit-curve for a given partition, a criterion for trajectory approximation must be decided. In statistical applications, a first-order polynomial trend line is typically fit to scatter data in such a way that the sum-of-squares differences is minimized (Figure 24a). One argument against this "blind" fitting method is that the assumption of a normally distributed noise about a treatment trend is not necessarily applicable: this noise is the object of measurement, not the assumption, and a scatter fit may have the least physiological relevance.

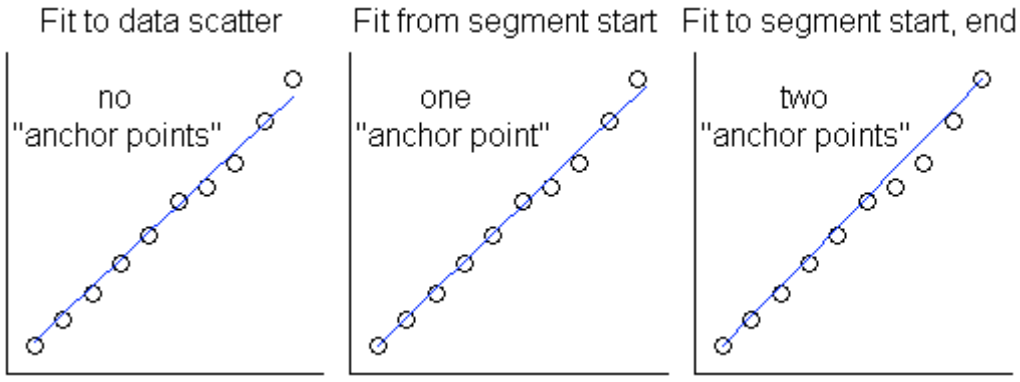


Figure 24 Approximant construction: Three linear approximations to the data: scatter fit, linear fit from first data point, linear fit to segment ends.

By "anchoring" the linear trend line to the initial segment data point, a more intuitive assessment of movement smoothness is made: starting from an arbitrary sample within the set of observed angles, determine the adherence to the best straight-line path described by all $| P_k |$ subsequent data (Figure 24b). This is implemented by defining a circle with center at the first data point, and radius determined by the distance between segment ends. At a user-determined resolution, Cartesian

coordinates for this polar data can be used to construct a set of | $P_k$ |-long rays; the minimum error to these lines would represent segment smoothness. Alternatively, two "anchor points" define a line spanning the precise segment range, which is equally meaningful from a motor control perspective (adding the stipulation "and ending at angle $\theta + \Delta\theta$" to the previous case "starting from an arbitrary sample within the observed angles"). The two-anchor method was selected based on its equivalent appeal to physiologic relevance (as opposed to no anchors) and its computational efficiency (over one anchor, requiring a single line of code).

Thus, on the $j^{th}$ iteration, the time sample domain $1 \leq i \leq$T will be partitioned into $j$ even intervals of motion described by $\tau$, the set of $j + 1$ boundary time points, and their corresponding angles of record $\Theta(\tau) \subset \theta(t)$. The $k^{\text{th}}$ segment of piecewise partition function $P$ is thus

$$P_k = \left[ \frac{\Theta_{k+1} - \Theta_k}{T/j} \cdot \left( i - \frac{k-1}{j} T \right) \right] + \Theta_k, \qquad \text{(Equation 26)}$$

where

$$k = \left| G \right| : G \subset \left\{ \frac{k-1}{j} \right\} < \frac{i}{T}. \qquad \text{(Equation 27)}$$

The result is then a single linear approximant spanning the local range of joint angles, matching to the first- and last data points defining the segment.

### 8.5.5 Distribution of error across segment domain

Comparison of each trajectory partition to a linear approximant will generate a set of errors, either for the entire segment (by methods described in Table 31) or for each data sample. These errors will be collected along the angular domain for representation as a spatial error function S($\theta$) function. Figure 25a demonstrates a domain-wide error, $E_3 > E_2 > E_1$, according to some error measurement method; Figure 25b-c depicts a specific assignment of deviation between a single sample (either on the approximant, or from the data record) to its corresponding locus on the opposite curve. This operation, likely a squared-difference, can be performed two different ways: the error can be measured as a angular distance at a given time (direct assignment), or the minimum distance (the vector normal) of each time sample of the observed motion to the linear approximant.

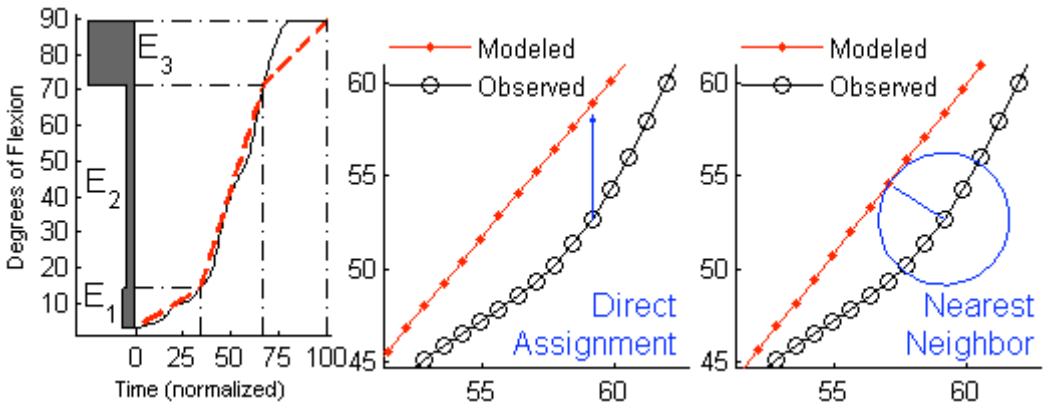


Figure 25 Three error assignment methods: domain-wide attribution, and point-wise error assignment (direct, or nearest-neighbor, shown for sub-region inset).

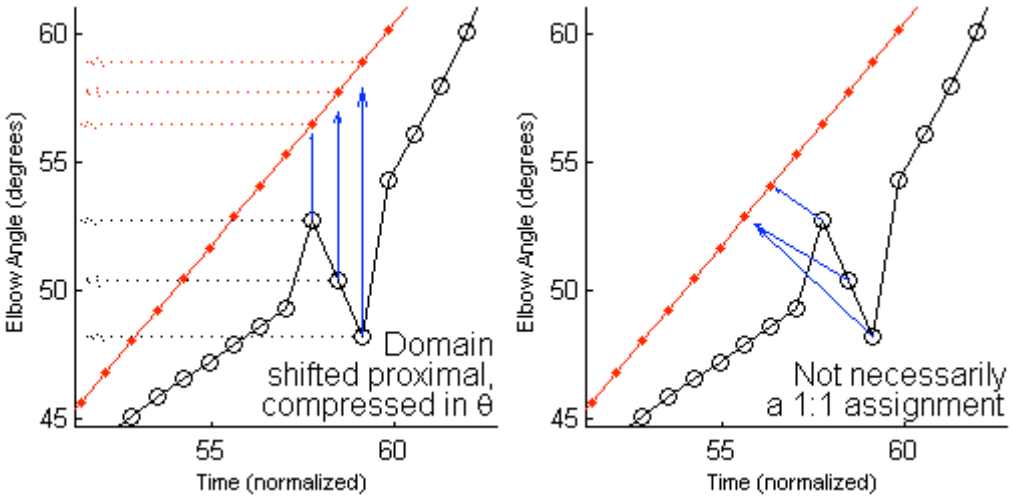


Figure 26 Shortcomings of point-wise assignment: domain shift and non-surjective transformations.

The principal utility for point-wise error assignment is in the limit of small deviations from the approximants, where high precision is desirable, and deviations are on the order of the inter-model sample distances. For partitions with moderate departure from the linear approximation, point-wise error assignment may cause misrepresentation in the S($\theta$) trace. In the case of direct assignment, the angular range over which a trajectory feature is observed may undergo transformation (expansion or compression, proximal or distal shift), if assigned the matching angular range within the model trace. Assignment to the $\theta$-domain according to the observed angles eliminates the presumption of monotonicity, resulting in ambiguity in the error assignment[27] (Figure 26).

Nearest-neighbor assignment runs additional risk of non-surjectivity in "poorly-behaved" trajectories. Non-monotonicities, in particular, present occasion for two data points to attribute to a single locus on the model curve, creating a quandary

[27] In "doubling-back" to an angular range previously considered, the error vector $E(\theta)$ for a given iteration will exhibit considerable "jumpiness" for a smooth performance (low error from the first transcription) overlaid with sparse large peaks of high error associated with the jerky feature.

of error assignment: should the errors be over-written, averaged, or treated as two sides of a triangle (rooting the sum of their squares?). Of course, with a model and assignment vector, each the same number of samples as the recorded signal, each double-assignment generates an empty-space in the assignment vector (Figure 26).

Though trans-partition error assignment loses considerable resolution, particularly in the early limit of large partitions, segmentation rate (Section 8.5.2) and normalization method (Section 8.5.7) can be chosen in such a way that this effect is minimized. After some number of iterations, resolution will be sufficient to discriminate between arbitrarily fine detail in the trajectory record; scale-factor (normalization) can be determined on a case-by-case basis. The flexibility of these two design parameters considerably outweigh the potential for skewed or non-surjective error vector dysfunctionality, thus meriting domain-wide error assignment.

### 8.5.6 Correlation-based measurement of approximant error

Metrics describing how two samples differ from one another by assessing the departure of one dataset $x$ from a substrate of comparison $a$ in a sum-of-squares way are expressed according to the general formulation

$$\left[\frac{1}{\kappa}\sum_{i=1}^{N}(x_i - a)(b - c)\right]^{\gamma}, \qquad \text{(Equation 28)}$$

where $\gamma$ and $\kappa$ are constants, and $a$, $b$, and $c$ are either constants or comparison vectors (Table 32)

| Table 32: Parameterization of domain transform | | | | | | |
|---|---|---|---|---|---|---|
| $\kappa$ | $a$ | $b$ | $c$ | $\gamma$ | Metric | |
| $N$ | $y_i$ | $x_i$ | $y_i$ | $\frac{1}{2}$ | Root-Mean Square Error | $RMSE$ |
| $T$ | $\bar{x}$ | $x_i$ | $\bar{x}$ | $\frac{1}{2}$ | Standard Deviation | $\sigma_X$ |
| $T$ | $\bar{x}$ | $x_i$ | $\bar{x}$ | 1 | Variance | $\sigma_X^2$ |
| $T$ | $\bar{x}$ | $y_i$ | $\bar{y}$ | 1 | Covariance | $\sigma_{XY}^2$ |
| $T \cdot \sigma_X \cdot \sigma_Y$ | $\bar{x}$ | $y_i$ | $\bar{y}$ | 1 | Correlation Coefficient | $\rho_{XY}$ |
| $N$ = Number of time points, $T$ = Total time ($N$ divided by the sampling | | | | | | |

Though segmentation within the time domain results in approximately equal partition cardinality (Section 8.5.2), segment distribution equivalence only normalizes error results *within* iterations. Between iterations, however, error scaling will increase rapidly with the span of the segments, suggesting the need for attenuation of the covariance. Thus, the Pearson product-moment correlation coefficient was selected as the performance metric for each segment

$$\rho(\theta_k, P_k) = \frac{1}{\frac{T}{j} - 1} \frac{1}{\sigma_\theta \sigma_P} \sum_{i \in \tau_k} (\theta_i - P_i)^2 , \qquad \text{(Equation 29)}$$

where $k$ is as defined in (Equation 27). Whereas strong correlation to a straight-line approximant indicates a smooth performance, we define movement error $E$ for the $k^{th}$ motion segment as the opposite:

$$E_k = 1 - \rho(\theta_k, P_k) . \qquad \text{(Equation 30)}$$

$E_k$ can range from 0 (perfectly smooth) to 1 (random motion) according to the unity scale of $\rho$.

### 8.5.7 Correlational error requires iterated normalization

For non-unitary metrics such as RMS- and variance-based metrics, normalization may be necessary to prevent large-scale bias of early iterations (low $j$), where partition angular range is large, and within-waveform variance is not accounted for. For correlation-based metrics, local details in the trajectory trace are less likely to be obscured from this scale disparity, however minor processing of the error vectors may diminish artefactual amplification of early iterations in the presence of global curvatures (Chapters 3 & 4).

Though iterative error vector S($\theta$) can in principle range from 0 to 1, this is not necessarily so, suggesting that neither bound is a guaranteed outcome, nor shall vector output necessarily exhibit large variation over the angular domain. Creating a template array A($\theta$), a $j \times \gamma$ array where $\gamma = T \cdot \eta$ and $\eta$ is a user-defined spatial resolution for visualization purposes[28], the $j^{th}$ row entry will be a normalized E($\theta$)

$$A_{j\cdot} = E^*(\theta) = \frac{E(\theta)}{\max(E(\theta))}, \qquad \text{(Equation 31)}$$

where E*($\theta$): indicates a normalized error vector. Writing in partition terms for the $j^{th}$ iteration

$$A_{j\xi} = E_k^* \quad \forall \quad \frac{k-1}{j} < \frac{\xi}{\eta} < \frac{k}{j}, \qquad \text{(Equation 32)}$$

$\xi$ has units of time or sample number. Subtraction of vector minimum was considered prior to normalization, but was considered to artefactually inflate relative feature size.

---

[28] $\eta = \frac{512}{T} s^{-1}$ is sufficient for approximately 0.25° resolution in for a motion of range of motion $\Delta\theta$ = 90°.

For example, if $j = 2$ error vector E($\theta$) will have two components, $E_1 = \alpha$ and $E_2 = \beta$. If $\alpha - \beta \neq 1$, subtracting the minimum ($\alpha$, if $\alpha < \beta$) will artificially inflate the inter-segmental difference; this difference amplification will be large in the limit as $\alpha$ approaches $\beta$.

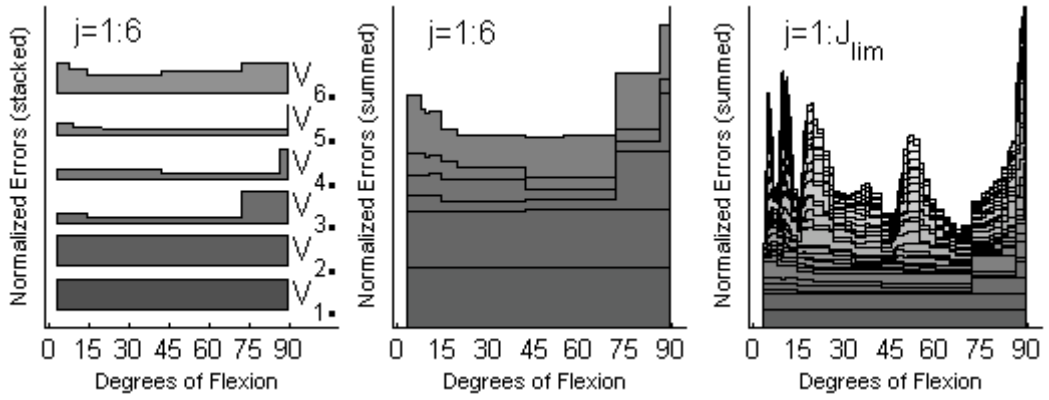


Figure 28 Spatial error vector generation: stacking, summing of $A_{1\rightarrow 6}$ ($\theta$); histogram representation of S($\theta$) (the sum is not subtracted or normalized).

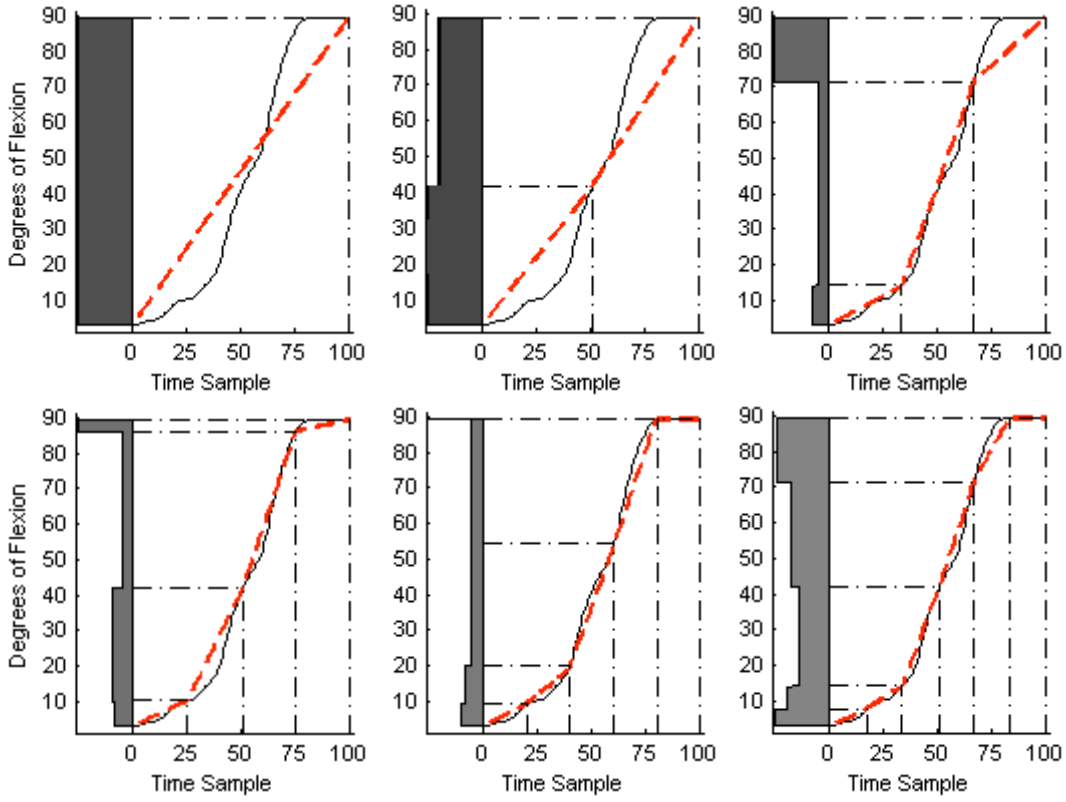


Figure 27 Error vector generation: The first six iterations of partition and projection of E($\theta$), bar graph rotated to rise in the reverse-time dimension.

## 8.6 Putting it all together: Creation of the spatial map

For each segmentation iteration, a vector E*($\theta$) is generated, consisting of $j$ partitions, each with an error $E_k$ for $1 \leq k \leq j$, determined by the correlation $\rho(\theta_k, P_k)$ of the $k^{th}$ linear approximant to its corresponding data segment. These errors are then distributed over the $\frac{T \cdot \eta}{j}$ samples in error template array A($\theta$), in the $j^{th}$ row (Figure 27). Summing over all iterations, a spatial error distribution vector S($\theta$) is defined as the sum of all errors $E$ found for a given angle $\theta$, as a function of deviation from a set of linear approximants $P$ to some arbitrary limit resolution $\frac{T}{J_{lim}}$ (Figure 28)

$$S(\theta) = \sum_{j} A_{j\cdot}(\theta). \qquad \text{(Equation 33)}$$

In all future use, unless otherwise stated, S($\theta$) will be discussed in terms of its min-subtracted, and normalized formulation:

$$S^*(\theta) = \frac{S(\theta) - \min(S(\theta))}{\max(S(\theta) - \min(S(\theta)))}. \qquad \text{(Equation 34)}$$

As shorthand, this normalization will be understood, but not acknowledged: S*($\theta$)→ S($\theta$).

Depiction of a trajectory's trace features presents the opportunity for creativity in the legibility and interpretability of the performance information. Plotting this vector in the number plane (error as a function of elbow flexion angle), though amenable to traditional plotting techniques and expeditious for single-joint (i.e. 1 DOF) motion, is not explicitly fidelious to motions of greater freedom. In order to enhance informational accessibility, spatial error vectors were converted to a single-

DOF heat map, and plotted as a band of colored tiles along the *x*-, *y*-, and *z*-coordinates comprising the hand's path through space. Heat map colors were chosen so that black signifying the "null" smoothness, S($\theta$) ≈ 0, and red the maximum error S($\theta$) ≈ 1, suggesting a "red light warning" of unsmooth performance (Figure 29).

Transverse planar motion, maintained by MAST constraint, is reflected in the circular arc segment of the resultant heat maps.

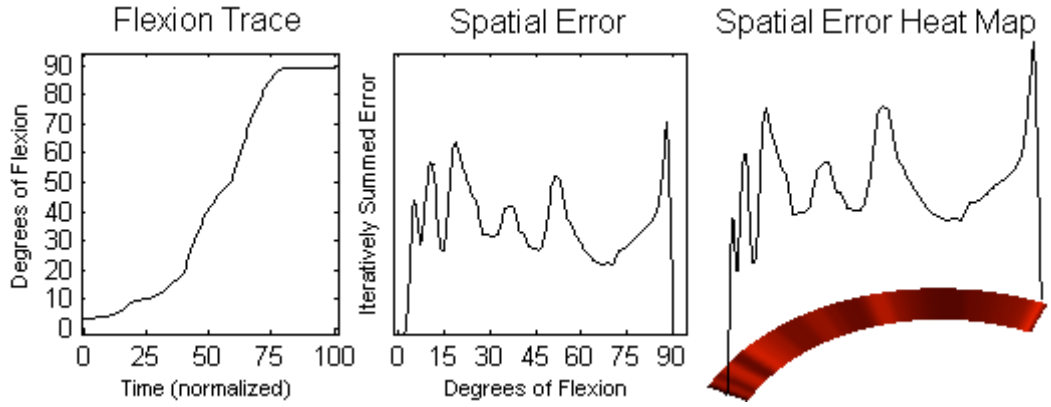


Figure 29 Spatial error heat map generation: side-by-side comparison of flexion trace $\theta$(t), spatial error generated from unsmooth trace features S($\theta$), and spatial error vector as a heat map.

## 8.7 Summary

Most measures of motor proficiency evaluate performance over time. Though this is a natural consequence of the nature of biomechanical data and its observation (the movement through a sequence of loci over time), it is not necessarily a meaningful domain by which to ascertain meaningful parameters related to motor function. Moreover, that many of these metrics require differentiation of temporal data, a notoriously noisy data transformation, these raters are not only ill-posed, but prone to artifact. Here, a pseudo-wavelet kinematical data transformation was

proposed, whereby the movement smoothness was assessed at progressively finer spatial resolution, against the criterion of locally constant angular velocity.

This pseudo-wavelet transform quantifies motor performance via a simple, well-established principle of motor behavior, while simultaneously obviating a potentially error-inducing differentiation, and expressing motor impairment as a function of joint angle, not time.

# 9 MAPPING ACCELERATIVE TRANSIENCE

## 9.1 Introduction

In Chapter 8, a pseudo-wavelet transform was proposed that determined smoothness in single-joint motion as adherence to a single simple criterion: constant angular velocity. It was suggested that in addition to rendering motor performance as a function of joint angle, as opposed to time, by obviating a potentially noisy differentiation of the SJT, the resultant spatial maps are robust to many movement conditions. In this chapter, this new method is compared against existing measures and the behavior of this novel wavelet transform is rigorously evaluated.

Furthermore, fundamentally limitations of this method are answered by the introduction of scalar parameters expressing motor performance in a way that is easily quantified or subject to traditional statistical analysis: the maps are vectors, not scalars. Additionally, a formal validation of the accuracy of this transform was performed on a set of SJTs performed by both individuals with compromised motor control due to chronic stroke, and healthy controls.

## 9.2 Experimental hypotheses

Here, the spatial acceleration vectors proposed in Chapter 8 are validated as a means of conveying information related to the performance of single-joint motion in all subjects.

| | |
|---|---|
| *Vectorial rendering of the single-joint trajectory, following transformation into the domain of linear approximant error as a function of angle, accurately reports movement proficiency in both healthy and impaired cohorts.* | (Hypothesis 11) |

As the primary index of neuromotor health, movement smoothness has been quantified by myriad raters in both healthy persons, and in persons recovering from neurologic trauma, e.g. stroke (Rohrer, Fasoli et al. 2002; Kahn, Zygman et al. 2006). However, despite their evaluation of salient features (ridges, curve behavior) of fundamentally relevant kinematical substrates (angular velocity, acceleration, etc.), standard smoothness metrics do not always detect differences in trajectories generated by drastically disparate subject cohorts. Average jerk, for instance, was not significantly different for cerebellopathy patients performing simple pointing tasks (Goldvasser, McGibbon et al. 2001), and was found to *increase* during recovery from hemiparetic stroke (Rohrer, Fasoli et al. 2002). Thus, it is important to show that any new metric derived to report trajectory smoothness was able to resolve significant performance differences of an obviously impaired cohort.

*Scalar smoothness metrics derived from the angular-domain trajectory transformation can discriminate healthy from impaired condition as well as standard metrics.* (Hypothesis 12)

The pseudo-wavelet transform permits precise location of unsmooth behaviors throughout the elbow workspace. It is therefore possible to assess the variability of accelerative behavior throughout the range of motion in both impaired and intact subjects.

*Measures derived from the angular domain are impervious to spurious co-dependence of angular velocity.* (Hypothesis 13)

Thus, it is tested 1) whether the novel pseudo-wavelet transform proposed here can identify the difference between healthy and impaired subjects, and 2) the

transformation out of the temporal domain is necessary to avoid spurious correlation to velocimetric parameters. A validation of this transform precedes the formal hypothesis testing.

## 9.3 Experimental methods

### 9.3.1 Subjects and protocol

Ten healthy individuals with no known neurological impairments voluntarily participated in this study, and were observed in a single session typically lasting less than 30 minutes. Additionally, a cohort of five outpatient clients of the JFK-Johnson Rehabilitation Institute (Edison, NJ) were recruited based on the inclusion criterion described in Section 1.2.3.2, also observed in a single session (Table 17). After a brief orientation period and adequate warm-up, subjects were seated in the MAST with their right arm supported against gravity, and instructed to flex and extend at a comfortable (self-selected) pace, and to maximize their smoothness. Stroke subjects were tested on their affected hand. A single day's data was collected.

### 9.3.2 Transform method validation

#### *9.3.2.1 Determining the sensitivity to various curvatures*

The proposed spatial acceleration transform identifies regions of non-linearity. However, it was found by the Essential Trajectory method (Chapter 5) that some SJTs adopt a regional curvature. In this way, it is incumbent to establish that the gentle regional curvatures observed do not overshadow the more transient accelerations constituting instances of non-smooth movement by iterated maximization of the regional error. That is to say, whereas some SJTs of ostensibly ideal performance are gently curved, it is imperative that these low-frequency curvatures generate local error

of comparatively trivial order in the presence of spontaneous and non-smooth behaviors.

#### *9.3.2.2 Spatial acceleration versus raw acceleration*

Prior to any interpretation of the transformed kinematic data, its accuracy and interpretability as a performance measure was assessed. Several SJT traces were selected at random for a side-by-side peak comparison between spatial acceleration vector S($\theta$) and the raw acceleration vector $\ddot{\theta}(t)$. Here, peaks were extracted manually from each trace, and their co-alignment determined manually. More elaborate assessments were foregone for the reason that it was not certain that the number of peaks in the respective profiles would equate. In the case where there were additional peaks in one trace, comparative metrics, e.g. the correlation of local maxima in terms of joint angle between the two traces, would require complex data conditioning, and would thus be beyond the scope of this analysis. Thus, all results presented here involve the direct observation of manually conditioned data.

### 9.3.3 Data treatment and analysis

#### *9.3.3.1 Signal processing*

Data traces were filtered with a low-pass Butterworth's filter (4 Hz cutoff), and divided into flexion and extension motions according to a thresholded local minimum; extension curves were discarded. Flexion traces were then subjected to a series of assessments of performance smoothness.

#### *9.3.3.2 Standard smoothness raters: Average jerk and velocity peaks*

Filtered angular data $\theta(t)$ was evaluated for the average jerk in the trajectory profile, as well as the number of peaks in the angular velocity trace. Time-averaged

jerk was determined by a trapezoidal integration of the triply differentiated angular position trace (Hogan 1984; Feng and Mak 1997; Todorov and Jordan 1998)

$$J = \frac{1}{T}\int_0^T \left| \frac{d^3}{dt^3}\theta(t) \right|^2 dt . \qquad \text{(Equation 35)}$$

The number of peaks in the velocity trace were counted over the singularly differentiate position trace (Rohrer, Fasoli et al. 2002)

$$N_V = \sum_t \left[ \left\{ \frac{d}{dt} \operatorname{sgn}\left( \frac{d}{dt}\theta(t) \right) \right\} > 0 \right]. \qquad \text{(Equation 36)}$$

Signals were filtered with identical filter characteristics after each successive differentiation (Feng and Mak 1997).

#### *9.3.3.3 Scalar metrics of smoothness as a function of angle*

In consideration of the two established metrics described above (average jerk and the number of velocity peaks), and in the interest of devising metrics with compatibility to existing scalars, two similar operations are proposed presently. In keeping with the theme of red as a heat-map index of poor performance, we define $R$ as the "redness" or total area under the regional performance error curve

$$R = \frac{1}{\Delta\theta}\int_{\Delta\theta} S(\theta) d\theta . \qquad \text{(Equation 37)}$$

$R$ thus has units of normalized error per degree of flexion. Additionally, we will count the number of curves $N_S$ in the $S(\theta)$ error-by-angle plot

$$\pi_S = \sum_{\Delta\theta} \left[ \frac{d}{dt} \left( \operatorname{sgn}\left( S(\theta) \right) \right) > 0 \right], \qquad \text{(Equation 38)}$$

yielding integer values.

#### *9.3.3.4 Trace feature analysis: Trace peak analysis*

In addition to the area-under-the-curve, and the number of trace peaks in S($\theta$), an analysis of the distribution of accelerative behaviors was performed. In order to determine the proportional homogeneity of transients in the motion profile, i.e. whether a few large ridges dominated the S($\theta$) trace, or whether many small features were observed, the ratio of peak error to average error

$$\varepsilon = \frac{\max\left( S(\theta) \right)}{\bar{S}}, \qquad \text{(Equation 39)}$$

was calculated. This yields a simple index of the relative weighting of trace peaks, analogous to a measure power-concentration. More complete identification of all trace peaks, for the purpose of correlation across repetitions would allow for an assessment of the variability of spontaneous accelerations across the joint workspace; correlation to the corresponding $J(t)$ trace might permit a determination of cause-and-effect to further illuminate metrical design. However, these analyses are beyond the scope of this preliminary assessment, and will not be performed here.

## 9.4 Results: Method validation

### 9.4.1 Robustness to global curvature, i.e. curved ETs

It has been shown previously (Section 5.5.1) that trajectories often exhibit gentle curvatures related to the acceleration or deceleration in single-joint articulation tasks. Whereas this is observed in healthy subjects, and is justifiable in the context of

normal motor function, smoothness metrics should not be overly-sensitive to these benign global trajectory curvatures such that otherwise proficient performances are rendered as unsmooth.

In order to determine the validity of the spatial error pseudo-wavelet transform method, a test of S($\theta$) was performed for a series of ideal waveforms. Curvature detection within the trajectory trace was tested by application of the linear approximant method to a single straight line appended with a gentle unimodal curvature at $t' = \frac{6 \cdot T}{10}$

$$y_1(t) = \begin{cases} A \cdot t & 0 \le t < 0.6 \\ B \cdot \left[ t \cdot (1 - t) \right] & 0.6 \le t \le 1 \end{cases}.$$

A second straight-line perturbation was designed wherein two Gaussian noise peaks were added to the linear trajectory at $t' = \frac{2 \cdot T}{10}$ and $t' = \frac{8 \cdot T}{10}$, simulating two unsmooth ridges in an otherwise perfect performance:

$$y_2(t) = A \cdot t + C \cdot e^{-k(t-0.01\alpha)^2} + D \cdot e^{-k(t-0.01\beta)^2} \Big|_{0 \le t \le 1}.$$

A composite curve was then created, superimposing two accelerative transients onto a gently curve trajectory

$$y_3(t) = E \cdot y_1(t) + F \cdot y_2(t).$$

Gentle curvatures in the linear trace were detected with high precision: the primary onset of curvature was correctly detected at 60% of the waveform's time-course (

Figure 30a). Simulated transient accelerations were also detected with considerable accuracy. The $t' = \frac{2 \cdot T}{10}$ peak, given an amplitude of C = 0.225created a peak in the S($\theta$) from approximately 20% to 20 + 22.5 = 42.5% percent of the normalized "range of motion." Likewise, the second ridge, extending through D = 0.15 percent of the workspace generates a smaller peak in the S($\theta$) trace from approximately 65 to 80%

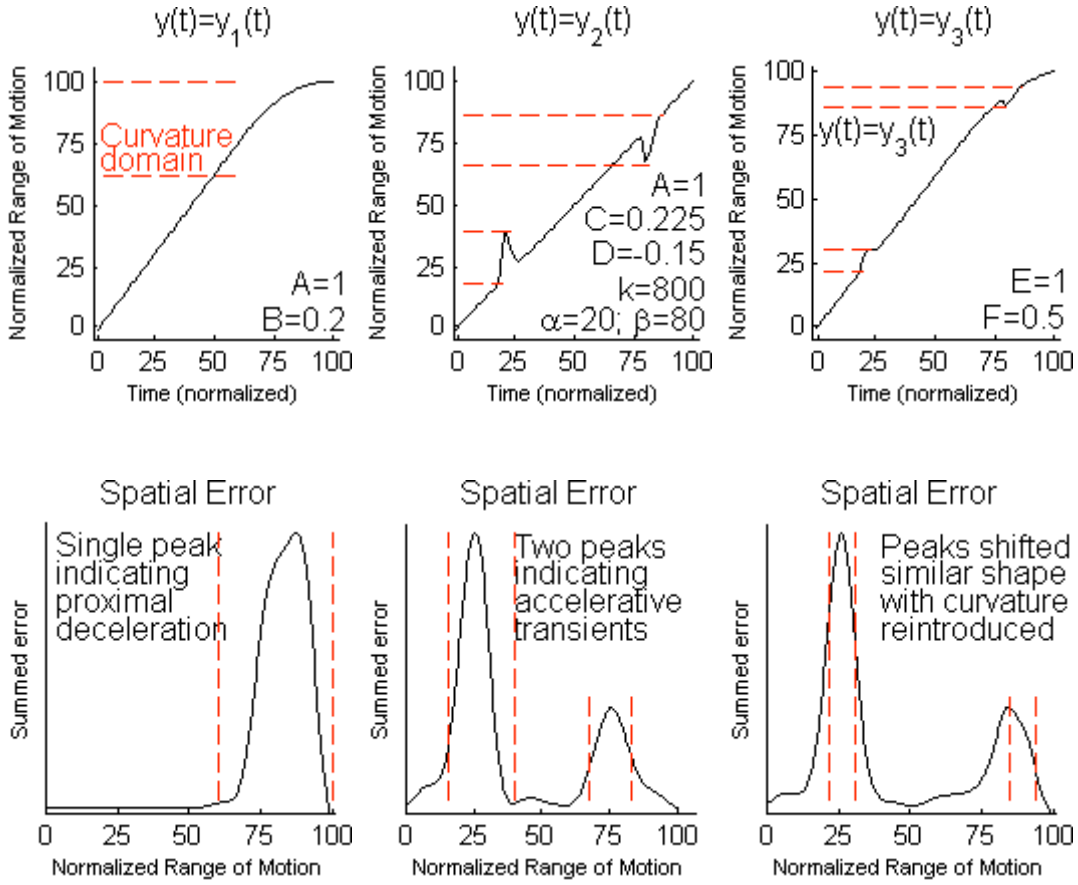


Figure 30 Inverse weighting scale: S($\theta$) detects both gentle global curvatures and locally unsmooth activity, preferentially weighting small transients.

of the joint range of motion[29].

[29] The S($\theta$) peak begins a bit earlier (at approximately 57%), suggesting a more drastic "limb regression." This is thought to be artefact due to the extreme change in velocity at peak onset (non-monotonicity in the trace), and is considered minor. In the subsequent case, where a deceleration is

Combining these two perturbations (gentle curvature and transient accelerations), the large peak associated with the simulated deceleration (Figure 30a) is absent from Figure 30c, but works to shift the peaks slightly to the right in the S($\theta$) curve. This is an expected consequence as the transient accelerations now appear at a more proximal angle than before (red highlights).

Thus, it is concluded that while gentle curvatures in the SJT are veridically detected, in the presence of even small transience, the spatial transform correctly prioritizes the swift accelerative behaviors, with only minimal skewing of the peaks of the S($\theta$) trace.

### 9.4.2 Comparison of spatial acceleration to raw acceleration trace

To assess spatial error vector S($\theta$) validity, a side-by-side comparison was made between peaks in S($\theta$), yielding the maximum spatial error by the segmented approximation described presently, and angular acceleration $\ddot{\theta}$ vector, yielding the maximally jerky features commensurate with the definition of average jerk (Equation 35). Single-repetition trajectories were selected from stroke subjects flexing their affected limb.

Peaks in the spatial error and angular acceleration profiles were found as the subset of points whose derivative was sufficiently small

$$\Theta_e = \{\theta'\} \ni' \ \frac{d}{d\theta} S(\theta') < \delta \qquad \text{(Equation 40)}$$

and

---

imposed over the second ridge (muting this abrupt velocity change), the second peak in the S($\theta$) trace appears closer to the expected 65%.

$$\tau_d = \{t'\} \ni' \frac{d}{d\theta}\ddot{\theta}(t') < \delta \qquad \text{(Equation 41)}$$

where $\delta$ is an arbitrarily small quantity. The time points $\tau_d$ corresponding to peaks in the acceleration profile were converted to their corresponding angles in the flexion trace

$$\Theta_d = \theta(\tau_d),$$

and compared against $\Theta_d$, the angles yielding peaks in S($\theta$). The average angular difference, scaled to percent of range of motion was calculated for all peaks common to $\Theta_d$ and $\Theta_e$ (determined manually):

$$\overline{\Delta p} = \frac{1}{\Delta\theta}\frac{1}{N_\cap}\sum_{i=1}^{N_\cap}\Theta_{ei} - \Theta_{di}, \qquad \text{(Equation 42)}$$

where $N_\cap$ is the number of elements shared between the sets[30]

$$N_\cap = \left|\Theta_e \cap \Theta_d\right|.$$

Acceleration traces were twice differentiated and filtered once (after both differentiations) with an inline smoothing function in the Matlab programming environment. Peaks of both profiles, when converted to the angular domain, exhibited an accuracy to within 5% of the trajectory range of motion (Figure 31). Though for many trajectories, the congruency $N_\cap = N_\cup = \left|\Theta_e \cup \Theta_d\right|$ [31] was observed, some

[30] More set-theoretic notation: $\cap$ : intersection (elements common to two sets)
[31] Still more set-theoretic notation: $\cup$ : union (all elements among two sets).

trajectory traces manifested fewer peaks in $S(\theta)$ (typically 1 missing peak). This suggests a soft limit on the sensitivity of the linear approximation method, but can probably be answered with adjustment of the protocols determined in the sections above (Sections 8.5.2-8.5.7).

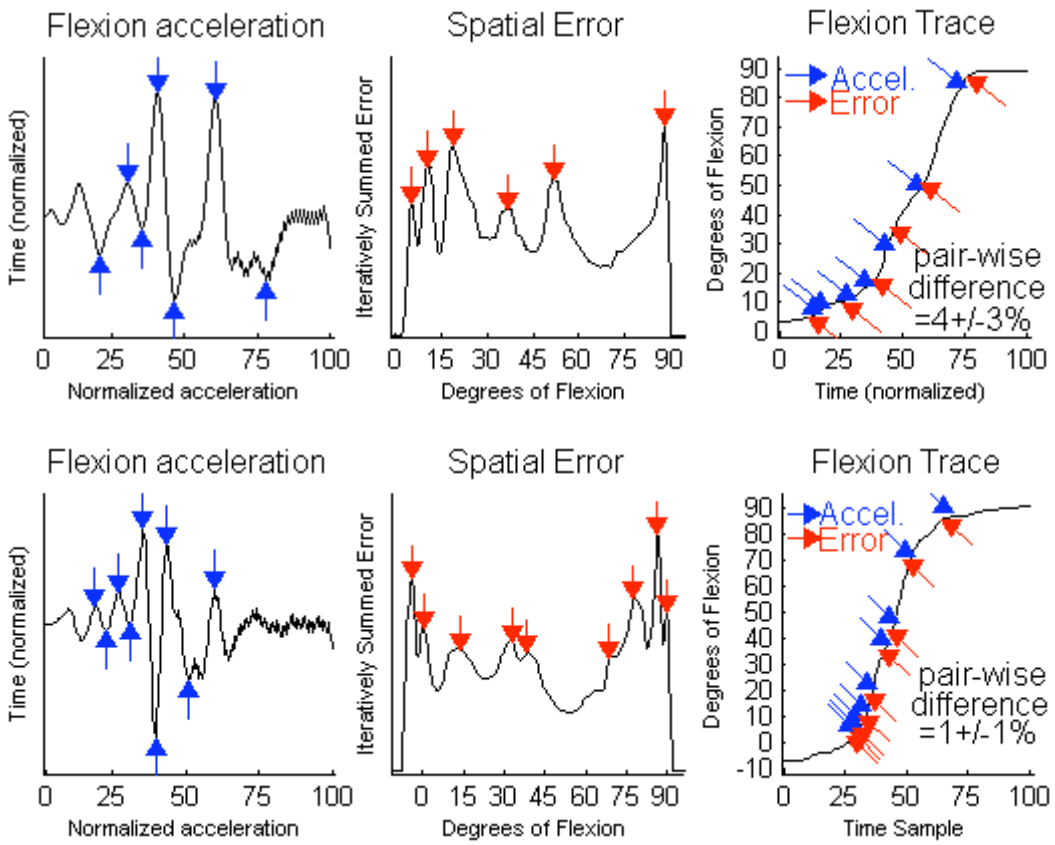


Figure 31 Accuracy and sensitivity of S($\theta$): two sample trajectories demonstrate the accuracy of spatial error vectors to <5% error from peaks in the acceleration profile.

Here, it is apparent that the correspondence between peaks in the raw acceleration profile is mostly well-matched to those of the spatial acceleration profile.

## 9.5 Results: Human subjects testing

### 9.5.1 Basic performance measures

As expected, the neurologically intact volunteers enacted large amplitude, swift motions, at a difference that showed significantly greater proficiency than the stroke subjects (Table 33):

| Table 33: Parameters of SJTs from 15 Subjects | | | |
|---|---|---|---|
| Metric | Normal (N = 10) | Stroke (N = 5) | Comparison |
| Movement amplitude $\Delta\theta$ | 88.4 ± 0.7º | 84.8 ± 5.5º | $P < 0.05$ |
| Average angular velocity $\bar{\dot{\theta}}$ | 91.0 ± 3.8º/s | 80.0 ± 13.1º/s | $P < 0.05$ |
| Mean Arrest Period Ratio | 0.09 ± 0.08º/s | 0.26 ± 0.19º/s | P < 0.001 |
| All values (μ ± σ). | | | |

Though speed of flexion was not strictly controlled, healthy subjects maintained a narrow range of velocities, versus stroke patients whose pace of movement was highly variable, and significantly slower ($P < 0.05$). As with the trajectory essence extraction (Chapters 3-5), healthy subjects moved with an average velocity of approximately 1 second ($\Delta\theta \approx \bar{\dot{\theta}}$), and that the movement amplitude was large, but did not approach the physiological limit of the elbow joint (generally presumed to exceed 120º). Thus, the movements observed here are considered to represent natural, smooth movement at a comfortable pace, over a comfortable range.

It is noted that the stroke subjects spent significantly greater time at extremely low angular velocity, as detected by MAPR.

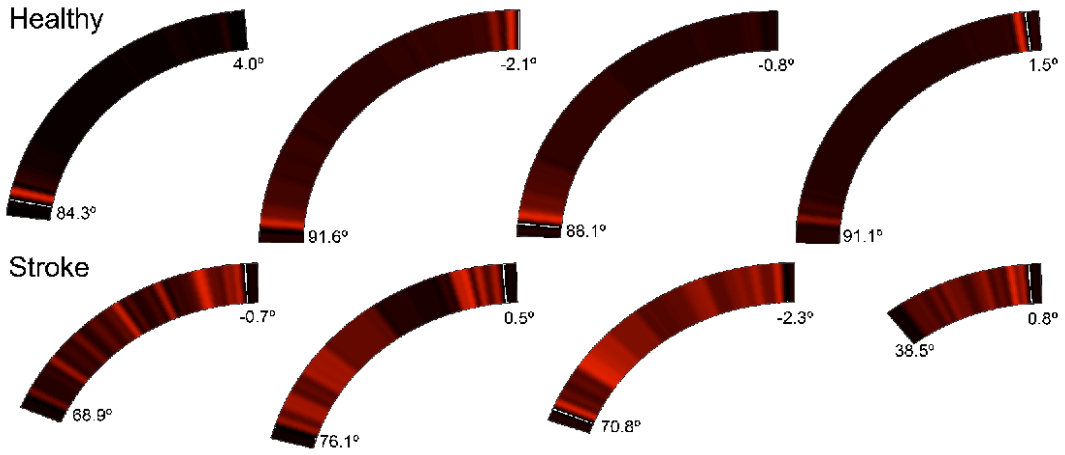


Figure 32 Sample spontaneous accelerations maps of healthy (*Top*) and stroke subjects (*Bottom*).

### 9.5.2 Integrated metrics: Area under *S*(θ) and *J*(t) curves

Two integrated metrics operated on the acceleration curves extracted from SJT data here: the "amount of redness" in the spatial map *R*, and the integrated average jerk *J*, each normalized to their respective independent variable (range of motion and time, respectively).

| Table 34: Peak counting of SJTs of 15 subjects | | | |
|---|---|---|---|
| Metric | Normal (N=10) | Stroke (N=5) | Comparison |
| Area under $S(\theta)$: $R$ x $10^{-3}$ | 3.1 ± 0.8 | 8.0 ± 2.9 | $P < 0.001$ |
| Area under $J(t)$: $J$ x $10^{-5}$ | 9.0 ± 6.7 | 40.6 ± 46.9 | ≈ |
| All values (μ ± σ). | | | |

Here, though the mean jerk is very different between cohorts, the variability in this metric among stroke subjects is sufficiently large so as to preclude significance at

the $P < 0.05$ level (Wilcoxon rank-sum). The area under the transformed kinematic data, however, yielded significantly lower $R$-values at $P < 0.001$ (Table 36).

### 9.5.3 Ratiometric indices: Peak maximum to trace mean

In order to estimate the sensitivity of each data trace (kinematic data in the temporal domain, versus transformed data in the angular domain), a peak-to-mean ratio of each trace was calculated, comparing the relative importance of the loci of greatest spontaneous acceleration to the rest of the trace.

Table 35: Ratiometric indices evaluated from SJTs of 15 subjects

| Metric | Normal (N=10) | Stroke (N=5) | Comparison |
|---|---|---|---|
| Ratiometry of $S(\theta)$ | 12.1 ± 1.9 | 6.6 ± 0.9 | $P < 0.001$ |
| Ratiometry of $J(t)$ | 9.9 ± 7.7 | 42.8 ± 49.4 | ≈ |

All values (μ ± σ).

Here again, though the time-domain metric demonstrated a large difference between cohort means, the variability within the stroke cohort prevented significance at the $P < 0.05$ level, whereas the transformed kinematic data provided a robust discrimination between groups at the level of $P < 0.001$ (Table 35).

### 9.5.4 Tallied metrics: Peak counting

Lastly, whereas it has been demonstrated that the number of peaks in the S($\theta$) trace correspond well (both in number, and in location in the $\theta$-domain), with peaks in the J($t$) trace, it was hypothesized that their ability to distinguish healthy from impaired motion would be approximately equivalent.

| Table 36: Peak counting of SJTs of 15 subjects | | | |
|---|---|---|---|
| Metric | Normal (N=10) | Stroke (N=5) | Comparison |
| Peak counting of $S(\theta)$: $\pi_{S(\theta)}$ | 9.3 ± 0.9 | 9.9 ± 1.6 | ≈ |
| Peak counting of $J(t)$: $\pi_{J(t)}$ | 14.4 ± 4.5 | 9.9 ± 5.7 | ≈ |
| All values (μ ± σ). | | | |

Unlike ratiometry and integration, the failure of peak counting in the jerk-versus-time trace failed to reach significance at the $P < 0.05$ level because an apparent similitude in group means. Similarly, and as predicted by the preliminary analysis above (Section 9.4.2), the number of peaks in the time-domain and angular-domain error representations are approximately similar in healthy subjects, and apparently identical for stoke subjects.

## 9.6 Speed, temporal metrics correlated in stroke cohort

### 9.6.1 Prolonged stall periods (high MAPR) skew jerk metrics

The need to normalize jerk-based metrics, in order to account for differences in angular range, movement speed, and experimental parameters between repetitions, over several subjects, or across protocols, was discussed in Section 2.2. The clear importance of normalization, however, occasionally competes with the preservation of jerk trace scale; this is especially true in the maintenance of the area under the curve under conditions of prolonged periods of zero-jerk during stalled motion (Section 7.6). Here, stroke subjects were observed to move with significantly longer periods of stall, as determined by the Mean Arrest Period Ratio (MAPR), measuring the percent of time spent below 10% velocity (Table 33). Thus, it is suggested that time-domain metrics extracted from subject groups with significantly different durations of low-velocity movement, such as features extracted from the jerk trace,

may be unreliable for cross-cohort comparison. A quantitative analysis supports this argument.

### 9.6.2 Spurious correlation: Jerk, speed in high-MAPR cohort

In order to determine the impact of prolonged stall periods on metrical behavior, a simple correlational analysis was performed. It has been established that whereas even healthy subjects are capable of performing single-joint tasks at a variety of movement speeds, with ostensibly similar performance quality, no measure of motor proficiency ought co-vary with movement speed under any circumstance. This, in many instances, holds true, but may unjustly presume the minimization of stall periods mid-motion.

Table 37: Correlation of smoothness metrics to average speed $\rho\left(\bar{\dot{\theta}}, X\right)$

| Metric | Domain | Healthy (MAPR = 0.09 ± 0.08) | Stroke (MAPR = 0.26 ± 0.19) |
|---|---|---|---|
| Integration | $J(t)$ | $J$ = 0.40 | $J$ = 0.85 |
| | $S(\theta)$ | $R$ = -0.22 | $R$ = 0.01 |
| Ratiometry | $J(t)$ | $\varepsilon_{J(t)}$ = 0.38 | $\varepsilon_{J(t)}$ = 0.85 |
| | $S(\theta)$ | $\varepsilon_{S(\theta)}$ = 0.03 | $\varepsilon_{S(\theta)}$ = 0.31 |

MAPR = Mean arrest period ratio (10%). $\varepsilon$ = Ratiometric index (max to mean).

Here, it was found that for stroke subjects, jerk-based measures correlate strongly, and spuriously, with average velocity. This metrical co-variation is attribute to the prevalence of stall (extremely low-velocity) periods in the trace, something not observed in healthy subjects jerk traces, or the spatial acceleration vector S($\theta$). Similarly, ratiometric indices evaluated from a trace with a small set of tall peaks, and

prolonged floors (zero-jerk regimes associated with movement stall), will be artificially reduced, erroneously decreasing jerk. Healthy subjects' ratiometry has relatively few periods of stall behavior, and are therefore less prone to correlation with average velocity; S($\theta$) is again impervious for its transform out of the temporal domain (Table 37).

## 9.7 Summary

Here, a novel angular-domain transformation is systematically tested for its response to a set of simple test cases, and is implemented in the analysis of empirical data recorded from both healthy and impaired subjects. Scalar metrics were devised for the analysis of vectorial spatial acceleration maps developed in Chapter 8. It was shown that the spatial acceleration maps S($\theta$) deliver an accurate and approximately surjective representation of peaks within the temporal acceleration profile, and selectively amplifies transient accelerations associated with spurious behavioral activity, virtually ignoring the gentle trajectory curvatures associated with the essential movement trends. Moreover, integrated and ratiometric scalars derived from these maps proved capable of discriminating an obviously impaired cohort, where similar time-domain metrics could not; in neither case were peak-counting metrics capable of reliably identifying impairment. It was determined that this limitation of jerk-based metrics may be explained by a spuriously high correlation between jerk and average movement velocity, observed under conditions of prolonged stall behaviors.

# 10 SUMMARY

## 10.1 Kinematical measurement of the upper-limb

### 10.1.1 Experimental methodology

#### *10.1.1.1 Instrumentation*

Kinematical analysis is the primary means by which motor impairment is assessed in both clinical and laboratory settings, and is considered a proxy to latent neurological processes occurring throughout the neuromotor hierarchy. In the present work, the motion of the upper-limb (UL) was studied in human subjects performing single-joint movements in the Mechanical Arm Support and Tracker (MAST). The MAST supports the UL against gravity, and rests the elbow and hand at or just below the plane of the shoulder, allowing for analysis of the elbow joint in repetitive movement tasks, providing both a comfortable interface, as well as continuous measurement of elbow angle.

#### *10.1.1.2 Subjects and protocol*

A variety of analytical paradigms, both traditional and novel, are discussed in terms of their origins, domain of application, and constraints. In order to test the limits of these tools, their incorporation into the analysis of trajectory data from subjects with a range of abilities was implemented: study recruitment comprised healthy persons with no known neurological impairment, as well as a cohort of hemiparetic individuals with compromised motor control due to chronic stroke, representing a wide distribution of age, gender, handedness, and (in the impaired cohort) side of cerebrovascular insult. Inclusion criteria for stroke subjects were pre-determined prior

to institutional review, and participant qualification was evaluated by an independent Occupational Therapist not involved with the study in any other capacity.

While subjects performed discrete single-joint articulations of the elbow, they were presented with a real-time GUI interface displaying not only instantaneous joint angle, but a buffer of approximately 2 seconds of movement history; their attention to this feedback was voluntary and not prompted in any way. Subjects were instructed to move "as smoothly as possible" within a "large, and comfortable range of motion." Prior to session start, all subjects were given complete instructions, and adequate time to warm-up; stroke subjects were provided with stretching exercises on request, as well as ample rest.

Some subjects made were observed in a single session, others performed the same movement task in independent sessions spanning several weeks, with a minimum of 24 hours in-between. When informative, a separate within-subjects analysis was performed on all subjects' data profiles, irrespective of the number of visits made to the lab; otherwise a within-session analysis was implemented on each session as an independent observation period.

### 10.1.2 Analysis: Standard, novel metrics

#### *10.1.2.1 Characterization*

The analyses performed here were primarily quantitative, reporting on parameters associated with movement proficiency, including basic spatiotemporal variables of the single-joint trajectory (SJT), symmetry, and smoothness. Where standard measures are reportedly flawed, these shortcomings are explained in the context of the data analyzed here (see, for example, Jerk Metrics among the differentiated smoothness metrics and Sections 2.2.4 and 7.4-7.7); in other cases,

certain metrics are discussed in terms of previously uncharacterized limitations (for example, dependence on average velocity of several jerk metrics under arrested motion, Section 7.6.2). Though derivation of these metrics is beyond the scope of this applied work, the origins of many objective smoothness measures are highlighted here where instructive.

#### *10.1.2.2 Implementation*

In addition to a light theoretical treatment of the standard measures of motor performance, these metrics were implemented directly the SJT traces recorded from the demographics described above, representing a spectrum of ability levels. Only through exhaustive, centralized evaluation of many subjects' movements can the true behavior of these performance measures be understood. In order for the results of these analyses to generalize beyond the setting of this work, and for validation against previous work, common practices were used in signal processing and metrical formulation as often as possible. Filter characteristics and use are consistent with what is found in there relevant literature, and departures from standard procedure are explained.

## 10.2 Results: Basic movement parameters

### 10.2.1 Cohorts not significantly different by standard measures

As expected, stroke subjects were found to have a large deficit in basic performance variables related to the range and speed of motion, as well as the amount of time spent in arrested motion. However, in most groupings, this only the mean arrest period ratio (MAPR) was found to yield significance at the $P < 0.05$ level, though range of motion $\Delta\theta$ and average velocity $\bar{\dot{\theta}}$ were nearly significant.

In terms of movement proficiency, stroke subjects were found to be markedly less smooth in their motion than healthy subjects, though none of the four jerk-based smoothness measures yielded significance at the $P < 0.05$ level. This result is consistent with others' findings as reported in the literature, where obviously impaired cohorts failed to yield significantly different measures (Goldvasser, McGibbon et al. 2001; Cozens and Bhakta 2003), and occasionally are observed to become *less* proficient with training, a counter-intuitive result, indeed (Rohrer, Fasoli et al. 2002). A summary is presented in Table 38.

| Table 38: Results Summary: Basic parameters of upper-limb motion | | | | | |
|---|---|---|---|---|---|
| | Healthy | | Stroke | | |
| Parameter | Value | Chapter ref. | Value | Chapter ref. | Cohort Comparison |
| | | | | | |
| Angular Range $\Delta\theta$ (º) | 91.3 ± 6.8º | 4.4.1 | 85.9 ± 7.3 | Chp 9 | $P \approx$ 1.5e-4 |
| | 88.4 ± 0.7 | 8.5.1 | 84.8 ± 5.5 | 8.5.1 | $P \approx$ 0.0753 |
| Angular velocity $\bar{\dot{\theta}}$ (º/s) | 90.6 ± 35.3 | 4.4.1 | 80.6 ± 23.5 | Chp 9 | $P \approx$ 0.0985 |
| | 76.0 ± 19.8 | 6.7.5 | 66.6 ± 49.1 | 6.7.5 | $P \approx$ 0.2761 |
| | 91.0 ± 3.8 | 8.5.1 | 80.0 ± 13.1 | 8.5.1 | $P \approx$ 0.2065 |
| MAPR 10% | 0.09 ± 0.08 | 6.7.5 | 0.26 ± 0.19 | 6.7.5 | $P \approx$ 0.0297 |
| | 0.15 ± .017 | n/a | 0.41 ± 0.22 | n/a | $P \approx$ 0.0193 |
| | | | | | |
| Smoothness measures | | | | | |
| IAJ ($\times 10^{-3}$) | 12.5 ± 9.1 | 6.7.6 | 33.8 ± 32.4 | 6.7.6 | $P \approx$ 0.3097 |
| AJ ($\times 10^{-4}$) | 0.9 ± 0.7 | 6.7.6 | 4.1 ± 4.7 | 6.7.6 | $P \approx$ 0.2097 |
| JM ($^\circ/s^2 \times 10^{-3}$) | 9.5 ± 7.2 | 6.7.6 | 11.2 ± 4.1 | 6.7.6 | $P \approx$ 0.1645 |
| NARJ | 15.2 ± 16.7 | 6.7.6 | 40.2 ± 21.5 | 6.7.6 | $P \approx$ 0.0992 |
| | | | | | |
| Movement variability | | | | | |
| Sess VR Flex | 0.09 ± 0.05 | 9.6.1 | 0.32 ± 0.24 | 9.6.1 | $P \approx$ 1.7e-4 |
| Sess VR Ext | 0.07 ± 0.03 | 9.6.1 | 0.34 ± 0.21 | 9.6.1 | $P \approx$ 9.7 e-7 |
| Var. $\bar{\dot{\theta}}$ Flex | 0.00 ± 0.00 | 9.6.2 | 0.19 ± 0.14 | 9.6.2 | $P \approx$ 0.0067 |
| Var. $\theta_{fin}$ Flex | 0.13 ± 0.04 | 9.6.2 | 0.03 ± 0.04 | 9.6.2 | $P \approx$ 2.4e-31 |
| Var $\bar{\dot{\theta}}$ Ext | 0.04 ± 0.01 | 9.6.2 | 0.19 ± 0.14 | 9.6.2 | $P \approx$ 0.0031 |
| Var. $\theta_{fin}$ Ext | 0.13 ± 0.05 | 9.6.2 | 0.09 ± 0.10 | 9.6.2 | $P \approx$ 1.3e-05 |
| | | | | | |
| Movement symmetry | | | | | |
| $\tau^{\dot{\theta}}_{\max}$ SJT, Flex | 0.36 ± 0.11 | 4.4.1 | 0.49 ± 0.15 | n/a | $P \approx$ 0.0020 |
| $\Gamma^{\ddot{\theta}}$ SJT, Flex | 0.71 ± 0.15 | 4.4.1 | 1.26 ± 0.48 | n/a | $P \approx$ 5.9e-7 |
| $\pi_{\dot{\theta}}$ SJT, Flex | 5.1 ± 5.2 | 4.4.1 | 5.2 ± 8.1 | n/a | $P \approx$ 0.0870 |
| $\tau^{\dot{\theta}}_{\max}$ SJT, Ext | 0.60 ± 0.13 | n/a | 0.40 ± 0.15 | n/a | $P \approx$ 4.8e-5 |
| $\Gamma^{\ddot{\theta}}$ SJT, Ext | 0.86 ± 0.28 | n/a | 1.45 ± 0.49 | n/a | $P \approx$ 2.5e-5 |
| $\pi_{\dot{\theta}}$ SJT, Ext | 5.87 ± 5.43 | n/a | 7.72 ± 9.88 | n/a | $P \approx$ 0.2208 |

MAPR = Mean Arrest Period Ratio. IAJ = Integrated average jerk, AJ = Average jerk, JM = Jerk metric, NARJ = Normalized average rectified jerk. VR = Variance Ratio, Flex = Flexion, Ext = Extension, Var. = Variability, $\theta_{fin} = \theta_{on} + \Delta\theta$. $\tau^{\dot{\theta}}_{\max}$ = Time to maximum velocity, $\Gamma^{\ddot{\theta}}$ = Symmetry ratio, $\pi_{\dot{\theta}}$ = Number of peaks in the velocity profile, SJT = Single-joint trajectory.

### 10.2.2 Significant deficit apparent in SJT symmetry, variability

There were, however, several domains in which cohort impairment was veridically resolved: movement variability and movement symmetry. Here, healthy subjects were found to perform single-joint motion with significantly less symmetry than stroke subjects, both in flexion and extension, and as measured by both the symmetry ratio, and the time to maximum velocity. Additionally, the SJTs recorded from stroke subjects exhibited significantly greater variation in average velocity and end-point positional error parameters, as well as holistic assessment of the trajectory profile over many cycles, as measured by the variance ratio (VR). The number of peaks in the velocity profile was not found to be a robust discriminant among cohorts.

## 10.3 Results: Trajectory domain transform

### 10.3.1 Method

Several standard measures of motor proficiency were found to insufficiently resolve obvious impairment in the cohorts involved in the present work. Furthermore, it was shown that these metrics were in some cases, highly correlated to average movement velocity, an untenable constraint in motion analyses where smoothness should not in any way reflect speed of motion. This metrical opacity was partly attributed to several shortcomings: 1) a dependency on the inherently noisy process of differentiation of discrete time-series data, 2) operation within the relatively uninformative domain of position versus time, and 3) no clear standard for normalization.

In order to address these limitations in performance measurement, a pseudo-wavelet transform was presented wherein goniometric data was parsed into segments of progressively finer resolution, testing regional partitions of the SJT against the standard of isogony: equal angle in equal time. This criterion can be tested directly by

a number of methods (here chosen to be the Pearson product moment correlation), and is related to the universally accepted notion of smooth movement: that of minimization of accelerative transience.

For each segment, an error was assigned, based on the correlation of the local SJT segment to its straight-slope approximant, to the corresponding domain of joint angle, yielding a plot of error-to-ideal versus joint angle. This transformation was validated for accuracy both in special test cases, and against empirical data, and scalar metrics were provided for the vector result.

### 10.3.2 Jerk correlates to average velocity in high arrest conditions

Task performance is considered "proficient" if the movement profile contains a minimum of transient accelerative behaviors; no dependence on speed should be inferred. Despite this supposed velocity independence, all four jerk metrics were found to correlate strongly ($\rho > 0.8$) to movement speed in the stroke cohort. It was concluded that this spurious interdependence of jerk and velocity could be explained by artificial decrease in the jerk integral, irrespective of its normalization, in situations of protracted periods of movement arrest. Indeed, the stroke subjects here had a significantly greater MAPR score than the healthy subjects.

| Table 39: Justification for, and analysis of, domain transform of kinematic data | | | | | |
|---|---|---|---|---|---|
| | Healthy | | Stroke | | |
| Parameter | Value | Chapter | Value | Chapter | Cohort |
| Correlation: Standard metrics to average velocity | | | | | |
| $\rho(\text{IAJ}, \bar{\dot{\theta}})$ | 0.05 | 6.7.5 | 0.84 | 6.7.5 | n/a |
| $\rho(\text{AJ}, \bar{\dot{\theta}})$ | 0.40 | 6.7.5 | 0.85 | 6.7.5 | n/a |
| $\rho(\text{JM}, \bar{\dot{\theta}})$ | 0.25 | 6.7.5 | 0.91 | 6.7.5 | n/a |
| $\rho(\text{NARJ}, \bar{\dot{\theta}})$ | 0.46 | 6.7.5 | 0.90 | 6.7.5 | n/a |
| | | | | | |
| Cohort discrimination: Temporal versus angular domain | | | | | |
| AUC $S(\theta)$ | 3.1 ± 0.8 | 8.5.2 | 8.0 ± 2.9 | 8.5.2 | $P \approx$ 6.6e-4 |
| AUC $J(t)$ | 9.0 ± 6.7 | 8.5.2 | 40.6 ± 46.9 | 8.5.2 | $P \approx$ 0.2544 |
| Ratiometry $S(\theta)$ | 12.1 ± 1.9 | 8.5.3 | 6.6 ± 0.9 | 8.5.3 | $P \approx$ 6.7e-4 |
| Ratiometry $J(t)$ | 9.9 ± 7.7 | 8.5.3 | 42.8 ± 49.4 | 8.5.3 | $P \approx$ 0.3097 |
| Peaks $S(\theta)$ | 9.3 ± 0.9 | 8.5.4 | 9.9 ± 1.6 | 8.5.4 | $P \approx$ 0.7892 |
| Peaks $J(t)$ | 14.4 ± 4.5 | 8.5.4 | 9.9 ± 5.7 | 8.5.4 | $P \approx$ 0.0992 |
| | | | | | |
| Correlation: Integrated metrics to average velocity | | | | | |
| $\rho(J(t)\ \text{Int}, \bar{\dot{\theta}})$ | 0.40 | 8.6.2 | 0.85 | 8.6.2 | n/a |
| $\rho(S(\theta)\ \text{Int}, \bar{\dot{\theta}})$ | -0.22 | 8.6.2 | 0.01 | 8.6.2 | n/a |
| $\rho(J(t)\text{Rat}, \bar{\dot{\theta}})$ | 0.38 | 8.6.2 | 0.85 | 8.6.2 | n/a |
| $\rho(S(\theta)\ \text{Rat}, \bar{\dot{\theta}})$ | 0.03 | 8.6.2 | 0.31 | 8.6.2 | n/a |
| AUC = Area under the curve. ρ = Pearson product moment correlation, IAJ = Integrated average jerk, AJ = Average jerk, JM = Jerk metric, NARJ = Normalized average rectified jerk. $\bar{\dot{\theta}}$ = average angular velocity. | | | | | |

### 10.3.3 Transformed metrics: Velocity-independent, discriminative

Whereas the transform enacted on SJT waveforms eliminates temporal information, metrics related to the vector of spontaneous acceleration S($\theta$) were found to correlate poorly to average velocity, with all values yielding cohort averages of $\rho <$ 0.5 (Table 39). From these traces, two classes of parameters were proposed: trace integrations, and trace ratiometrics. Though both metric classes were devoid of velocity dependence in both jerk and S($\theta$) traces recorded from healthy subjects,

temporal domain (jerk) metrics persisted in spuriously high velocity-dependence in the stroke cohort; transformed data exhibited no such correlation.

## 10.4 Results: Essential movement patterns

### 10.4.1 Method

Whereas proficiency can be readily assessed from the transient accelerations in the SJT profile, these features in the trajectory profile can obscure highly informative features of the movement profile such as the basic movement pattern and parameters related to movement symmetry. This noise can be related either to the generation of movement, or in its empirical observation; three such sources of trace artifact are proposed as 1) legitimate motor behavior unrelated to the essential motor plan, 2) machine error related to the acquisition and digitization data, not necessarily restricted to goniometry, and 3) noise related to the processing of kinematical data, not necessarily restricted to its differentiation.

In order to prevent contamination of certain trajectory analyses from noise inherent in the kinematical record, a trajectory surrogate was proposed where in the observed trace was reconstructed by one of a small set of analytical traces, parameterized to match average angular velocity, total range of motion, and delay of movement onset. These traces, selected from a set of ideal trajectory models selected to represent a modest (but complete) range of motor behaviors, involve a single presumption: that of monotonic angular velocity. From these noise-free trajectory approximants, selected via a standard minimization of the mean-squared difference, it is argued that both the essential motor behavior, and parameters related to trajectory symmetry, can be accurately extracted.

Beyond the first-order validation of method accuracy by direct waveform comparison (here by the coefficient of determination), a comprehensive analysis of

trace velocity feature identification was performed on both SJT data and their corresponding ET waveforms.

### 10.4.2 Cohorts similar in essential motor behaviors, not symmetry

#### *10.4.2.1 Degenerate movement patterns*

In all tasks, the single best model-based reconstruction of the SJT, the so-called Essential Trajectory (ET), was found to fit to the observed motion with a high degree of accuracy. The single most prolific model type in terms of the proportion of each dataset for which the greatest number of ETs were of a given curve type, was denoted as the Principal Trajectory (PT), irrespective of the proportion of its representation within the dataset. A Significant Trajectory (ST) was a model curve for which a "large" proportion of the dataset could be best-fit by a given class, as determined by a broken-stick scree analysis. The designation of a model curve as an ST is inclusive, but not limited to the ET.

In flexion tasks, a single ET was not sufficient to explain the totality, nor even a majority of subjects' datasets, in either within-subjects or within-session analysis. The average number of STs was greater than 2, indicating a degeneracy in movement themes. Indeed the proportion of traces for which the PT was the best-fit was approximately 50%, indicating that a variety of movement patterns could be expected from subjects. In datasets for which $| ST | > 1$, i.e. degenerate sets, no prediction between movement type could be found among basic movement parameters (average velocity, angle of movement onset, or performance sequence).

#### *10.4.2.2 Identical model trace distributions*

The movement patterns of both healthy and impaired cohorts, as depicted by histograms of proclivity per a given ET among subjects, revealed a nearly identical

propensity for subjects to "select" from among the six possible trajectory patterns. The primary movement class was that of linear traces, followed by sigmoidal traces (notably both symmetric), though a wide variety of movement patterns manifested as Significant Trajectories. In fact, not only were the distributions and degeneracies of PT model types nearly identical among cohorts, but there was little difference in setting: within-subject and within-session analyses yielded equivalent results.

Table 40: Results summary: Flexion pattern via Essential Trajectory modeling

| | Healthy | | Stroke | | |
|---|---|---|---|---|---|
| Parameter | Value | Chapter ref. | Value | Chapter ref. | Cohort Comparison |
| Goodness of Fit | | | | | |
| ET $R^2$ | 0.99±0.01 | 4.4.2 | 0.99±0.01 | 9.3.1 | $P \approx 0.9878$ |
| | | | | | |
| Symmetry | | | | | |
| $\tau^{\dot{\theta}}_{\max}$ ET | 0.39 ± 0.10 | 4.4.3 | 0.51 ± 0.16 | 9.5.5 | $P \approx 0.0193$ |
| $\Gamma^{\ddot{\theta}}$ ET | 0.71 ± 0.26 | 4.4.3 | 0.93 ± 0.23 | 9.5.5 | $P \approx 0.9878$ |
| | | | | | |
| Scree analysis | | | | | |
| \|ST\| Subject | 2.02 ± 0.72 | 5.5.2 | 2.27 ± 1.1 | 9.5.1.1 | $P \approx 0.5973$ |
| \|ST\| = 1 Subject | 0.24 | 5.5.2 | 0.27 | 9.5.1.1 | |
| PT prop Subject | 0.49 ± 0.14 | 5.5.2 | 0.48 ± 0.18 | 9..1.1 | $P \approx 0.4733$ |
| \|ST\| Session | 1.93 ± 0.64 | 5.5.3 | 1.93 ± 0.46 | 9.5.1.2 | $P \approx 0.6578$ |
| \|ST\| = 1 Session | 0 | 5.5.3 | 0 | 9.5.1.2 | |
| PT prop Session | 0.53 ± 0.13 | 5.5.3 | 0.52 ± 0.17 | 9.5.1.2 | $P \approx 0.1658$ |
| | | | | | |
| Correlation: ET type to basic movement parameters | | | | | |
| $\rho(ET, \bar{\dot{\theta}})$ | 0.14 | 5.6.4 | 0.13 | 9.4.4 | n/a |
| $\rho(ET, \theta_{on})$ | 0.09 | 5.6.4 | 0.05 | 9.4.4 | n/a |
| ρ(ET, #) | 0.09 | 5.6.4 | 0.10 | 9.4.4 | n/a |

ET = Essential Trajectory, $R^2$ = Coefficient of determination. $\tau^{\dot{\theta}}_{\max}$ = Time to maximum velocity, $\Gamma^{\ddot{\theta}}$ = Symmetry ratio. ST = Significant Trajectory, |ST| = Number of STs, PT prop = Proportion of movement profile ETs fitted to the Principal Trajectory (PT). ρ = Pearson product moment correlation, $\bar{\dot{\theta}}$ = average angular velocity, $\theta_{on}$ = angle of motion onset, # = Sequence number in dataset.

#### *10.4.2.3 Stroke subjects move with greater symmetry*

Whereas the Essential Trajectory was validated as a measurement substrate for extraction of parameters associated with the veridical movement behaviors, symmetry in the SJT was extracted from the corresponding ET movement patterns. Similar to the results generated in a symmetry analysis of SJT waveforms, stroke subjects were found to move with a highly symmetric rhythm, reaching significance at the $P < 0.01$ level in the time-to-maximum velocity, and near-significance via the symmetry ratio; healthy subjects were found to spend less time in acceleration, and more time in deceleration. It is noted that despite the apparent equivalence between symmetry analysis via ET and via SJT, this is an artifact resulting from a randomly-distributed noise in the trajectory traces. Indeed, on a trace-by-trace basis, the differences between the observed velocity peak in the raw trace (low-pass filtered), and the differentiated-and-filtered Essential Trajectory was large, with the Essential Trajectory demonstrably accurate in extracting the veridical velocity peak.

### 10.4.3 Extension movement patterns reveal additional insight

#### *10.4.3.1 PT distributions, degeneracy similar to that of flexion*

In extension tasks, the linear and sigmoidal ET traces most-often yielded Principal Trajectories. Here again, the movement profiles both in sessional and subject analysis, were found to be degenerate with multiple STs, and less than 40% of subjects yielding single-ST datasets. As with flexion tasks, the proportion of each dataset for which the PT was found to yield the ET was approximately 50-60%, and no correlation to basic movement parameters was found.

#### *10.4.3.2 Poor prediction across movement direction*

For degenerate datasets, an analysis of the correspondence between flexion and extension movement patterns was performed by inspection of the ST sets. Here, the average overlap between flexion STs and extension STs was low (approximately $\overline{O}$ = 0.4-0.5), with less than 10% of subjects' ST sets completely identical among movement tasks (unity overlap,$O_1$); a large proportion of subjects' ST sets yielded a null overlap: $O_0$= 0.2 - 0.5. Thus, it is concluded that there is relatively little predictive power across direction of between movement theme generation.

| Table 41: Results summary: Extension pattern via Essential Trajectory modeling | | | | | |
|---|---|---|---|---|---|
| | Healthy | | Stroke | | |
| Parameter | Value | Chapter ref. | Value | Chapter ref. | Cohort Comparison |
| Symmetry | | | | | |
| $\tau^{\dot{\theta}}_{\max}$ ET, Ext | 0.66 ± 0.07 | n/a | 0.47 ± 0.10 | n/a | $P \approx$ 2.4e-7 |
| $\Gamma^{\ddot{\theta}}$ ET, Ext | 0.67 ± 0.23 | n/a | 1.04 ± 0.43 | n/a | $P \approx 0.0120$ |
| | | | | | |
| Scree analysis | | | | | |
| \|ST\| Subject | 1.92 ± 0.81 | 5.6.2 | 1.63 ± 0.50 | 9.5.1.3 | $P \approx 0.3482$ |
| \|ST\| = 1Subject | 0.31 | 5.6.2 | 0.36 | 9.5.1.3 | n/a |
| PT prop Subject | 0.56 ± 0.16 | 5.6.2 | 0.52 ± 0.13 | 9.5.1.3 | $P \approx 0.5014$ |
| \|ST\| Session | 1.93 ± 0.64 | n/a | 1.72 ± 0.43 | n/a | $P \approx 0.2694$ |
| \|ST\| = 1 Session | 0.05 | n/a | 0 | n/a | n/a |
| PT prop Session | 0.61 ± 0.17 | n/a | 0.59 ± 0.18 | n/a | $P \approx 0.4363$ |
| | | | | | |
| Correlation: ET type to basic movement parameters | | | | | |
| $\rho(\text{ET}, \bar{\dot{\theta}})$ | 0.12 | 5.6.4 | 0.07 | 9.4.4 | n/a |
| $\rho(\text{ET}, \theta_{on})$ | 0.12 | 5.6.4 | 0.07 | 9.4.4 | n/a |
| ρ(ET, #) | 0.10 | 5.6.4 | 0.10 | 9.4.4 | n/a |
| | | | | | |
| Prediction: Flexion, Extension | | | | | |
| $PT^f = PT^e$ Subj | 0.29 | n/a | 0.27 | n/a | n/a |
| ST $\bar{O}$ Subj | 0.39 ± 0.36 | n/a | 0.45 ± 0.30 | n/a | $P \approx 0.9589$ |
| ST $O_1$ Subj | 0 | n/a | 0.10 | n/a | n/a |
| ST $O_0$ Subj | 0.35 | n/a | 0.20 | n/a | n/a |
| $PT^f = PT^e$ Sess | 0.24 | 5.6.3.3 | 0.5 | 9.5.3 | n/a |
| ST $\bar{O}$ Sess | 0.39 ± 0.36 | 5.6.3.3 | 0.44 ± 0.30 | 9.5.3 | $P \approx 0.3461$ |
| ST $O_1$ Sess | 0.09 | 5.6.3.3 | 0.08 | 9.5.3 | n/a |
| ST $O_0$ Sess | 0.41 | 5.6.3.3 | 0.25 | 9.5.3 | n/a |

ET = Essential Trajectory, $\tau^{\dot{\theta}}_{\max}$ = Time to maximum velocity, $\Gamma^{\ddot{\theta}}$ = Symmetry ratio. ST = Significant Trajectory, |ST| = Number of STs, PT prop = Proportion of movement profile ETs fitted to the Principal Trajectory (PT). ρ = Pearson product moment correlation, $\bar{\dot{\theta}}$ = average angular velocity, $\theta_{on}$ = angle of motion onset, # = Sequence number in dataset. $\bar{O}$ = Average ST overlap, $O_1$ = Proportion of profiles with unity ST intersection, $O_0$ = Proportion of profiles with null ST.

## 10.5 Conclusions to hypotheses

### 10.5.1 Overview

The present work represents a series of investigations into the characterization and analysis of human performance vis-à-vis both basic movement parameters and holistic assessments of movement proficiency via a family of smoothness metrics. A series of experimental hypotheses were put forth related to the assessment of human movement, and features of movement concerning both basic behavioral patterns, and their alteration under neurological deficit. A review of these hypotheses and their conclusions follows:

### 10.5.2 Chapter 4: Essential Trajectory as a valid SJT surrogate

It was hypothesized that the Essential Trajectory, an analytical curve parameterized to match the observed trajectory, would serve as a valid trajectory surrogate,

> *The single-joint trajectory can be accurately reconstructed by a parameterized analytic curve selected from among a small set of model traces, the so-called Essential Trajectory.* (Hypothesis 1)

and that the parameters extracted thereof would accurately reflect the veridical movement parameters contained within the SJT.

> *Features extracted from the Essential Trajectory will report information relevant to the observed movement with an accuracy that is competes with or exceeds those extracted from the observed single-joint trajectory.* (Hypothesis 2)

It was, indeed determined that the ET was a valid and highly accurate representation of the single-joint trajectory, and that the parameters associated with the essential motor behavior were accurately extracted via the Essential Trajectory.

### 10.5.3 Chapter 5: SJTs symmetric, but unpredictably degenerate

Based on empirical laws, e.g. the isogony principle, and on copious abstraction within the literature, it was supposed that the basic motor behaviors of healthy subjects would yield highly linear, or at least symmetric SJT traces.

> *Subjects single-joint movements will be largely isogonic and symmetric in both flexion and extension tasks.* (Hypothesis 3)

Additionally, it was suggested that the basic motor behaviors of these subjects were highly stable and stereotyped in the absence of external perturbations, and with the movement constrained, as in the MAST.

> *Irrespective of the isogonic nature of the movement profile* (Hypothesis 3)*, model adoption by subjects will be highly uniform, showing relatively high stability among the available model types.* (Hypothesis 4)

While the predominance of linear and sigmoidal Principal Trajectories in the subjects' datasets indicated a highly symmetric movement, these movement patterns were hardly exclusive. Indeed, there was a considerable degeneracy in the movement themes, and many asymmetric ETs were found to contribute significantly. In these pluralistic cases, it was further hypothesized that "selection" of ET type could be related to basic parameters of the observed motion.

*In the cases where the primary model type is not observed in a given movement cycle, this deviation from the central behavioral theme can be explained as the result of some perturbation in basic movement patterns, i.e. angular velocity, angle of motion onset, or time.* (Hypothesis 5)

This was found not to be the case. It is noted that mixed-effects analyses were not performed, however this would be beyond the scope of the present work. It is concluded that humans without apparent neurologic deficit do not necessarily adopt uniformly linear or symmetric movement behaviors, but fluctuate in a way that cannot necessarily be predicted by initial conditions.

### 10.5.4 Chapter 6: Stroke patients equivalently isogonic, degenerate

In order to characterize the essential movement behaviors of an impaired cohort, a validation of the Essential Trajectory model in stroke subjects' SJTs was performed.

*Essential Trajectory approximants of the SJT trace will yield equivalently strong trace reconstructions of trajectories recorded from hemiparetic individuals.* (Hypothesis 6)

As expected, the ET traces yielded highly accurate representations of stroke subjects' movements, with an equivalently high coefficient of determination as that of the healthy subjects. Lastly, it was hypothesized that the compromised motor skills of chronic stroke patients would manifest as a deviation from the highly symmetric and linear trajectories observed in stroke patients.

*Subjects with impaired motor control exhibit motor deficiency in the way of asymmetric movement patterns.* (Hypothesis 7)

Furthermore, it was suggested that the "choice" of movement pattern would depart even further from the pluralistic PT model results of healthy subjects, resulting in a higher degeneracy.

> *Motor impairment will manifest as an increased variability in trajectory patterns, and this instability will have greater co-dependence on basic movement parameters.* (Hypothesis 8)

Contrary to expectation, it was determined that the impaired cohort performed the single-joint movement task with surprisingly similar basic behavior as that of the healthy subjects. No significant difference was found in the number of significant trajectories, nor in the adoption of ETs as Principal Trajectories. Here, a cohort similarity is identified, where dissimilarity was expected.

### 10.5.5 Chapter 8: Failure of jerk measures in cohort discrimination

Whereas it has been reported in the literature that standard jerk-based smoothness raters occasionally fail to report significant differences between cohorts, it was supposed that this may relate to a spurious co-dependence of average angular velocity,

> *Standard jerk metrics are independent of average velocity in "well-behaved" movements performed by healthy individuals.* (Hypothesis 9a)

and that this might pertain only to persons with impaired motor control.

> *Jerk metrics exhibit spurious dependence on movement velocity in the special case of spastic movements characterized by significant periods of stall behavior.* (Hypothesis 9b)

Indeed, it was shown that in highly arrested motion, the jerk integral, irrespective of its normalization, was artificially decreased, resulting in the artificial appearance of reduced performance deficit: the greater the movement arrest, the greater the decrease in jerk.

*Jerk metrics can discriminate between healthy individuals and those with impaired motor control due to chronic stroke.* (Hypothesis 10)

It was further shown that this effect is sufficiently powerful and so highly variable among subjects that cohort impairment is no longer resolvable at a significant level.

### 10.5.6 Chapter 9: Domain transformation yields valid substrates

Temporal domain analysis of kinematic data results proficiency metrics that are not only highly prone to error, but are dependent on a relatively meaningless variable: time. In order to obviate the pitfalls of position-versus-time analysis, a pseudo-wavelet data transformation was proposed.

*Vectorial rendering of the single-joint trajectory, following transformation into the domain of linear approximant error as a function of angle, accurately reports movement proficiency in both healthy and impaired cohorts.* (Hypothesis 11)

Here, subjective analysis of both special test cases, and empirical data yielded convincing evidence of the accuracy of the representation of spontaneous accelerations in the angular domain transform. In order to support traditional analyses and hypothesis testing, a set of scalars was defined from which the spatial acceleration map could be evaluated.

*Scalar smoothness metrics derived from the angular-domain trajectory transformation can discriminate healthy from impaired condition as well as standard metrics.* (Hypothesis 12)

It was determined that these scalars were not only capable of resolving cohort differences, but exhibited a metrical independence of angular velocity not observed in temporal domain (jerk) metrics.

*Measures derived from the angular domain are impervious to spurious co-dependence of angular velocity.* (Hypothesis 13)

Thus it is concluded that the angular domain transform is not only an accurate and utilitarian paradigm in the resolution of spatio-temporal behavioral idiosyncrasies, but may be necessary in order to avoid corruption of the proficiency assessment due to average velocity in the case of highly arrested movement.

## 10.6 Concluding remarks

### 10.6.1 Thesis scope

For many standard performance measures, there is no central work in which a given metric is compared against other metrics: it is atypical for a metric's use to be justified beyond cursory explanation, particularly in clinical studies. Furthermore, despite their evaluation of obviously impaired cohorts, many measures have an imperfect record in cohort discrimination. This can be explained by a dearth of best-practices in performance assessment, starting with which metrics are best used for what research hypothesis, and including metrical normalization, and other standardization practices that would allow for generalization across protocols, thus

greatly increasing the power of experimental and clinical activities and their dissemination in the scientific literature.

Here, an in-depth, but by no means comprehensive, analysis is performed on several widely-adopted measures, including an overview of their origins and limitations. Alternative methods are proposed to balance the typically mutually exclusive needs of identification of the essential movement pattern, and isolation of specific loci of motor deficiency. As well as possible, these novel methods are validated and compared against the state-of-the-art paradigms, hopefully to the satisfactory demonstration of their accuracy. It is the presumption of the author that their utility is self-evident.

### 10.6.2 Thesis self-consistency

There are many consistencies among the analyses performed here that suggest the veracity of these results. One subtle but noteworthy aspect of these data bears mention. It is reported (Table 38) that stroke subjects move with significantly (or near-significance) greater symmetry than the healthy subjects. Elsewhere, their symmetry is reported as not significantly different (Figure 16). To explain: these apparently contradictory conclusions result from two entirely different analyses: quantitative assessment by symmetry ratio and time-to-maximum velocity, and by categorical analysis of the Principal Trajectory type. These results are not necessarily incongruous: quantitative measurement assesses the entire movement trace, without discriminating for periods of relatively slow movement at the motion extrema; the Essential Trajectory model (and thus the PT), accounts for this “stall” behavior automatically, and reports only the “important” movement activity above a given threshold of movement.

## 10.7 Concluding philosophy

Here, simple substrates of single-joint motion are decomposed into their two primary aspects: the movement essence, and their incidence. Beyond the impact on experimental observation or research into the human motor system it is suggested that this work may contain implications for broader impacts on the approach of neuromotor scientists and clinicians: While it is certainly relevant to ask "in what way are we different," (*we* referring to any two individuals or cohorts, here chronic stroke patients and the unimpaired), just as important a question may be "in what way are we similar?" Indeed, it is not necessarily the way a question is answered that is informative but the question, itself, that was posed.

# APPENDIX

## 10.8 Variables: Classical Latin alphabet

| Variable | Description | First mentioned |
|---|---|---|
| A | Arbitrary simulation parameter | 7.3.2 |
| A($\theta$) | Template error array | 8.5.7 |
| $a$ | Activation | 3.2.1.2 |
| $a$ | Muscle activation | 8.3.2 |
| $a$ | Coefficient of correlation metrics | 8.5.6 |
| $B$ | Viscosity | 3.2.1.1 |
| $B$ | Baseline-padded curve $b$ | 3.4.2 |
| $b$ | Basic model curve | 3.4.2 |
| $b$ | Coefficient of correlation metrics | 8.5.6 |
| $C$ | Curvature | 5.4.1.1 |
| $c$ | Time sample | 2.2.3 |
| $C$ | Coefficient of correlation metrics | 8.5.6 |
| $d_{\mathrm{m}}$ | Moment arm of muscle $m$ | 3.2.1.1 |
| E($\theta$) | Domain of approximation error | 8.5.5 |
| E*($\theta$) | Normalized error array | 8.5.7 |
| $E$ | Regional scalar value for E($\theta$) | 8.6 |
| $F_{\mathrm{m}}$ | Force of muscle $m$ | 3.2.1.1 |
| G | Partition subset | 8.5.4 |
| H | Histogram | 5.3.3.1 |
| $h$ | Filter coefficients | 4.5.1.1 |
| $I$ | Inertia | 3.2.1.1 |
| $i$ | Time sample | 2.2.3 |
| $i$ | Index of flexion/extension | 8.3.2 |
| $J$ | Jerk integral | 2.3.2.1 |
| $\bar{J}$ | Average jerk | 7.2.1 |
| J($t$) | Jerk as a function of time | 7.4 |
| $j$ | Cycle iteration | 5.4.2.1 |
| $K$ | Elastic stiffness | 3.2.1.1 |
| $K$ | Curvature | 3.2.2.2 |
| $k$ | Arbitrary coefficient | 3.2.2.2 |
| $k$ | Arbitrary simulation parameter | 7.3.2 |
| $k$ | Partition index | 8.5.4 |
| $k$ | Coefficient of correlation metrics | 8.5.6 |
| $\dot{L}$ | Rate of change of muscle length | 3.2.1.2 |
| $L$ | Muscle length | 3.2.1.2 |
| $L$ | Vector of ET labels | 4.3.2 |
| MAPR | Mean arrest period ratio | 2.3.2.2 |
| MR | Movement range | 2.2.3 |
| $N_{\mathrm{p}}$ | Number of points in partition | 8.5.2 |
| $N_{\mathrm{s}}$ | Number of samples | 2.3.1.1 |

| | | |
|---|---|---|
| $O$ | Overlap of ST sets | 5.6.3.1 |
| PT | Principal Trajectory | 5.3.3.2 |
| $PT^{f,e}$ | PT in flexion, extension | 5.6.3.1 |
| P | Temporal domain partition | 8.5.3 |
| $p$ | Zero-pad duration | 3.4.2 |
| $p$ | Pace | 7.6.4 |
| $R$ | Radius of curvature | 5.4.1.1 |
| $R$ | Spatial error map (heat map) | 9.5.2 |
| $r_{vp}$ | Rank of veridical max. $\dot{\theta}$ peak | 4.6.2 |
| S | Sorted histogram | 5.3.3.2 |
| ST | Significant Trajectory | 5.3.3.2 |
| $S(\theta)$ | Spatial acceleration vector | 8.5.5 |
| $S^*(\theta)$ | Normalized $S(\theta)$ | 8.6 |
| $s$ | Second | 2.2.3 |
| s | Motion segment | 3.2.2.2 |
| $T$ | Total movement time | 2.3.1.1 |
| $T_m$ | Torque of muscle group $m$ | 3.2.1.1 |
| $T$ | Torque | 3.2.1.1 |
| $T^*$ | Normalized time | 5.4.2.1 |
| $T'$ | Transformed movement duration | 7.6.4 |
| $t$ | Time | 2.3.2.1 |
| $u$ | Muscle activation input | 3.2.1.2 |
| $u_{ifd}$ | Stretch reflex | 8.3.2 |
| V | Voltage | 2.2.3 |
| $v_{mj}$ | Minimum jerk velocity | 3.2.1.2 |
| $V$ | Angular velocity | 5.4.1.1 |
| X | Arbitrary dataset | 5.4.2.1 |
| $\overline{X}_i$ | Average across time points of X | 5.4.2.1 |
| $\overline{\overline{X}}$ | Grand mean of X | 5.4.2.1 |
| $X(\omega)$ | Fourier transform of position | 7.6.4 |
| $x(t)$ | Position as a function of time | 7.6.4 |

## 10.9 Variables: Greek alphabet

| Variable | Description | First mentioned |
|---|---|---|
| $\alpha$ | Positive constant of 2/3-PL | 3.2.2.2 |
| $\alpha$ | Arbitrary simulation parameter | 7.3.2 |
| $\alpha$ | Partition lower-bound | 8.5.2 |
| $\alpha$ | Arbitrary error value | 8.5.7 |
| $\beta$ | Exponent of 2/3-PL | 3.2.2.2 |
| $\beta$ | Arbitrary simulation parameter | 7.3.2 |
| $\beta$ | Partition upper-bound | 8.5.2 |
| $\beta$ | Arbitrary error value | 8.5.7 |
| $\Gamma^{\ddot{\theta}}$ | Symmetry ratio | 2.3.1.2 |
| $\gamma$ | Arbitrary parameter | 6.6.2 |
| $\gamma$ | Coefficient of correlation metrics | 8.5.6 |
| $\Delta\theta$ | Range of motion | 2.3.1.1 |
| $\Delta\theta_{\text{cal}}$ | Calibration range of motion | 2.2.3 |
| $\Delta$ | Range of motion | 3.2.2.1 |
| $\delta$ | MAPR Velocity threshold | 2.3.2.2 |
| $\delta$ | Derivative resolution/step size | 7.6.2 |
| $\delta$ | Arbitrary threshold | 9.4.2 |
| $\varepsilon$ | Ratio of trace peak-to-mean | 9.3.3.4 |
| $\eta$ | Viscosity | 3.2.1.1 |
| $\eta$ | User-defined spatial resolution | 8.5.7 |
| $\dot{\theta}$ | Velocity vector | 2.2.3 |
| $\overline{\dot{\theta}}$ | Average velocity | 2.3.1.1 |
| $\theta_{\text{min}}$ | Angle of motion onset | 2.3.1.1 |
| $\theta_{\text{max}}$ | Angle of motion cessation | 2.3.1.1 |
| $\dot{\theta}_{\text{max}}$ | Maximum angular velocity | 2.3.1.2 |
| $\ddot{\theta}_{\text{max}}$ | Maximum angular acceleration | 2.3.1.2 |
| $\theta(t)$ | Joint angle as a function of time | 2.3.2.1 |
| $\Theta_{\text{eq}}$ | Equilibrium joint angle | 3.2.1.1 |
| $\theta_{ROM}$ | Angular range of motion | 3.4.2 |
| $\theta_{on}$ | Angle of motion onset | 3.4.2 |
| $\theta_{off}$ | Angle of motion cessation | 3.4.2 |
| $\Theta_{\text{d,e}}$ | Angles of raw error comparison | 9.4.2 |
| $\kappa$ | Jerk normalization coefficient | 2.3.2.1 |
| $\mu$ | Mean | 1.2.3.1 |
| $\mu$ | Migration coefficient | 8.5.2 |
| $\xi$ | Partition sample | 8.5.7 |
| $\pi_{\dot{\theta}}$ | Number of peaks in velocity trace | 4.4.1 |
| $\rho$ | Correlation coefficient | 4.3.3 |
| $\rho_{XY}$ | Correlation of two traces | 8.5.6 |
| $\sigma$ | Standard deviation | 1.2.3.1 |
| $\sigma_{\dot{\theta}}^2$ | Velocity variance | 7.2.1 |
| $\sigma_X$ | Standard deviation of a single trace | 8.5.6 |

| | | |
|---|---|---|
| $\sigma_{XY}$ | Standard deviation of a two traces | 8.5.6 |
| $\boldsymbol{\tau}_{\max}^{\theta}$ | Time to max. elbow flexion | 2.3.1.1 |
| $\boldsymbol{\tau}_{\max}^{\dot{\theta}}$ | Time to max. angular velocity | 2.3.1.2 |
| $\boldsymbol{\tau}_{\max}^{\ddot{\theta}}$ | Time to max. angular acceleration | 2.3.1.2 |
| $\tau$ | Temporal landmark | 4.6.2 |
| $\tau_d$ | Selected points of a given trace | 9.4.2 |
| $\nu$ | Sampling Frequency | 2.2.3 |
| $\varphi$ | Parameter variability | 6.6.2 |
| $\chi$ | *b* class (= A → F) | 3.4.2 |
| $\Psi$ | Arbitrary waveform feature | 4.6.1 |
| $\omega$ | Angular frequency | 7.6.4 |

# REFERENCES

Adamovich, S. V., P. S. Archambault, et al. (2001). "Hand trajectory invariance in reaching movements involving the trunk." Exp Brain Res 138(3): 288-303.

Adamovich, S. V., M. F. Levin, et al. (1997). "Central modifications of reflex parameters may underlie the fastest arm movements." J Neurophysiol 77(3): 1460-9.

Akazawa, K. and R. Okuno (2006). "Estimating torque-angle relations of human elbow joint in isovelocity flexion movements." IEICE Transactions on Information and Systems E89-D(11): 2802-2810.

Amirabdollahian, F., R. Loureiro, et al. (2002). A case study on the effects of a haptic interface on human arm movements with implications for rehabilitation robotics. 1st Cambridge Workshop on Universal Access and Assistive Technology (CWUATT) (incorporating 4th Cambridge Workshop on Rehabilitation Robotics). Cambridge, UK, University of Cambridge.

Archambault, P., P. Pigeon, et al. (1999). "Recruitment and sequencing of different degrees of freedom during pointing movements involving the trunk in healthy and hemiparetic subjects." Exp Brain Res 126(1): 55-67.

Asatryan, D. G. and A. G. Feldman (1965). "Functional timing of the nervous system with control of movements or maintenance of a steady posture: I. Mechanographic analysis of the work of the joint on execution of a postural task." Biophys USSR 10: 925-935.

Atkeson, C. G. and J. M. Hollerbach (1985). "Kinematic features of unrestrained vertical arm movements." J Neurosci 5(9): 2318-30.

Bartkowiak, A., S. Lukasik, et al. (1991). "Statistical Evaluation of the Effect of Gemfibrosil, a Cholesterol Reducing Drug, on Some Biochemical Coronary Heart-Disease Risk Variables." Biometrical Journal 33(6): 711-718.

Bastian, A. J., K. M. Zackowski, et al. (2000). "Cerebellar ataxia: torque deficiency or torque mismatch between joints?" J Neurophysiol 83(5): 3019-30.

Beppu, H., M. Nagaoka, et al. (1987). "Analysis of Cerebellar Motor Disorders by Visually-Guided Elbow Tracking Movement .2. Contribution of the Visual Cues on Slow Ramp Pursuit." Brain 110: 1-18.

Beppu, H., M. Suda, et al. (1984). "Analysis of cerebellar motor disorders by visually guided elbow tracking movement." Brain 107 ( Pt 3): 787-809.

Binet, A. and J. Courtier (1893). "On the speed of graphic movements." Revue Philosophique 35: 664-671.

Bizzi, E., N. Accornero, et al. (1984). "Posture control and trajectory formation during arm movement." J Neurosci 4(11): 2738-44.

Blakeley, J. and J. Jankovic (2002). "Secondary paroxysmal dyskinesias." Mov Disord 17(4): 726-34.

Bouisset, S. and F. Goubel (1973). "Integrated electromyographical activity and muscle work." J Appl Physiol 35(5): 695-702.

Brooks, V. B., J. D. Cooke, et al. (1973). The continuity of movements. New York, Plenum.

Camilleri, M. J., M. L. Hull, et al. (2007). "Sloped muscle excitation waveforms improve the accuracy of forward dynamic simulations." J Biomech 40(7): 1423-32.

Cangelosi, R. and A. Goriely (2007). "Component retention in principal component analysis with application to cDNA microarray data." Biol Direct 2: 2.

Chang, J. J., T. I. Wu, et al. (2005). "Kinematical measure for spastic reaching in children with cerebral palsy." Clin Biomech (Bristol, Avon) 20(4): 381-8.

Corcos, D. M., G. L. Gottlieb, et al. (1989). "Organizing principles for single-joint movements. II. A speed-sensitive strategy." J Neurophysiol 62(2): 358-68.

Cozens, J. A. and B. B. Bhakta (2003). "Measuring movement irregularity in the upper motor neurone syndrome using normalised average rectified jerk." J Electromyogr Kinesiol 13(1): 73-81.

Dabroom, A. M. and H. K. Khalil (1999). "Discrete-time implementation of high-gain observers for numerical differentiation." International Journal of Control 72(17): 1523-1537.

Daly, J. J., N. Hogan, et al. (2005). "Response to upper-limb robotics and functional neuromuscular stimulation following stroke." J Rehabil Res Dev 42(6): 723-36.

Derwort, A. (1938). "Investigations on the timecourse of tracing movements." Pflugers Archives fur die GesamtePhysiologie des Menschen und der Tiere 240: 661-675.

Dewald, J. P., P. S. Pope, et al. (1995). "Abnormal muscle coactivation patterns during isometric torque generation at the elbow and shoulder in hemiparetic subjects." Brain 118 ( Pt 2): 495-510.

Doeringer, J. A. and N. Hogan (1998). "Intermittency in preplanned elbow movements persists in the absence of visual feedback." J Neurophysiol 80(4): 1787-99.

Engelbrecht, S. E. (2001). "Minimum Principles in Motor Control." J Math Psychol 45(3): 497-542.

Engelbrecht, S. E. and J. P. Fernandez (1997). "Invariant characteristics of horizontal-plane minimum-torque-change movements with one mechanical degree of freedom." Biological Cybernetics 76(5): 321-329.

Fang, Y., G. H. Yue, et al. (2007). "Abnormal cognitive planning and movement smoothness control for a complex shoulder/elbow motor task in stroke survivors." J Neurol Sci 256(1-2): 21-9.

Feldman, A. G. and M. L. Latash (1982). "Afferent and efferent components of joint position sense; interpretation of kinaesthetic illusion." Biol Cybern 42(3): 205-14.

Feng, C. J. and A. F. Mak (1997). "Three-dimensional motion analysis of the voluntary elbow movement in subjects with spasticity." IEEE Trans Rehabil Eng 5(3): 253-62.

Fetters, L. and J. Todd (1987). "Quantitative assessment of infant reaching movements." J Mot Behav 19(2): 147-66.

Fitts, P. M. (1954). "The information capacity of the human motor system in controlling the amplitude of movement." J Exp Psychol 47(6): 381-91.

Fitts, P. M. and J. R. Peterson (1964). "Information Capacity of Discrete Motor Responses." J Exp Psychol 67: 103-12.

Flanagan, J. R. and D. J. Ostry (1990). Trajectories of human mulit-joint arm movements: Evidence of joint level planning. London, Springer-Verlag.

Flash, T. and E. Henis (1991). "Arm Trajectory Modifications during Reaching Towards Visual Targets." Journal of Cognitive Neuroscience 3(3): 220-230.

Flash, T. and N. Hogan (1985). "The coordination of arm movements: an experimentally confirmed mathematical model." J Neurosci 5(7): 1688-703.

Goldvasser, D., C. A. McGibbon, et al. (2001). "High curvature and jerk analyses of arm ataxia." Biol Cybern 84(2): 85-90.

Gomi, H. and Kawato (1996). "Equilibrium-point control hypothesis examined by measured arm stiffness during multijoint movement." Science 272(5258): 117-20.

Gottlieb, G. L., D. M. Corcos, et al. (1989). "Organizing principles for single-joint movements. I. A speed-insensitive strategy." J Neurophysiol 62(2): 342-57.

Gottlieb, G. L., M. L. Latash, et al. (1992). "Organizing principles for single joint movements: V. Agonist-antagonist interactions." J Neurophysiol 67(6): 1417-27.

Gowland, C., P. Stratford, et al. (1993). "Measuring physical impairment and disability with the Chedoke-McMaster Stroke Assessment." Stroke 24(1): 58-63.

Gresham, G. E., P. W. Duncan, et al. (1995). Post-stroke rehabilitation. A. f. H. C. P. a. R. US Department of Health and Human Services. Bethesda, MD. 95.

Gribble, P. L. and D. J. Ostry (1999). "Compensation for interaction torques during single- and multijoint limb movement." J Neurophysiol 82(5): 2310-26.

Hancock, P. A. and K. M. Newell (1985). The movement speed-accuracy relationship in space-time. Berlin, Springer-Verlag.

Harris, C. M. and D. M. Wolpert (1998). "Signal-dependent noise determines motor planning." Nature 394(6695): 780-4.

Hastie, T., R. Tibshirani, et al. (2001). The Elements of Statistical Learning. New York, NY, Springer.

Heller, A., D. T. Wade, et al. (1987). "Arm function after stroke: measurement and recovery over the first three months." J Neurol Neurosurg Psychiatry 50(6): 714-9.

Hoff, B. (1994). "A Model of Duration in Normal and Perturbed Reaching Movement." Biological Cybernetics 71(6): 481-488.

Hoffman, D. S. and P. L. Strick (1990). "Step-tracking movements of the wrist in humans. II. EMG analysis." J Neurosci 10(1): 142-52.

Hogan, N. (1984). "An organizing principle for a class of voluntary movements." J Neurosci 4(11): 2745-54.

Hogan, N., H. I. Krebs, et al. (2006). "Motions or muscles? Some behavioral factors underlying robotic assistance of motor recovery." J Rehabil Res Dev 43(5): 605-18.

Hollerbach, J. M. (1981). "An oscillation theory of handwriting." Biological Cybernetics 39: 135-156.

Hsiang, S. M., C. C. Chang, et al. (1999). "Development of a set of equations describing joint trajectories during para-sagittal lifting." J Biomech 32(8): 871-6.

Hurley, J. F. (1981). Multivariable Calculus. Philadelphia, PA, Saunders College Publishing.

Jack, W. R. (1895). "The Analysis of Voluntary Muscular Movements by Certain New Instruments." J Anat Physiol 29(Pt 4): 473-8.

Jackson, D. (1993). "Stopping rules in principal components analysis: A comparison of heuristical and statistical approaches." Ecology 74: 2204-2214.

Jaric, S., S. Blesic, et al. (1999). "Changes in movement final position associated with agonist and antagonist muscle fatigue." Eur J Appl Physiol Occup Physiol 80(5): 467-71.

Jaric, S., G. L. Gottlieb, et al. (1998). "Changes in the symmetry of rapid movements. Effects of velocity and viscosity." Exp Brain Res 120(1): 52-60.

Jaric, S., S. Milanovic, et al. (1999). "Changes in movement kinematics during single-joint movements against expectedly and unexpectedly changed inertial loads." Human Movement Science 18(1): 49-66.

Ju, M. S., C. C. Lin, et al. (2002). "Performance of elbow tracking under constant torque disturbance in normotonic stroke patients and normal subjects." Clin Biomech (Bristol, Avon) 17(9-10): 640-9.

Kahn, L. E., P. S. Lum, et al. (2006). "Robot-assisted movement training for the stroke-impaired arm: Does it matter what the robot does?" J Rehabil Res Dev 43(5): 619-30.

Kahn, L. E., M. L. Zygman, et al. (2006). "Robot-assisted reaching exercise promotes arm movement recovery in chronic hemiparetic stroke: a randomized controlled pilot study." J Neuroeng Rehabil 3: 12.

Kawato, M., Y. Maeda, et al. (1990). "Trajectory formation of arm movement by cascade neural network model based on minimum torque-change criterion." Biol Cybern 62(4): 275-88.

King, R. B. (1996). "Quality of life after stroke." Stroke 27(9): 1467-72.

Kluger, A., J. G. Gianutsos, et al. (1997). "Patterns of motor impairment in normal aging, mild cognitive decline, and early Alzheimer's disease." Journals of Gerontology Series B-Psychological Sciences and Social Sciences 52(1): P28-P39.

Krebs, H. I., M. L. Aisen, et al. (1999). "Quantization of continuous arm movements in humans with brain injury." Proc Natl Acad Sci U S A 96(8): 4645-9.

L'Insalata, J. C., R. F. Warren, et al. (1997). "A self-administered questionnaire for assessment of symptoms and function of the shoulder." J Bone Joint Surg Am 79(5): 738-48.

Lacquaniti, F., C. Terzuolo, et al. (1983). "The law relating the kinematic and figural aspects of drawing movements." Acta Psychol (Amst) 54(1-3): 115-30.

Lei, M., Z. Z. Wang, et al. (2001). "Detecting nonlinearity of action surface EMG signal." Physics Letters A 290(5-6): 297-303.

Lemay, M. A. and P. E. Crago (1996). "A dynamic model for simulating movements of the elbow, forearm, and wrist." Journal of Biomechanics 29(10): 1319-1330.

Levin, M. F. (1996). "Interjoint coordination during pointing movements is disrupted in spastic hemiparesis." Brain 119 ( Pt 1): 281-93.

Levin, M. F. and M. Dimov (1997). "Spatial zones for muscle coactivation and the control of postural stability." Brain Res 757(1): 43-59.

Levin, M. F., R. W. Selles, et al. (2000). "Deficits in the coordination of agonist and antagonist muscles in stroke patients: implications for normal motor control." Brain Research 853(2): 352-369.

Liang, N., T. Yamashita, et al. (2008). "Temporal modulations of agonist and antagonist muscle activities accompanying improved performance of ballistic movements." Hum Mov Sci 27(1): 12-28.

Marsden, C. D., J. A. Obeso, et al. (1983). "The function of the antagonist muscle during fast limb movements in man." J Physiol 335: 1-13.

Milner, T. E. (2002). "Contribution of geometry and joint stiffness to mechanical stability of the human arm." Exp Brain Res 143(4): 515-9.

Mustard, B. E. and R. G. Lee (1987). "Relationship between EMG patterns and kinematic properties for flexion movements at the human wrist." Exp Brain Res 66(2): 247-56.

Mutha, P. K. and R. L. Sainburg (2007). "Control of velocity and position in single joint movements." Hum Mov Sci 26(6): 808-23.

Nagasaki, H. (1989). "Asymmetric velocity and acceleration profiles of human arm movements." Exp Brain Res 74(2): 319-26.
Nelson, W. L. (1983). "Physical principles for economies of skilled movements." Biol Cybern 46(2): 135-47.
Nielsen, J. F., J. B. Andersen, et al. (1998). "Input-output properties of the soleus stretch reflex in spastic stroke patients and healthy subjects during walking." Neurorehabilitation 10(2): 151-166.
O'Dwyer, N. J., L. Ada, et al. (1996). "Spasticity and muscle contracture following stroke." Brain 119 ( Pt 5): 1737-49.
O'Haver, T. C. and T. Begley (1981). "Signal-to-noise ratio in higher order derivative spectrometry." Annals of Chemistry 53: 1876-1878.
Osu, R., N. Kamimura, et al. (2004). "Optimal impedance control for task achievement in the presence of signal-dependent noise." J Neurophysiol 92(2): 1199-215.
Osu, R., Y. Uno, et al. (1997). "Possible explanations for trajectory curvature in multijoint arm movements." J Exp Psychol Hum Percept Perform 23(3): 890-913.
Pfann, K. D., D. S. Hoffman, et al. (1998). "Common principles underlying the control of rapid, single degree-of-freedom movements at different joints." Exp Brain Res 118(1): 35-51.
Piazzi, A. and A. Visioli (2000). "Global minimum-jerk trajectory planning of robot manipulators." Ieee Transactions on Industrial Electronics 47(1): 140-149.
Plamondon, R., A. M. Alimi, et al. (1993). "Modelling velocity profiles of rapid movements: a comparative study." Biol Cybern 69(2): 119-28.
Platz, T., P. Denzler, et al. (1994). "Motor learning after recovery from hemiparesis." Neuropsychologia 32(10): 1209-23.
Pohlmeyer, E. A., S. A. Solla, et al. (2007). "Prediction of upper limb muscle activity from motor cortical discharge during reaching." J Neural Eng 4(4): 369-79.
Prasad, T., K. S. Wasson, et al. (1984). "Modeling the non-linear stochastic characteristics of EMG/tension relationship." International Journal of Systems Science 15(12): 1311-1322.
Reina, G. A., D. W. Moran, et al. (2001). "On the relationship between joint angular velocity and motor cortical discharge during reaching." J Neurophysiol 85(6): 2576-89.
Richardson, M. J. and T. Flash (2002). "Comparing smooth arm movements with the two-thirds power law and the related segmented-control hypothesis." J Neurosci 22(18): 8201-11.
Rohrer, B., S. Fasoli, et al. (2002). "Movement smoothness changes during stroke recovery." J Neurosci 22(18): 8297-304.
Sainburg, R. L., C. Ghez, et al. (1999). "Intersegmental dynamics are controlled by sequential anticipatory, error correction, and postural mechanisms." J Neurophysiol 81(3): 1045-56.
Schaal, S. and D. Sternad (2001). "Origins and violations of the 2/3 power law in rhythmic three-dimensional arm movements." Exp Brain Res 136(1): 60-72.
Schmidt, R. A., H. Zelaznik, et al. (1979). "Motor-output variability: a theory for the accuracy of rapid motor acts." Psychol Rev 47(5): 415-51.
Semmlow, J. S. (2004). Biosignal and Biomedical Image Processing. New York, NY, Marcel Dekker, Inc.

Shannon, C. E. (1998). "Communication in the presence of noise (Reprinted from the Proceedings of the IRE, vol 37, pg 10-21, 1949)." Proceedings of the Ieee 86(2): 447-457.

Shreiber, D. I., V. H. Barocas, et al. (2003). "Temporal variations in cell migration and traction during fibroblast-mediated gel compaction." Biophys J 84(6): 4102-14.

Soechting, J. F., F. Lacquaniti, et al. (1986). "Coordination of arm movements in three-dimensional space. Sensorimotor mapping during drawing movement." Neuroscience 17(2): 295-311.

Soechting, J. F. and C. A. Terzuolo (1986). "An algorithm for the generation of curvilinear wrist motion in an arbitrary plane in three-dimensional space." Neuroscience 19(4): 1393-405.

Suzuki, M., D. M. Shiller, et al. (2001). "Relationship between cocontraction, movement kinematics and phasic muscle activity in single-joint arm movement." Exp Brain Res 140(2): 171-81.

Tian, J. and J. He (2003). Can EMG machine interface be used to model brain machine interface? 25th Annual International Conference of the IEEE Engineering in Medicine and Biology Society.

Todorov, E. (2004). "Optimality principles in sensorimotor control." Nat Neurosci 7(9): 907-15.

Todorov, E. and M. I. Jordan (1998). "Smoothness maximization along a predefined path accurately predicts the speed profiles of complex arm movements." J Neurophysiol 80(2): 696-714.

Trombly, C. A. (1993). "Observations of improvement of reaching in five subjects with left hemiparesis." J Neurol Neurosurg Psychiatry 56(1): 40-5.

Uno, Y., M. Kawato, et al. (1989). "Formation and control of optimal trajectory in human multijoint arm movement. Minimum torque-change model." Biol Cybern 61(2): 89-101.

Usui, S. and I. Amidror (1982). "Digital low-pass differentiation for biological signal processing." IEEE Trans Biomed Eng 29(10): 686-93.

van Galen, G. P. and W. P. de Jong (1995). "Fitts' Law as the outcome of a dynamic noise filtereing model of motor control." Human Movement Science 14: 539-571.

van Mourik, A. M. and P. J. Beek (2004). "Discrete and cyclical movements: unified dynamics or separate control?" Acta Psychol (Amst) 117(2): 121-38.

van Soest, A. J. and M. F. Bobbert (1993). "The contribution of muscle properties in the control of explosive movements." Biol Cybern 69(3): 195-204.

Viviani, P. and T. Flash (1995). "Minimum-jerk, two-thirds power law, and isochrony: converging approaches to movement planning." J Exp Psychol Hum Percept Perform 21(1): 32-53.

Viviani, P. and R. Schneider (1991). "A developmental study of the relationship between geometry and kinematics in drawing movements." J Exp Psychol Hum Percept Perform 17(1): 198-218.

Viviani, P. and C. Terzuolo (1982). "Trajectory determines movement dynamics." Neuroscience 7(2): 431-7.

Voight, M. L. and G. Cook (2001). Impaired neuromuscular control: Reactive neuromuscular training. New York, NY, McGraw-Hill.

Wann, J., I. Nimmo-Smith, et al. (1988). "Relation between velocity and curvature in movement: equivalence and divergence between a power law and a minimum-jerk model." J Exp Psychol Hum Percept Perform 14(4): 622-37.

Wiegner, A. W. and M. M. Wierzbicka (1992). "Kinematic models and human elbow flexion movements: quantitative analysis." Exp Brain Res 88(3): 665-73.

Wolpert, D. M., Z. Ghahramani, et al. (1995). "Are arm trajectories planned in kinematic or dynamic coordinates? An adaptation study." Exp Brain Res 103(3): 460-70.

Yan, J. H., S. Rountree, et al. (2008). "Alzheimer's disease and mild cognitive impairment deteriorate fine movement control." J Psychiatr Res 42(14): 1203-12.

Yang, Z. and G. Zhao (1998). Application of symbolic techniques in detecting determinism in time series. 20th Annual International Conference of the IEEE Engineering in Medicine and Biology Society.

# CURRICULUM VITA

Michael T. Wininger

## Education

2004-2009 Rutgers, The State University of New Jersey (New Brunswick, NJ)
Ph.D. Biomedical Engineering

1999-2004 University of Connecticut (Storrs, CT)
B.S. Physics *General/Theoretical*
B.A. Mathematics *General/Analytical*

## Positions Held

2009 Max Planck-Institut für Informatik (Saarbrücken, Germany)
Max Planck Institute for Informatics
Computational Biology & Applied Algorithmics
Visiting Scholar

2007 Industrial Technology Research Institute (Hsinchu, Taiwan)
Biomedical Engineering Research Lab
Cell Engineering Division
Visiting Fellow

2004 Adidas America (Portland, OR)
Adidas Innovation Team
Engineering Research Intern

## Publications

2009 Yungher DA, Wininger MT, Craelius W, Barr JB, Threlkeld AJ. Surface muscle pressure as a measure of active and passive behavior of muscles during gait. *Clinical Biomechanics.* In Revision.

2009 K-A Norton, Wininger MT, Bhanot G, Ganesan S, Shinbrot T. A 2-D mechanistic model of ductal carcinoma in situ (DCIS) morphology and progression. *Journal of Theoretical Biology.* In Revision.

2009 MT Wininger, Kim N-H, Craelius W. Spatial resolution of spontaneous accelerations in reaching tasks. *Journal of Biomechanics*. 42(1):29-34, 2009.

2009 T Morris, Newby NA, Wininger MT, Escaldi S, Craelius W. Inter-limb transfer of learned ankle movements. *Experimental Brain Research*. 192(1):33-42, 2009.

2008 MT Wininger, Kim N-H, Craelius W. Pressure signature of the forearm as a predictor of grip force. *Journal of Rehabilitation Research and Design.* 45(6):883-892, 2008.